AN INVESTIGATION OF UREA DECOMPOSITION AND SELECTIVE NON-CATALYTIC REMOVAL OF NITRIC OXIDE WITH UREA

A Thesis

by

YONG HUN PARK

Submitted to the Office of Graduate Studies of
Texas A&M University
in partial fulfillment of the requirements for the degree of

MASTER OF SCIENCE

May 2003

Major Subject: Mechanical Engineering

AN INVESTIGATION OF UREA DECOMPOSITION AND SELECTIVE NON-CATALYTIC REMOVAL OF NITRIC OXIDE WITH UREA

A Thesis

by

YONG HUN PARK

Submitted to Texas A&M University
in partial fulfillment of the requirements
for the degree of

MASTER OF SCIENCE

Approved as to style and content by:

Jerald A. Caton (Chair of Committee)	Denis J. Phares (Member)
Don R. Collins (Member)	John A. Weese (Head of Department)

May 2003

Major Subject: Mechanical Engineering

ABSTRACT

An Investigation of Urea Decomposition and Selective Non-Catalytic Removal of Nitric Oxide with Urea. (May 2003)

Yong Hun Park, B.E., Kyungpook National University

Chair of Advisory Committee: Dr. Jerald A. Caton

The use of urea (NH_2CONH_2) to remove nitric oxide (NO) from exhaust streams was investigated using a laboratory laminar-flow reactor. The experiments used a number of gas compositions to simulate different combustion exhaust gases. The urea was injected into the gases as a urea-water solution. The decomposition processes of the urea-water solutions and urea powder were examined. For both the nitric oxide removal and the urea decomposition experiments, a Fourier transform infrared (FTIR) spectrometer was used to determine the concentrations of the product species.

The products from the decomposition were examined every 50 K from 500 K to 800 K. The dominant products were ammonia (NH_3), isocyanuric acid (HNCO) and carbon dioxide (CO_2). In case of urea-water solution decomposition, for gas temperatures between 550 and 650 K, the highest concentrations were for NH_3 and HNCO. On the other hand, the concentrations of CO_2 were highest for gas temperatures of about 500 – 550 K. For temperatures above about 650 K, the amount of these three dominant products slightly decreased as temperature increased.

For the nitric oxide removal (SNCR) experiments, the gas mixture was heated to temperatures between 800 K and 1350 K. Depending on the temperature, gas composi-

tion, residence time, and urea feed rate, removal levels of up to 95% were obtained. Other by-products such as N_2O were detected and quantified. The effects of the urea/NO (beta) ratio were determined by varying the urea concentration for a constant NO concentration of 330 ppm. The effects of the levels of oxygen (O_2) in the exhaust gases and the residence time also were investigated. Increasing the urea/NO ratio and residence time resulted in higher NO removal and increased the temperature “window” of the nitric oxide removal.

DEDICATION

I would like to dedicate this thesis to my parents who have been a major influence in my life. They have supported me wholeheartedly in all my endeavors. I also would like to dedicate this thesis to Jyoug-Yuop Baek who has been my best friend and brother as well for the majority of the years. His encouragement has kept me going, throughout my student life.

ACKNOWLEDGEMENTS

I would like to thank my adviser, Dr. Jerald A. Caton for the opportunity to work on the project described in this thesis. Dr. Caton enhanced my knowledge about scientific work in countless discussions in addition to his extensive knowledge about combustion chemistry and especially the chemistry of nitric oxide removal processes.

Many thanks also go to Ki-Hyun Baek who helped me a lot to understand the complex chemistry.

This research project was sponsored in part by a grant from the Texas Advanced Research Program of the State of Texas under Grant No. 000512-0191-1999. The contents of this paper, however, do not necessarily reflect the opinions or views of the sponsors.

TABLE OF CONTENTS

LIST OF FIGURES

FIGURE Page

FIGURE Page

FIGURE Page

FIGURE Page

FIGURE Page

FIGURE Page

FIGURE Page

FIGURE Page

LIST OF TABLES

1. INTRODUCTION

The use of automobiles, trucks, power plants and other such fuel burning devices are very common nowadays. Unfortunately, the use of these devices continues to worse the environment. The reason is that there are many undesirable products such as NO, NO_2, N_2O and CO from the combustion process [1].

Among the unwanted products, nitrogen oxides (NO_x) play an important role in science and industry since the formation of nitrogen oxides is inevitable when fuel is burnt at high temperature in a combustion process. There are lots of sources for producing NO_x like motor vehicles, an electric utility power plant, other industrial facilities and even residential sources that burn fuel. Serious concern is that the formation of NO_x contributes to air pollution. It can cause acid rain and photochemical smog destroying the environment [2, 3]. Figure 1 shows the photochemical smog concentration in LA [6]. The unwanted air pollutants and the limited natural sources of fuels require efficient control system for all chemical process [2, 4, and 5].

Figure 1. Photochemical smog concentration in LA [6].

This thesis follows the format and style of Journal of Fluids Engineering.

1.1 What Is NO_x and Why Is It So Important?

NO_x is used to refer to NO (nitric oxide) and NO_2 (nitrogen dioxide). They are two of the most common oxides of nitrogen. Many nitrogen oxides are colorless and odorless, but NO_2 is a reddish-brown gas having a sharp odor. The oxidation from NO to NO_2 is part of the processes that result in the creation of ozone in the lower level of the atmosphere [7]. On the other hand, ozone in the upper level of the atmosphere adsorbs the ultraviolet rays from the sun. Ground level ozone contributes to smog and causes human respiratory problems [8]. Figure 2 shows the ozone in earth's atmosphere [8].

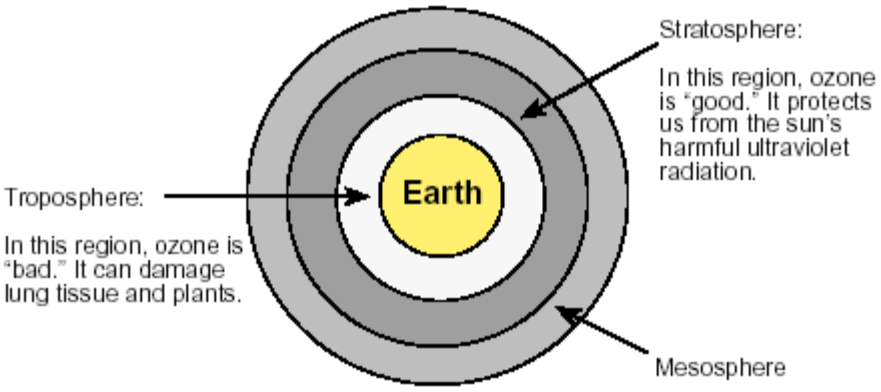

Figure 2. Ozone in earth's atmosphere [8].

1.2 Formation of NO_x

The formation of nitrogen oxide occurs through mainly three processes – Thermal NO_x, Fuel NO_x, and Prompt NO_x. Thermal NO_x is produced while nitrogen and air with excess oxygen are presented at elevated temperatures (greater than 1800 K) in the combustion process since fixation of nitrogen requires the breaking of the strong N_2 triple bond [9]. The quantity of NO_x formation depends on reaction temperature, residence

time, the local stoichiometric and turbulence. Two of the main reactions for formation of thermal NO_x are described by the Zeldovich mechanism

$$O + N_2 = N + NO \quad (1)$$

$$N + O_2 = O + NO \quad (2)$$

An additional reaction has been shown to be necessary for near-stoichiometric and in fuel-rich mixtures:

$$N + OH = H + NO \quad (3)$$

Although the formation rate of thermal NO_x is slow, compared to other processes, it contributes the largest portion to the total NO_x [10].

Fuel NO_x is formed in the combustion system reaction from chemically bound nitrogen in fuels such as coal, coke and heavy oils [11]. Between 20 and 80 percent of the bound nitrogen is typically converted to NO_x, depending on fuel pyrolysis and sub-sequent reaction between many intermediate nitrogenous species and the oxidant species [12].

The third process that results in NO_x is known as " Prompt NO_x". The breakdown of hydrocarbon fragments such as C, CH, CH_2 may react with atmospheric nitrogen and their subsequent combination to produce other nitrogen species such as CN, H_2CN, HCN

and NH under fuel-rich conditions [11, 13]. The route now accepted is the following reactions [9]:

$$CH + N_2 = HCN + N \quad (4)$$

$$N + O_2 = NO + O \quad (5)$$

$$HCN + OH = CN + N_2O \quad (6)$$

$$CN + O_2 = NO + CO \quad (7)$$

This is referred to as prompt NO_x since the rapid formation of NO_x is confined to regions near flame front.

1.3 General Methods for Control of NO_x Emission

The most promising methods of NO_x control technologies are categorized as pre and post combustion techniques. For engines, NO_x control technologies include lowering the compression rate, retarding the timing, using EGR (exhaust gas recirculation) and enriching the fuel mixture. These techniques provide pre-combustion NOx control by keeping combustion temperatures low. Post-combustion technologies reduce NO_x in the exhaust gases [2].

Combustion modifications and pre-combustion techniques provide significant NOx removal but often are not enough to meet regulations. To get more reduction in emission, post-combustion control is necessary. These include, for example, selective cata-

lytic reduction (SCR), selective non-catalytic reduction (SNCR), and electron beams radiation.

1.4 Selective Non-Catalytic Reduction of NO_x

The selective non-catalytic reduction (SNCR) process is one of the technologies for NO_x removal. Depending on which agent is being used, these are classified into three main processes: Thermal $DeNO_x$ (using ammonia), $RAPRENO_x$ (using cyanuric acid), and NO_xOUT (using urea). NO_x reduction is achieved by injecting one of these agents into the exhaust gas stream at an elevated temperature. Even though a SNCR technique has some drawbacks like a narrow temperature window for operation and, for certain conditions, conversion of ammonia to NO_x, it has advantages like considerably lower capital cost and easy installation relative to the selective catalytic reduction (SCR).

1.4.1 The Thermal $DeNO_x$ Process – Using Ammonia

The thermal $DeNO_x$ Process injecting ammonia (NH_3) downstream of the combustion zone was invented by Lyon and Hardy [14]. They found that mixtures of NO, O_2 and NH_3 within appropriate circumstances reduced NO_x [14]. One concern of this process is the possibility of unreacted ammonia being emitted into the environment, since ammonia is a toxic chemical. Commercial use of the thermal DeNOx was used in 1985 [15]. The overall reactions for the NOx removal using ammonia (NH_3) are commonly represented through the following overall reactions:

$$4NO + 4NH_3 + O_2 \rightarrow 4N_2 + 6H_2O \quad (8)$$

$$6NO_2 + 8NH_3 \rightarrow 7N_2 + 12\ H_2O \quad (9)$$

1.4.2 The RAPRENO$_x$ Process – Using Isocyanuric Acid

The RAPRENO$_x$ process was developed by Perry and Sibers [16]. The HNCO molecule (isocyanuric acid) was obtained from sublimation of cyanuric acid when its temperature was high. Other possible sources for HNCO are ammelide and ammeline [17]. Using HNCO for NO reduction, a possible reaction mechanism was proposed [18]:

$$HNCO \rightarrow NH + CO \quad (10)$$

$$NH + NO \rightarrow H + N_2O \quad (11)$$

$$H + HNCO \rightarrow NH_2 + CO \quad (12)$$

$$NH_2 + NO \rightarrow N_2H + OH \quad (13)$$

$$NH_2 + NO \rightarrow N_2 + H_2O \quad (14)$$

1.4.3 The NO$_x$OUT Process – Using Urea

Arand *et al.* in 1980 patented the process of using either urea powder (NH_2CONH_2) or urea-water solution to reduce NOx [19]. Figure 3 shows the molecular model of urea. Benefits of using urea instead of ammonia (NH_3) include easier handling, safer, and non-regulated. Ammonia is toxic and has federal, state and local regulations [4, 19].

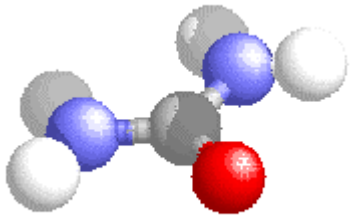

Figure 3. Molecualr model of Urea.

The thermal decomposition of dry urea has been shown to produce NH_3 and HNCO [20], while the thermal decomposition of urea-water solution has been shown to produce NH_3 and CO_2 [21]:

$$NH_2CONH_2 \rightarrow NH_3 + HNCO \quad (15)$$

$$NH_2CONH_2+H_2O \rightarrow 2NH_3+ CO_2 \quad (16)$$

Itaya *et al.* suggested that the overall NO reduction from urea solution may proceed through the following reaction [21]:

$$2NO+(NH_2)_2CO+(0.5)O_2\rightarrow 2N_2+CO_2+ 2H_2O \quad (17)$$

SNCR techniques of NOx reduction will be described in the literature review.

2. LITERATURE REVIEW

In this section, previous work on selective-non-catalytic reduction will be presented: Thermal $DeNO_x$, and NO_xOUT processes.

2.1 Thermal $DeNO_x$ Process

The effective removal of NO from combustion gases by injection of NH_3 was discovered by Lyon who named it the thermal $DeNO_x$ process [22].

2.1.1 Kinetic Modeling of the $DeNO_x$ Process

The chemical details of the Thermal $DeNO_x$ process have been developed and improved over the years. Lyon and Benn developed a chemical kinetics model including 24 reactions [23] and Saliman and Hanson presented a chemical kinetics scheme including 49 reactions to predict the thermal $DeNO_x$ process [24].

The two main reactions to remove of NO with NH_2 radicals which are produced through the reaction of OH with NH_3 in reaction (18) are reactions (19) and (20) [24]:

$$NH_3 + OH = NH_2 + H_2O \quad (18)$$

$$NH_2 + NO = N_2 + H_2O \quad (19)$$

$$NH_2 + NO = N_2 + H + OH \quad (20)$$

Two other reactions also remove NO directly [24]:

$$NH + NO = N_2 + OH \quad (21)$$

$$NH + NO = N_2O + H \quad (22)$$

Reaction (18) is chain terminating since chain carriers were not directly or indirectly produced [25]. The reaction for the chain carrier producing path is either reaction (19) or reaction (20) [26]. The temperature window, which explains the region of NO reduction effectively, shift obtained by the addition of H_2 [24]:

$$H + O_2 = O + OH \quad (23)$$

$$H_2 + O = H + OH \quad (24)$$

$$O + H_2O = OH + OH \quad (25)$$

$$H + H_2O = OH + H_2 \quad (26)$$

In the above reactions, OH is not produced fast enough at low temperatures [24]. Figure 4 shows a scheme with 73 reactions is used with the main reaction path [24].

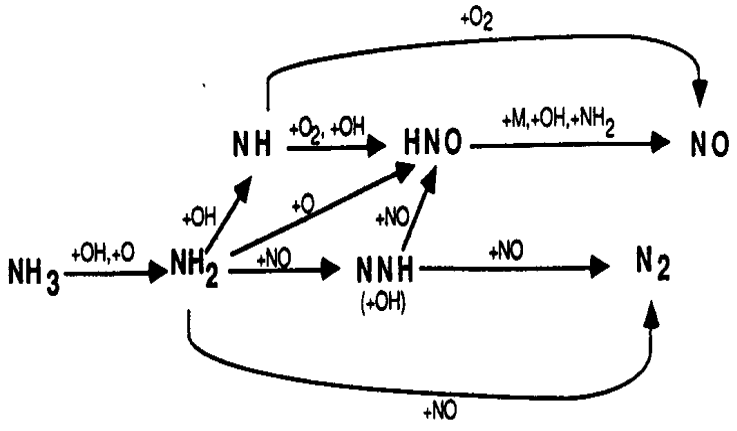

Figure 4. Reaction path diagram for the thermal DeNOx process [24].

Miller and Bowman introduced 82 reactions and they presented several key kinetic parameters [25]:

$$NH_3 + O = NH_2 + OH \quad (27)$$

$$NH_2 + O = HNO + H \quad (28)$$

$$NH_2 + O = NH + OH \quad (29)$$

$$NH + O_2 = NO + OH \quad (30)$$

$$NH_2 + NO = NNH + OH \quad (31)$$

$$NNH + NO = N_2 + HNO \quad (32)$$

$$HNO + M = H + NO + M \quad (33)$$

$$NH_2 + NO = N_2 + H_2O \quad (34)$$

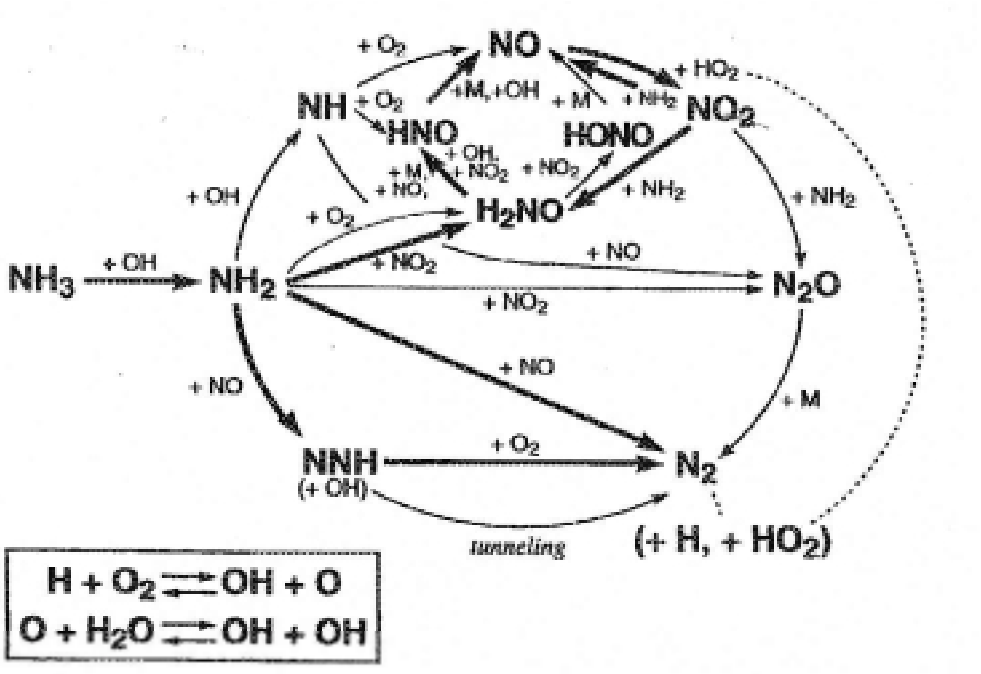

Figure 5. Reaction path diagram for the thermal DeNOx process. The bold arrows represent the dominant paths [29].

Figure 5 shows the reaction path diagram for the thermal $DeNO_x$ process [29]. First, the ammonia is converted to NH_2 principally by reaction with OH with reaction (18) but also in the absence of water vapor by reaction with oxygen atoms with reaction (27) and HNO, NH produced with reaction (28) and (29) as product distribution for the $NH_2 + O$ reaction. OH and O continue the $NH_3 \rightarrow NH_2$ conversion, which should be re-generated through $NH_2 + NO$ reaction to be self-sustaining [24]. This regeneration is accomplished by reaction (31), (32) and (33). Compared to the previous attempts, these mechanisms give a good fit to experimental data [24]. Compared with Glarborg *et al.*'s mechanism [30], Kjaergaard *et al.* presented a few changes [29]:

$$NNH + O_2 = N_2 + HO_2 \quad (35)$$

$$HO_2 + NO = NO_2 + OH \quad (36)$$

$$NH_2 + NO_2 = H_2NO + NO \quad (37)$$

$$NH_2 + NO = NNH + OH \quad (38)$$

NO_2 is an essential intermediate in the process compared with Miller and Bowman and to allow a short lifetime for NNH, it is necessary to have a fast reaction between NNH and O_2 in reaction (25) [24, 29]. A consequence of a large value for reaction (35) is that NO_2 is formed readily by the reaction (36) [26].

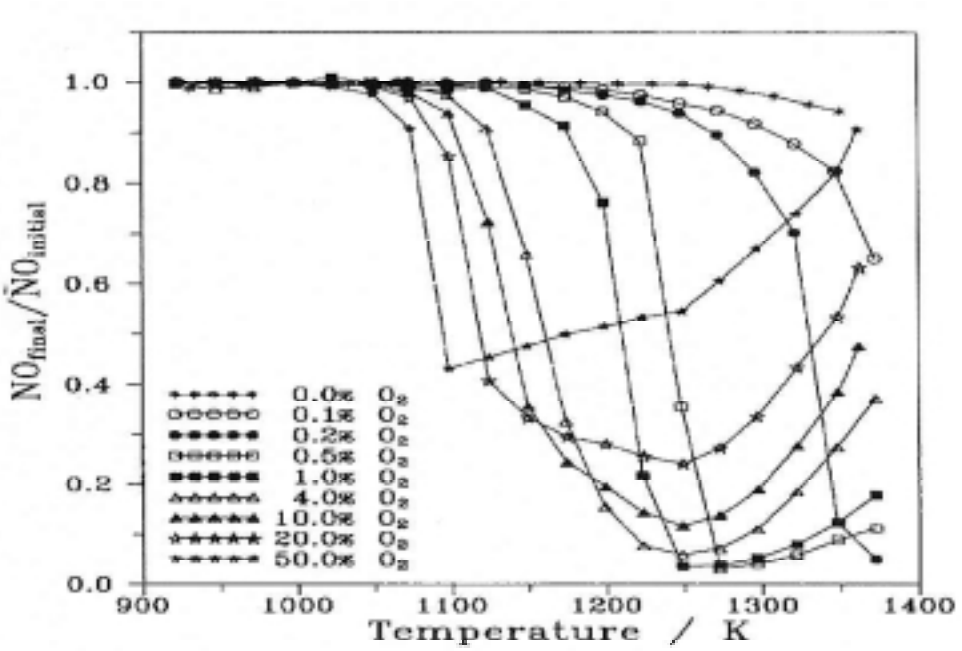

Figure 6. Effect of different O_2 concentration on NO reduction [27].

2.1.2 O_2 Concentration Effect

Miller and Bowman mentioned the necessity of excess oxygen in order to run the process properly [24]. To be reduced by NH_3, the presence of O_2 is required [27]. As the O_2 concentration is increased, the boundary for the process is shifted toward lower temperatures and broadened temperature range while the potential of the NO reduction is diminished as shown in figure 5 [27].

Figure 6 shows for higher oxygen concentrations, the overall NO removal is less but occurs at lower temperature, minimizes any “ammonia slip”, and increases the emission of N_2O [28]. Figure 7 shows the measured percentage NO removal as a function of the reactor temperature with different O_2 concentration [28]. When the oxygen level increases, the temperature range for NO reduction is widened but the NO reduction poten-

tial decreases as shown in figure 8 [29]. As the oxygen level increases, the effect of pressure on the initiation temperature is reduced. [29]. As the oxygen concentration decreases, the temperature window shifts significantly toward higher temperature [31].

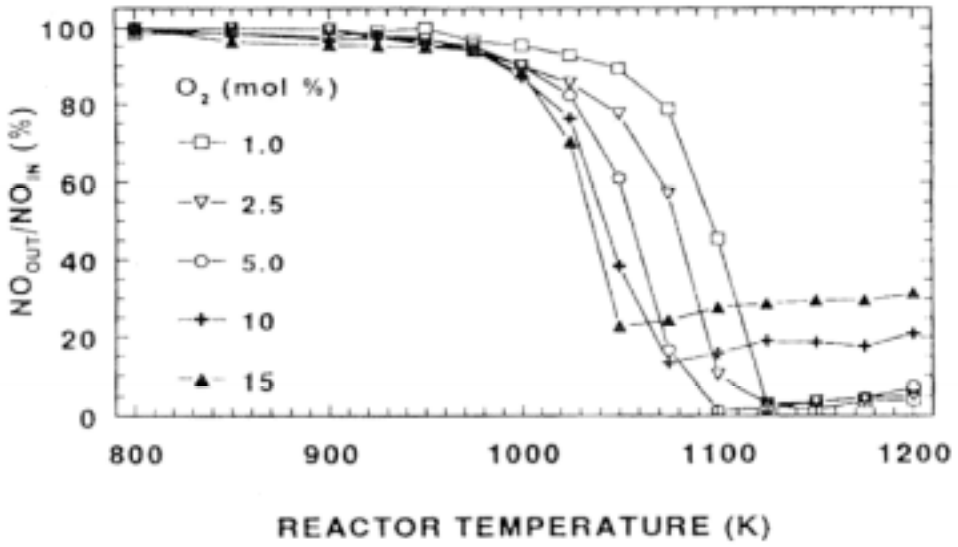

Figure 7. Measured percentage NO removal as a function of the reactor temperature with different O_2 concentration [28].

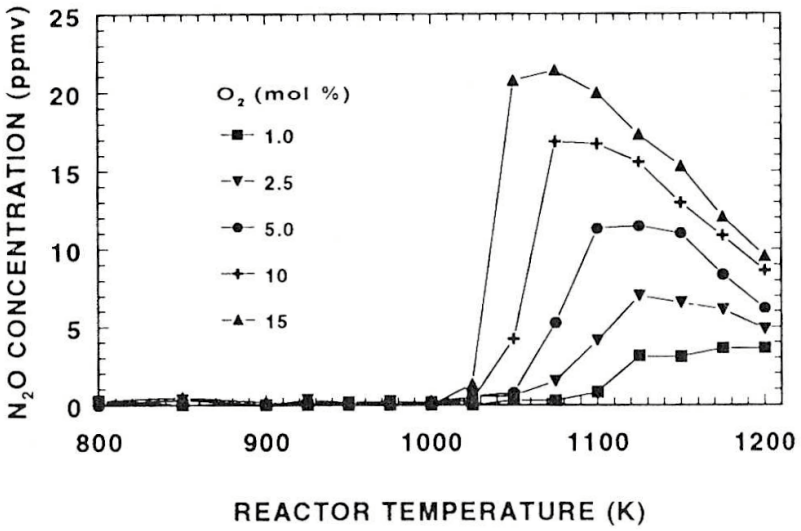

Figure 8. Measured N_2O concentration as a function of the reactor temperature [28]

Figure 9 shows a sharp distinction between a very slow reaction regime at lower temperatures and a rapid oxidation regime at higher temperatures. The low-temperature boundary is very sensitive to small variations in the O_2 concentration [31].

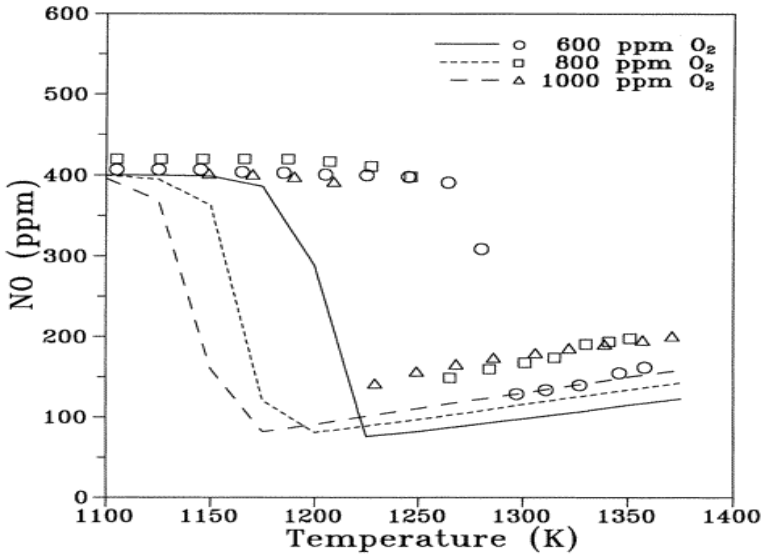

Figure 9. Comparison of experimental data and model predictions for reduction of NO by NH_3 at near-stoichiometric conditions and 1400 ppm CO: effect of O_2 concentration. Symbols: experiment, lines: calculations [31]

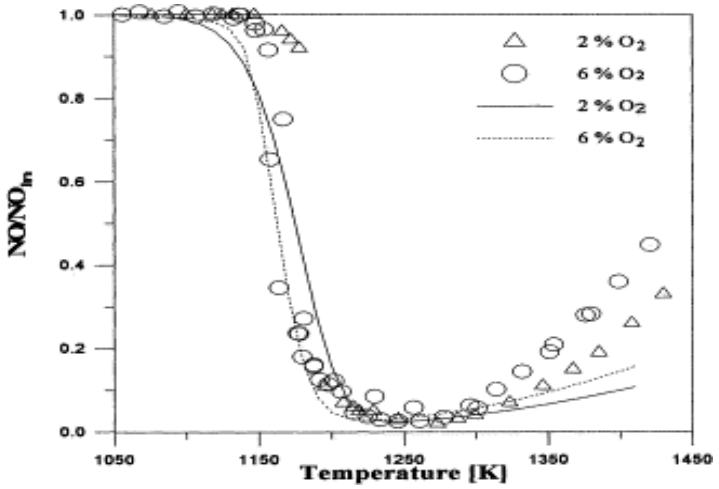

Figure 10. Influence of O_2 concentration in high partial pressures conditions: NO=1400 ppm; NH_3=2800 ppm; O_2=4%; H_2O=5% [32].

Increasing O_2 concentration shits the NO reduction profile toward lower temperatures without affecting the maximum degree of abatement as shown in figure 10 [32].

2.1.3 CO Concentration Effect

Dill and Sowa found when the CO concentration is larger than the initial NO in higher temperature reactions (T>1010^{o}C), NO reduction is more inefficient, while good NO reduction and an NH_3 slip under 5 ppm can be reached for low temperature cases [33]. So, CO has a great effect on low temperature cases but in all cases, NO reduction becomes less dependent on initial CO concentration as initial NO decreases. The results

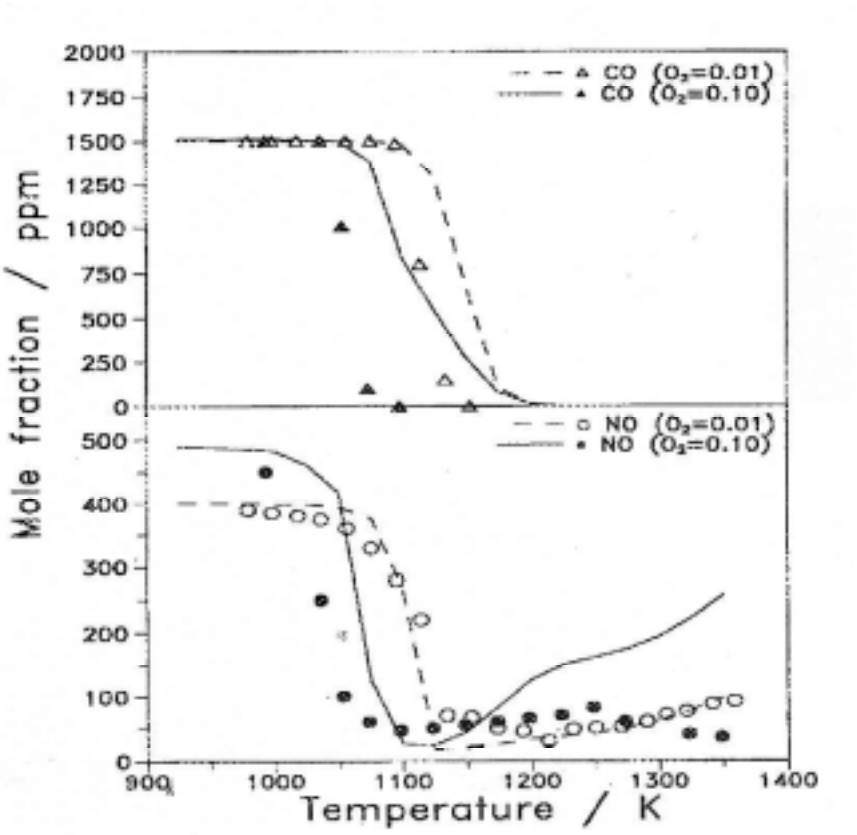

Figure 11. Effect of inlet CO and O_2 level and temperature on NH_3 and NO outlet concentrations at high temperature [29].

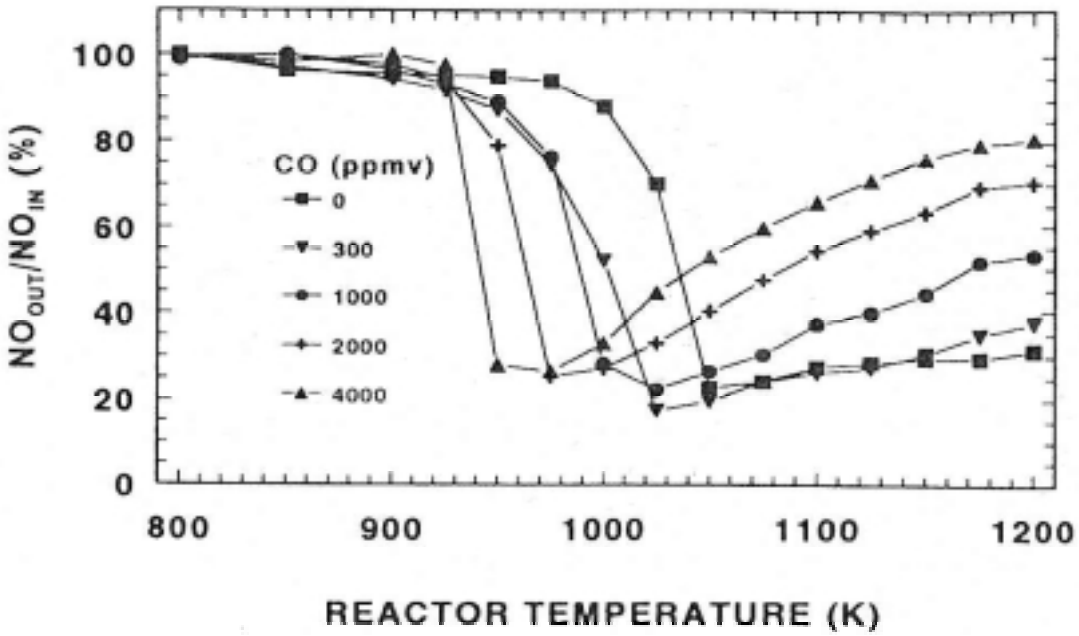

Figure 12. Measured percentage NO removal as a function of the reactor temperature and inlet CO concentration [28].

for residual CO differ greatly from the predicted results, which comes from relationship between CO and the important radical species include H, OH, and O [33].

For temperatures higher than the one for maximum NO reduction, the higher CO concentration cases causes less NO reduction [28]. CO was added to shift the region for NO_x removal to lower temperatures as shown in figure 11 [29]. The effect of CO shifts the reaction regime to lower temperature [29]. Figure 12 shows NO removal as a function of reactor temperature for five different CO concentrations for base case conditions for 15% oxygen [28]. For higher CO concentration, the temperature for maximum NO removal decreases. Increasing the initial CO concentrations not only shifts the regime for NO reduction to below 1000 K temperature, but causes a narrowing of the temperature

window [29]. In higher CO concentration, CO causes an adverse effect on the width of the temperature regime for NO reduction [29].

2.1.4 NO_2 and N_2O Formation

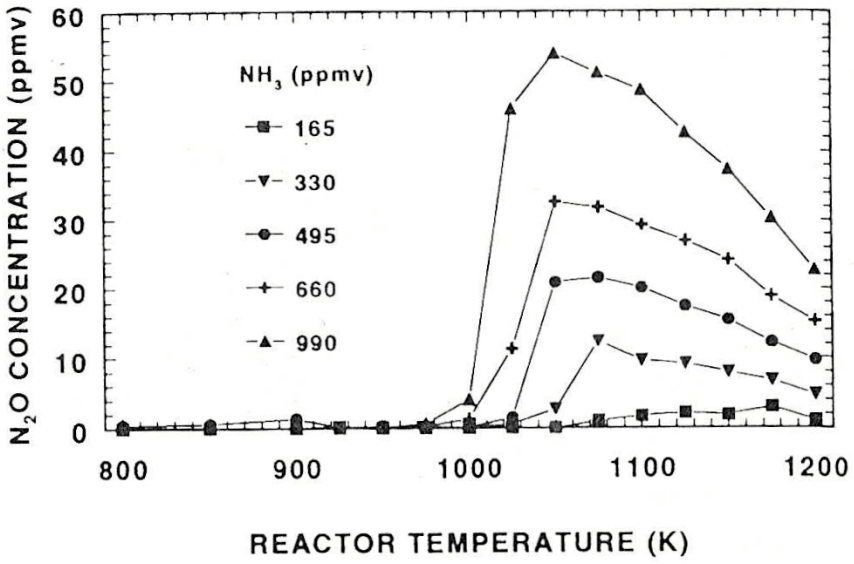

Figure 13. Measured N_2O concentration as a function of the reactor temperature [28].

Figure 13 shows the measured N_2O concentration as a function of the reactor temperature [28]. As inlet NH_3 increases, the formation of N_2O concentration increases [28]. The amount of NO_2 observed is high at higher temperatures and low O_2 concentrations, while N_2O is dominant at lower temperatures and high O_2 level. [27]. The ammonia process had substantial NO_2 formation at 515 Kpa condition [34]. NO_2 emissions in the high-pressure cases had an increase of four to six times the NO_2 level of the low-pressure case.

2.1.5 Pressure Effect

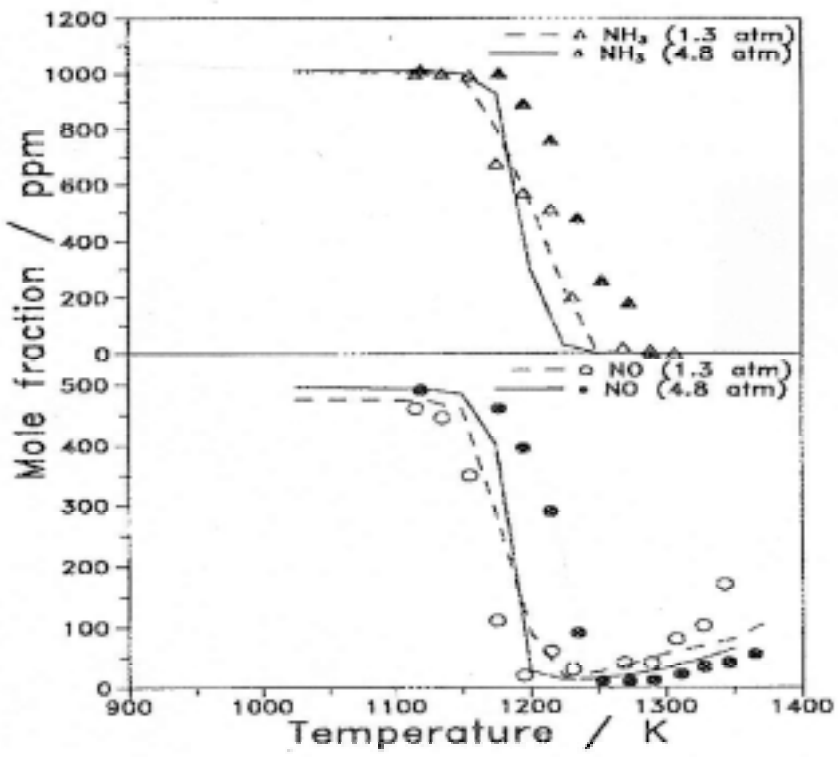

Figure 14. Effect of pressure and temperature on NH_3 and NO outlet concentrations [30].

High partial pressures in the thermal $DeNO_x$ process have a significant impact on the performance. Elevated pressures have an adverse effect on the NO_x reduction potential as shown in figure 14 [27]. Lower pressure case showed significantly more NO reduction than higher case [34]. The ammonia-slip levels for the high-pressure cases were of similar magnitude with the low-pressure case [34]. Increasing pressure, both the lower and the higher boundaries for the process are shifted toward higher temperatures and the temperature range for NO_x removal slightly broadened [29]. Pressure change from 1 to

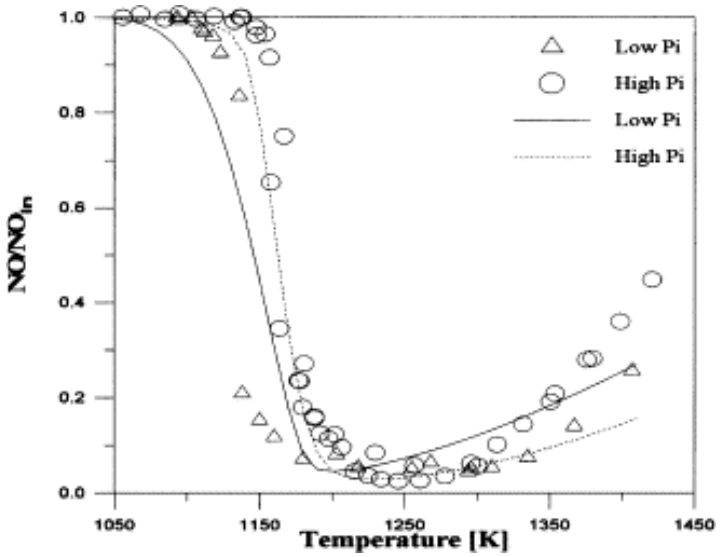

Figure 15. Influence of partial pressures on NO reduction. Symbols: experimental results, line: model prediction [32].

10 bar leads to at least 100 K temperature window width [30]. The effect of pressure is most pronounced at low O_2 levels [30]. As the partial pressures increase, it causes a reduction of operating window width and a small shift towards higher temperature [32]. In figure 15, as the partial pressures of oxygen increases, the maximum reduction of NO decreases [32].

2.1.6 β – Ratio Effect

The β – ratio is the ratio of the concentration of the reducing agent and the concentration of the nitric oxide. This means that the β – ratio for the thermal $DeNO_x$ process is defined as the molar ratio of NH_3 injected to the initial NO_x present. This ratio is important to determine the most efficient use of the reducing agent. As β – ratio

(NH_3/NO ratio) increases, the NO reduction at the optimum temperature increases, but there is an increase of NH_3 slip as a disadvantage [35].

2.2 NO_xOUT Process

2.2.1 Urea Decomposition

According to the material data sheet, the melting point of urea is 405 K (132.7°C). Schaber *et al.* [36] mentioned that mass loss of urea began around 413 K (140°C) and suggested 19 reactions for the urea thermal decomposition as the temperature rises. First, urea powder can be vaporized, and then NH_3 and HNCO evolve around 425 K (152°C). Biruet is produced from isocyanic acid reaction with urea through the following reaction:

$$NH_2CONH_2+HNCO\rightarrow H_2NCONHCONH_2 \quad (39)$$

Around 448 K (175°C), cyanuric acid ($C_3H_3N_3O_3$) and ammelide ($C_3H_4N_4O_2$) are produced through the following reactions [36]:

$$H_2NCONHCONH_2+HNCO\rightarrow C_3H_3N_3O_3 + NH_3 \quad (40)$$

$$H_2NCONHCONH_2+HNCO\rightarrow C_3H_4N_4O_2 + H_2O \quad (41)$$

$$HNCO+NH3\rightarrow H_2O + H_2NCN \quad (42)$$

The products HNCO and H_2O, from reaction (41) and (42), react to form CO_2 for temperature of about 700 K (427°C). After 700 K, NH_3 and CO_2 are produced as HNCO is consumed from reaction (43).

$$HNCO + H_2O \rightarrow CO_2 + NH_3 \quad (43)$$

Fang and DaCosta [37] studied the thermal decomposition of urea. The mixture of urea and biuret was found at about 473 K. The main component between 500 K and 600 K was cyanuric acid having a pale beige color deposit. Ammeline and ammelide having a dark beige color deposit were found as major components between 600 K and 700 K.

NH_3 and HNCO are the main decomposition products of dry urea for certain conditions [38]. The main route up to 593K seems to proceed through

$$NH_2CONH_2 \rightarrow NH_3 + HNCO \quad (44)$$

However, Jodal *et al.* proposed for high temperatures other reaction channels: NH_2 can be removed instead of NH_3 [39].

$$NH_2CONH_2 \rightarrow NH_2 + H2NCO \quad (45)$$

$$H_2NCO \rightarrow H_2 + NCO \quad (46)$$

Bilbao proposed direct elimination of NH_2 and H radicals from urea [40].

$$NH_2CONH_2 \rightarrow NH_2 + H + HNCO \quad (47)$$

In presence of water, urea has been suggested to react [41]

$$NH_2CONH_2 + H_2O \rightarrow 2NH_3 + CO_2 \quad (48)$$

When performed thermal decomposition experiments, obtained significantly less ammonia that the amount predicted theoretically [41].

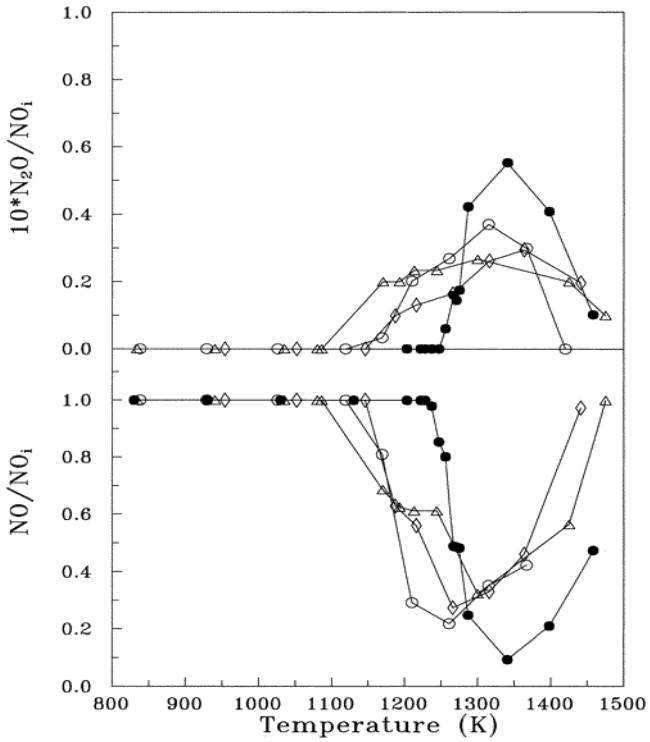

Figure 16. Experimental NO and N_2O concentrations versus temperature for different oxygen concentrations: solid circle: 0.5% O_2, empty triangular: 1.0% O_2, empty diamond: 4.0% O_2, empty circle: 10% O_2. (Inlet concentrations: 300 ppm NO, 150 ppm urea, 4% H_2O, N_2 to balance) [40].

2.2.2 O_2 Concentration Effect

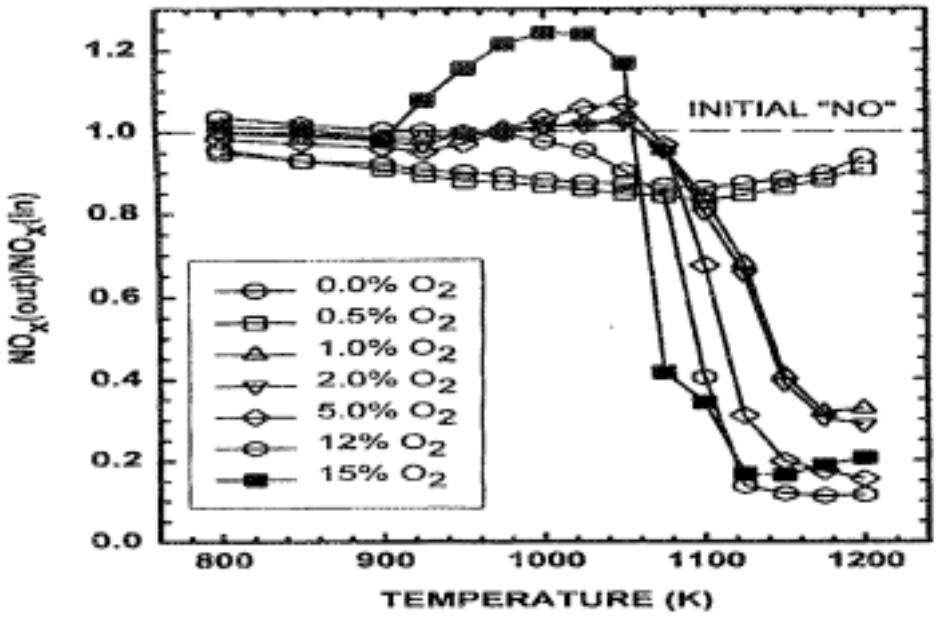

Figure 17. The removal of NOx as a function of reactor temperature for seven levels of oxygen for 100 ppm carbon monoxide and a heated residence time of 2.11 sec. [42].

As the oxygen concentration diminishes, the NO reduction increases and the lowest oxygen concentration case obtained the major N_2O production as shown in figure 16 [40]. Srivatsa and Caton completed experiments with different O_2 concentration cases. In their experiments, the highest NO_x reduction are obtained between 5% and 15% O_2 concentration for 1100 and 1200 K [42]. Figure 17 shows the cases of lower 0 and 0.5% O_2 concentration, the maximum NO_x reduction is extremely low (5% and 20%) [42]. As the initial O_2 concentration increases, window range for NO_x reduction slightly shifts to lower temperature regime [42]. Not only increasing O_2 concentration, but also higher urea solution, the reduction of NO is increased [41].

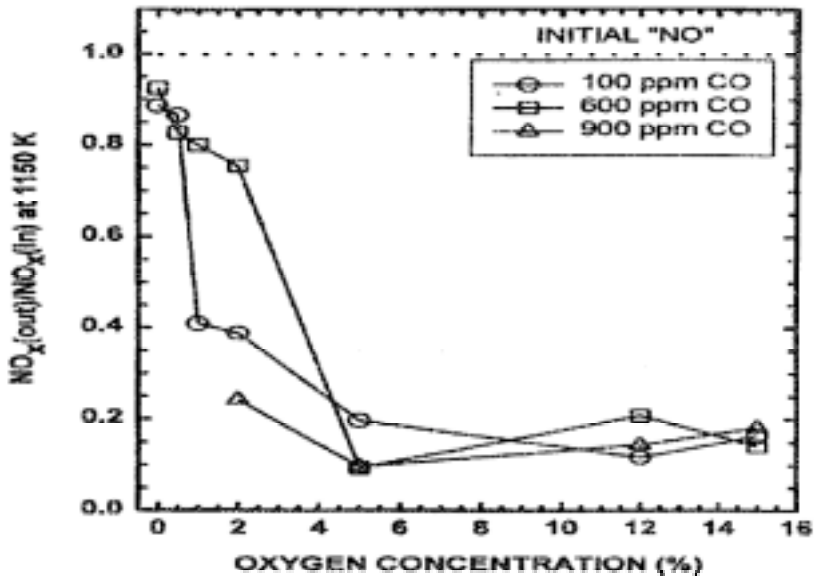

Figure 18. The removal of NOx as a function of oxygen concentration for three levels of carbon monoxide (100, 600 and 900 ppm) for a reactor temperature of 1150 K and a heated residence time of 2.11 secs. [42].

2.2.3 CO Concentration Effect

The effect of CO on NO reduction process has been studied [14, 43 and 44], which indicated that the presence of CO shifts the selectivity by increasing the rate of NH_2 formation and the rate of NH_3 oxidation to NO [45]. The presence of CO is detrimental under slow conditions but beneficial under rapid conditions because it enhances the radical pool at lower temperature regions [45].

Figure 18 shows the effects of the CO which were not clear, and no conclusions may be obtained [42]. Rota *et al.* also mentioned that the effect of adding an amount of CO, only small shift towards to lower temperatures of the NO reduction "window" as shown in figure 19 [46].

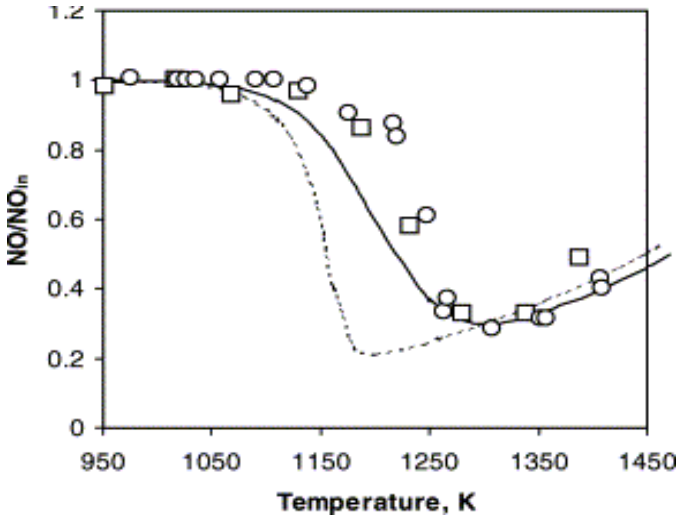

Figure 19. Influence of CO/NO ratio in the feed on the NO reduction. Experimental results and model predictions. Symbols: experiments for (O) CO/NO=0 and (□) CO/NO=1. Curves: model predictions for (—) CO/NO=0 and (- -) CO/NO=1 [46].

2.2.4 NO_2 and N_2O Formation

N_2O is a major product in fluidized bed combustors and lead to the depletion of stratoshperic ozone. Moreover, N_2O has been classified as a greenhouse gas, which have become a concern since the levels of atmospheric N_2O have been steadily rising.

Maximum N_2O concentrations nearly coincide with the regions where the minimum NO concentration is obtained, and the major N_2O levels is obtained for the lowest oxygen concentrations [40].

Figure 20 shows that the amount of N_2O is typically 2-3 times higher when using urea compared to the use of ammonia [40]. The higher N_2O values for the urea cases suggest HNCO presence from the urea decomposition. Perry *et al.* [17] suggested the following reactions to describe HNCO process and N_2O formation as the following reaction:

$$HNCO \rightarrow NH^{-} + CO^{-} \quad (49)$$

$$NH^{-} + NO \rightarrow N_2O + H^{-} \quad (50)$$

First, HNCO is produced from decomposition from urea, then HNCO is decomposed as NH^{-} and CO^{-}, then the reaction between NH^{-} and NO leads to formation of N_2O. Glarborg *et al.* [47] proposed that radical NCO from HNCO was the key element for NO reduction as following reaction and also reaction (52) explains the large formation of N_2O when used HNCO from urea solution.

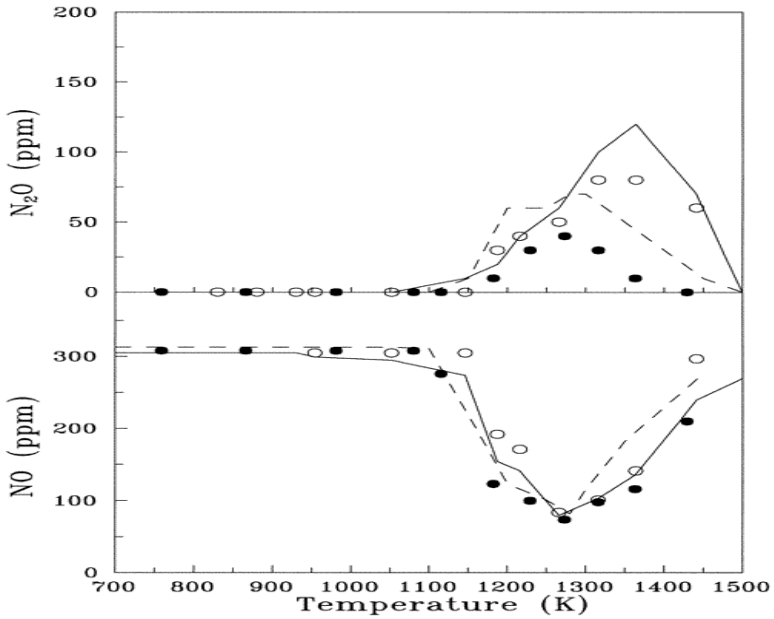

Figure 20. Experimental and calculated results of NO and N_2O concentrations versus temperature, when using either urea (o) or ammonia (●) as reducing agent. Solid lines denote calculations for urea and dashed lines for ammonia. (Inlet concentrations: 300 ppm NO, 150 ppm urea, 300 ppm NH_3, 4% O_2, 4% H_2O, N_2 to balance) [40].

$$HNCO + OH \rightarrow NCO + 6H_2O \quad (51)$$

$$NCO + NO \rightarrow N_2O + CO \quad (52)$$

$$NCO + NO \rightarrow N_2 + CO_2 \quad (53)$$

HNCO from urea decomposition react with radical OH, then radical NCO is made from reaction (51), after the radical NCO react with NO, NO converts to N_2O, N_2, CO, and CO_2.

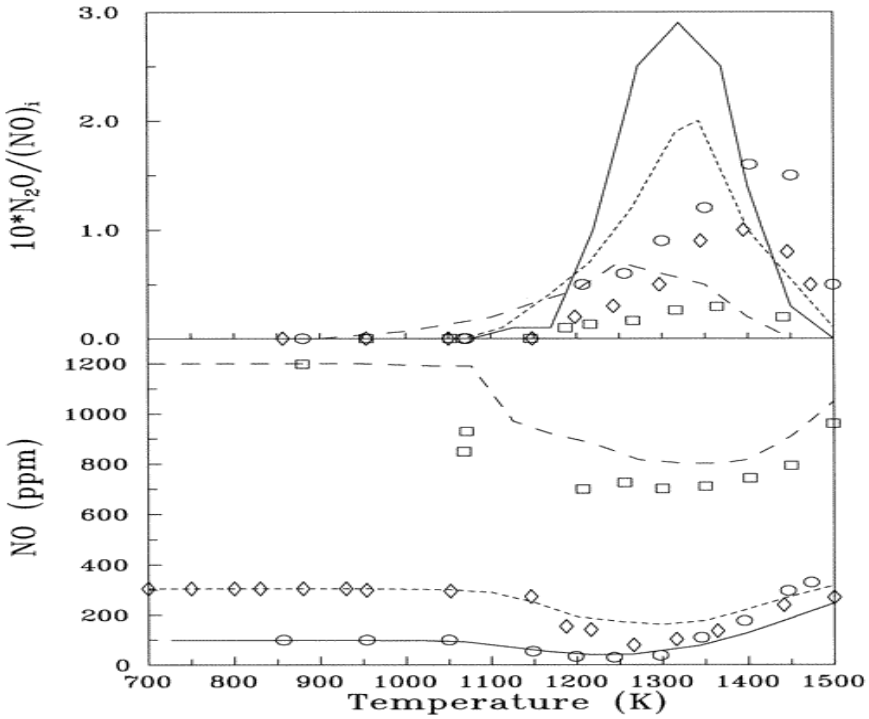

Figure 21. Experimental and calculated results of NO and N_2O concentrations versus temperature for different urea/NO ratios. The urea/NO ratio is varied changing the NO concentration (i.e., 100, 300, and 1200 ppm) for a given urea concentration (150 ppm). Symbols denote experimental results, and lines model calculations. (solid lines: 100 ppm NO, short-dashed lines: 300 ppm NO, long-dashed lines: 1200 ppm NO.) (Inlet concentrations: 4% O_2, 150 ppm urea, 4% H_2O, N_2 to balance) [40].

Figure 21 shows the experimental and calculated results of NO and N_2O concentration versus temperature for different β-ratio [40].

2.2.5 β - Ratio Effect

Rota *et al.* conducted the experiment for two values of β - ratio. The increasing β - ratio leads to the better NO reduction as shown in figure 22 [40]. In the urea solution of 40 wt%, NO reduction reached almost 100% at temperature above 1173 K, but in case of 10 wt%, NO reduction obtained only 40% at a higher reactor temperature of 1273 K in Itaya *et al.* experiment [21].

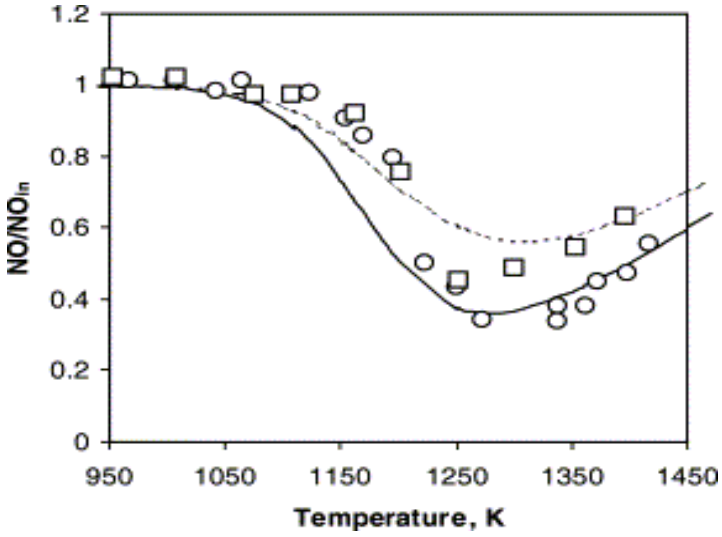

Figure 22. Influence of beta-ratio on NO reduction. Experimental results and model predictions. Symbols: experiments for (□) =1.2 and (o) =2.4. Curves: model predictions for (- -) =1.2 and (—) =2.4 [46].

3. OBJECTIVES

The overall goal of this research project is to investigate the selective non-catalytic reduction (SNCR) of NO_x by urea. The first part of this work is to determine the products of the urea thermal decomposition. The second part of this work is to obtain fundamental data on NO_x reducing using urea under varying residence time, oxygen concentration, β-ratio (the molar ratio between NH_3 and NO in the feed), and inlet gas compositions. The results for these experiments will be compared to NO_x removal using ammonia.

4. EXPERIMENTAL APPARATUS

The apparatus used to conduct the experiments consist of five distinct systems: (1) source of simulated exhaust gas, (2) mass flow controllers, (3) urea-water solution feed system, (4) the furnace and reactor assembly (reaction zone), and (5) the output gas mixture analysis system (Fourier transform infrared spectrometer). Each of these systems is described in the following section.

4.1 Overview of the Experimental Setup

Figure 23 shows the experimental apparatus. First, the mass flow controllers were calibrated individually with various gases (NO, CO, O_2, CO_2, N_2O, NO and N_2) and had accuracies ± 1.0% of full scale. The urea solution was placed in a 250 ml plastic flask and using a calibrated pressure control gauge was pressurized with N_2 gas. The urea solution flowed out due to the nitrogen gas pressure and then flowed through an injection pipette. The solution was vaporized by wrapped heating tape and then injected into the simulated exhaust gas stream in the pre-heat section before entering the reactor unit.

The mixture entered the reactor inside the furnace. The total flow rate of the gas was 1100 sccm (standard cubic centimeter per minute at O°C and 1 atm). To avoid too much H_2O in the gas mixture, the feeding rate of the urea solution was set to have 5% of H_2O in all gas mixtures. A quartz tube (ID=10 mm, length=1.04 m) was placed in a three-zone reactor that has an electronic control unit to furnish accurate temperature

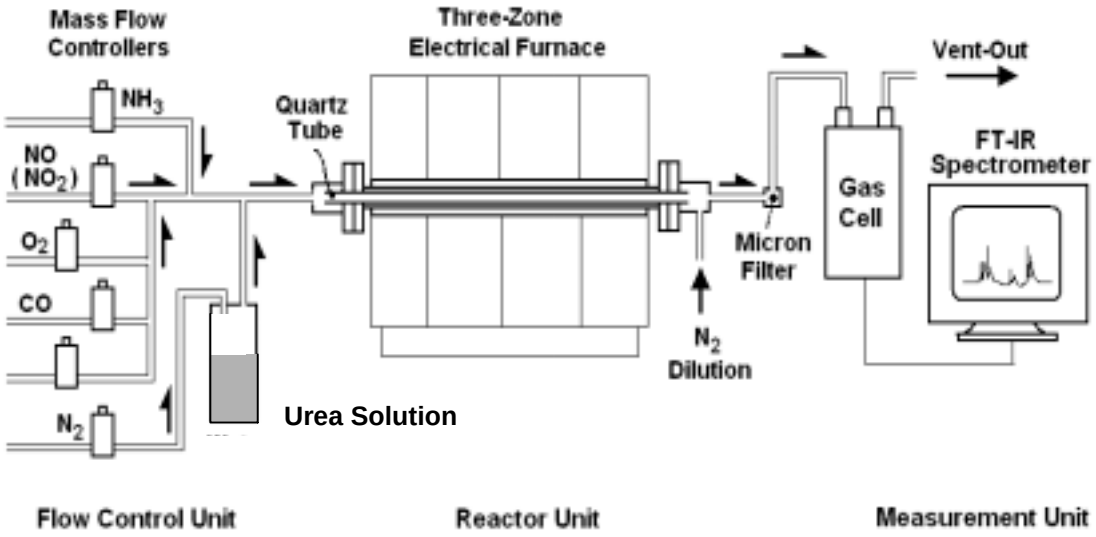

Figure 23. Schematic setup of the experimental apparatus used to perform NO removal experiments.

control. By operating different heating zones (i.e., heating lengths), and using different inside diameters for the quartz tube, the residence time could be varied. A condenser for H_2O was placed right after the end of reactor to minimize the H_2O in the gas cell of the FTIR (Fourier transform infrared) spectrometer. The output gas from the condense passed through a 0.7 micron-filter and then was diluted by 5000 sccm of nitrogen gas. The output gases from the reactor, including the dilution gas, flowed into the gas cell of the FTIR spectrometer. Necessary calibrations were completed to quantify the FTIR spectrum for each species, prior to the main experiments. Then, the gases were vented out to the atmosphere.

4.2 Source of Simulated Exhaust Gas

To avoid the inherent complexities of dealing with the exhaust from an actual combustion source, such as particulate emissions and transient irregularities in NO con-

centrations, a source of simulated exhaust gas was used. All the gases and gas mixtures were stored in standard gas cylinders. The concentration of each tank is listed in table 1.

Table 1. Cylinder concentrations used for experiments

Species	Mixture	Purity
N_2	100 % N_2	99.99%
O_2	49.7% O2, 50.3% N_2	± 1%
CO_2	4.11% CO_2, 95.89% N_2	± 1%
N_2O	1% N_2O, 99% N_2	± 1%
NO_2	0.994% NO_2, 99.006% N_2	± 1%
NO	1.99% NO, 98.01% NO	± 1%
NH_3	0.5207% NH_3, 99.4793% NH_3	± 1%
CO	1.79% CO, 98.21% N_2	± 1%

4.3 Mass Flow Controller

As a means of controlling the flow of each constituent into the system, a series of seven mass flow controllers was used (the PFD 401 series by Precision Flow Devices Inc., and MKS type 1179A by MKS Instruments). Note that mass flow controllers for different maximum flow rates were used in the experimental setup. Table 2 is a list of all controllers, and lists their flow capacity and other gases. Figure 24 shows the front panel controls of MKS type 247D four-channel readout.

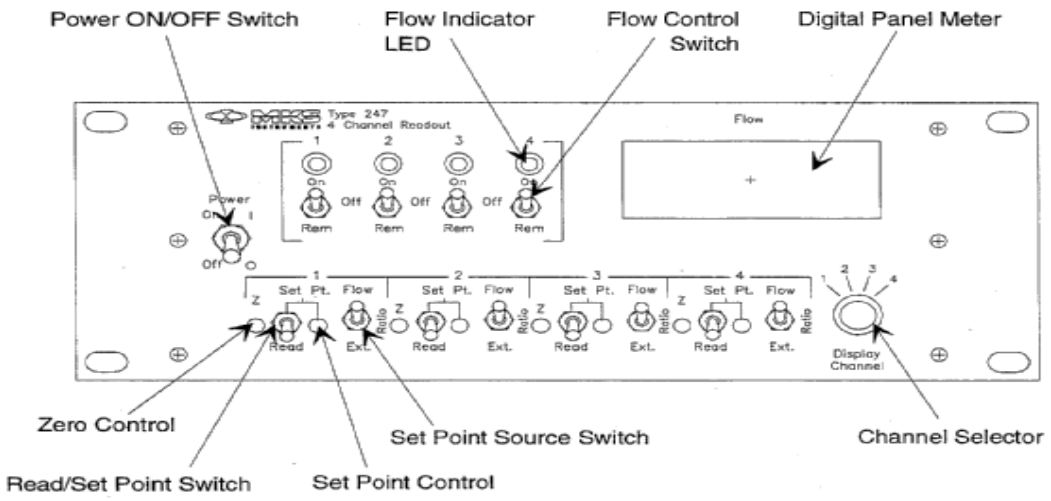

Figure 24. Front panel controls of MKS type 247D four-channel readout.

4.3.1 Calibration Process

The gas that flows through the system is collected in a glass flask. This flask is completely filled with water, which is displaced by the gas over time [48].

Table 2. Mass flow controllers in the experimental setup

MFC-Number	Manufacturer	Flow capacity (sccm)	Alternate gas
1-1	MKS Instruments	50	CO/N_2
1-2	MKS Instruments	100	CO_2/N_2
1-3	MKS Instruments	200	NO/N_2
1-4	MKS Instruments	5000	N_2
2-1	Precision Flow Devices	300	NH_3/N_2
2-2	Precision Flow Devices	300	O_2/N_2
2-4	Precision Flow Devices	1000	N_2

The time and volume displaced are measured through following equation [49]:

$$\frac{\partial V}{\partial t} \equiv \frac{M_1 - M_2}{\rho_{H2O} * t} \tag{54}$$

To include the pressure difference from changing water level in the flask during the process of displacement, a correction term for the volume is needed [48]:

$$\frac{\partial V_{adjusted}}{\partial t} = \left(\frac{P_{atm} - \rho_{H2O} gh}{P_{atm}} \right) \left(\frac{M_1 - M_2}{\rho_{H2O} t} \right) \tag{55}$$

The procedure is described in more detail in Appendix A1.

4.4 Urea-Water Solution Feed System

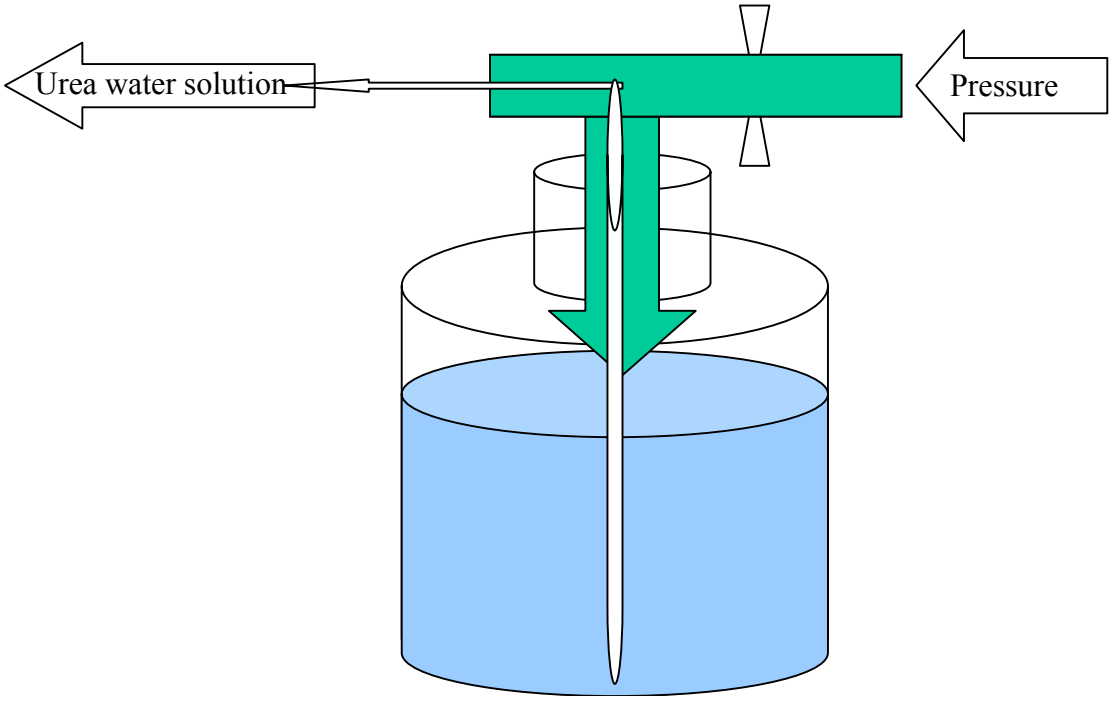

Figure 25. Feeding solution setup using pressure.

The urea solution was placed in a 250 ml plastic flask and using a calibrated pressure control gauge was pressurized with N_2 gas as shown in figure 25. The urea solution flowed out due to the nitrogen gas pressure and then flowed through an injection pipette. The solution was vaporized by wrapped heating tape and then injected into the simulated exhaust gas stream in the pre-heat section before entering the reactor unit. The calibration procedure is described in more detail in Appendix A2.

4.5 The Furnace and Reactor Assembly (Reaction Zone)

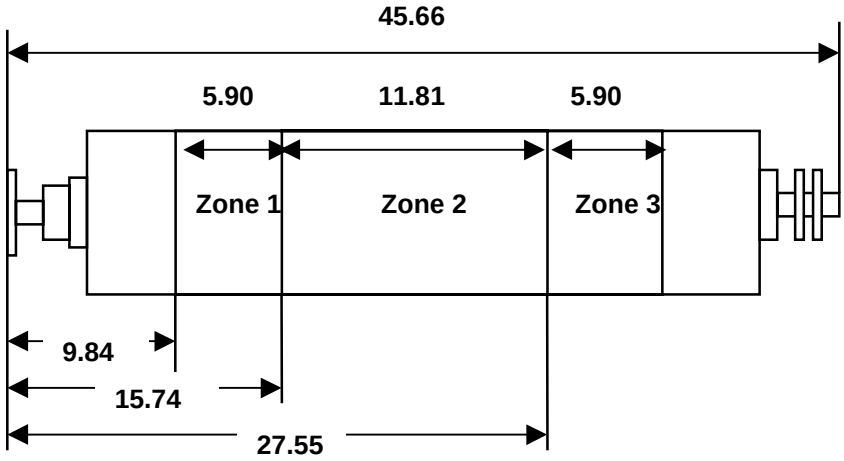

Figure 26. Schematic of the furnace setup. All lengths in inches [48].

Heating the flowing gases to the temperature needed in the flow reactor was performed by a three-zone tube furnace (Lindberg model number 54259), which has an electronic control unit (Lindberg model number 58475). The initial and final zones of the furnace are 15.2 cm in length while the center zone is 30.5 cm in length as shown in figure 26. The energy produced by the heating zones is transferred to an Inconel 600

pipe in the entire length of the furnace. The quartz reactor, which prevents catalytic reactions with the steel surface, is centrally located within this pipe. The reactor is 25.4 mm internal diameter tube of Inconel 600 which is 1.06 m long. The tube is threaded at both ends and two 6.35 mm bolt flanges of 304 stainless steel are screwed on the ends. The reactor end-flange assembly on the upstream side is connected to the stainless steel heated chamber which mixes urea-water solution with simulated gases. The reactor end-flange assembly on the downstream side is connected to the condenser which collected the H_2O after the reactor. The quartz tube is located in the center of the reactor with the support of graphite gaskets made from Grafoil^{TM} sheets. These gaskets also seal the flanges on each end of the reactor. The furnace temperature distribution is described in more detail in Appendix A3.

4.6 The Output Gas Mixture Analysis System (Fourier Transform Infrared Spectrometer).

In order to determine the concentration of the various species exiting the reactor, a Fourier transform infrared (FTIR) spectrometer was used (Biorad FTS-60A). After dilution the total simulated exhaust stream of 6100 sccm passed through a permanently aligned long path cell. A liquid nitrogen cooled MCT (Mercury-Cadmium-Tellurium) detector which works in the range of 4000 to 400 cm^{-1} was used.

To operate the FTIR properly, the FTS 60A uses cold. Besides, since the beam splitter is made out of KBr crystal, which is sensitive to ambient air conditions, a purge air generator is used to ensure proper air conditions.

The calibration procedure and data for the different species used in the experiments is described in more detail in Appendix A4.

5. EXPERIMENTAL PROCEDURE

Before describing the actual experiments, the standard conditions of the experiments are provided. The total flow rate of the gas in the reactor was 1100 sccm (standard cubic centimeter per minute at 0°C and 1 atm), which is regulated by the mass flow controllers. This standard condition is consistent with former studies by Gentemann [48] and Srivasta [50].

5.1 Procedure for Conducting Experiments

First, liquid nitrogen is added to the MCT detector. The mass flow controllers should be turned on at least an hour before the experiment began. The whole system was tested for leakage everyday before the experiment. MFC # 1-4 and # 2-4 of the nitrogen part were switched on first to take background scans with FTIR.

The setting of each mass flow controller was determined using an Excel spreadsheet, which included the calibration data for each specific mass flow controller. The mass flow controller setting was double-checked to ensure the flow of the correct quantities of each mixture component. The furnace was turned on a half hour before testing to ensure thermal stability.

After calculating the weight of urea to be used as ppm unit for one experiment, the calculated amount of urea was mixed with H_2O in a flask. Heating tape for the urea solution was switched on. The desired nitrogen pressure from the calibrations was determined to feed urea-water solution at the proper rate.

The temperature of the furnace was increased every 100 K from 273 K to 773 K. After all heating zone reached the desired temperature, every 50 K from 800 to 1350 K was measured the output species using FTIR.

5.2 Data Collection Procedure

To process the data of a FTIR scan, Biorad WinIR-pro version 2.96 software was used. The scan of the gas mixture in the FTIR was taken after steady-state was established, which could be monitored by comparing scans of the FTIR repeatedly. That is to say, the final value was reached once the change of the measured concentration was within ± 0.5 ppm, which was assumed as a steady state. Typically, the final values were obtained in about 20 minutes. The furnace needed a certain time to reach the set temperature. The measured temperature was for the outside Inconel 600 steel tube.

An FTIR measurement was the average of 16 scans, which were reported as one data value. All data were obtained from low to higher temperature in the reactor. The concentration data was then plotted as a function of temperature.

5.3 Residence Time

In the reactor unit, a quartz-tube reactor designed for obtaining plug (or laminar) flow, is placed in a three-zone electrically heated furnace providing a uniformly heated section of the reactor. The number of zones activated for the furnace controls the length of the uniformly heated section on the quartz-tube reactor. Figure 27 shows the normalized temperature profiles (i.e., $T(x)/T_{set}$, where T_{set}= reactor set temperature) on the

quartz tube for a 1.0-cm inside diameter with 1100 sccm (standard cubic centimeter per minute) nitrogen flow for two-reactor set temperatures (i.e., T_{set} = 1100 and 1300 K) when measured by a thermocouple. The uniformly heated length provided on the quartz tube reactor is 30 cm when 2 zones in the furnace are heated, while the length increases to 51 cm when all 3 zones are activated, securing maximum uncertainties of ± 1.3 %, but within ± 15 K over the uniformly heated length. Thus, by varying inside diameters for the quartz tube reactor, different residence time (or reaction time) will be provided under a constant mass flow [51].

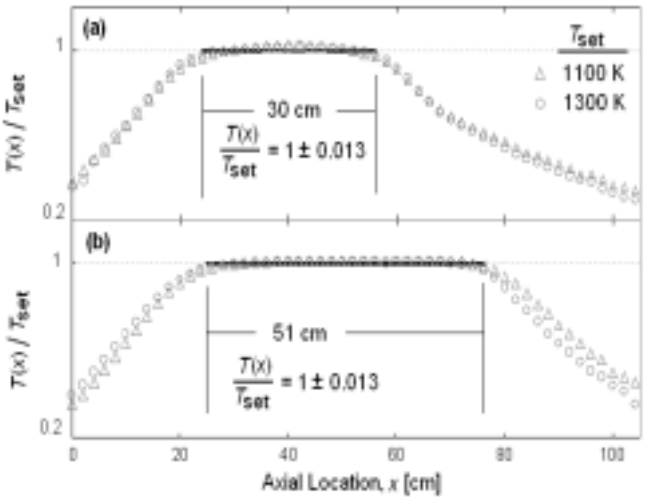

Figure 27. Normalized temperature profiles for two reactor set temperatures: (a) 2-zone heating, and (b) 3-zone heating [51].

$$t_{res.time} = \frac{V_{heating}}{Q} * 60 * (\frac{T_{cold}}{T_{reactor}}) \quad (56)$$

$$V_{heating} = \frac{D^2 \pi}{4} * L_{heating} \quad (57)$$

where D is the quartz tube inside diameter, $L_{heating}$ is the heating length, $T_{reactor}$ is the temperature of the reactor, and T_{cold} is the temperature of the ambient temperature (298 K). All experiments, except one case using ammonia to check oxygen percentage effect, used a 10 mm diameter quartz tube. Table 3 shows an example of residence time calculation corresponding to the number of activated heating zones. The value for residence time calculation can be found in appendix 3

Table 3. Residene time calculation example using equation (56) and (57)

Heating zone	Q (sccm)	T_{cold} (K.)	L (cm)	D (cm)	Area (cm^2)	Volume (cm^3)	Residence time (sec.)
1, 2, 3	1100	298	54	1.0	0.79	42.41	689/ $T_{reactor}$
2, 3	1100	298	36	1.0	0.79	28.27	460/ $T_{reactor}$
3	1100	298	8	1.0	0.79	6.28	102/$T_{reactor}$

6. EXPERIMENTAL RESULTS AND INTERPRETATION

The results obtained for urea decomposition, and for the NO removal using urea and ammonia will be reviewed and discussed. As a preface to this section, lines in all graphs used to connect data points are only for the purpose of helping the reader differentiate one set of data from another.

6.1 Decomposition Study of Urea-Water Solution

The NO_xOUT process using urea for NO reduction has been widely used, but the actual reaction of NO removal does not occur directly between NO and urea. The reason is that urea decomposes at elevated temperature. So, the decomposition process is essential to understand NO removal using urea.

6.1.1 Urea Powder Decomposition Experiment

The first decomposition experiment used urea powder. Dry urea powder (3.0 g) was placed in the entrance of the reactor. The reactor temperature was increased as only nitrogen gas flowed through the reactor. Figure 28 shows the concentrations of NH_3, CO_2, and the absorbance of HNCO as function of temperature. Due to a lack of an HNCO calibration gas, HNCO can only be reported as absorbance. HNCO and NH_3 were produced between 500 K and 700 K. After 700 K, the amounts of NH_3 and CO_2 increased as HNCO decreased which is consistent with reaction (43).

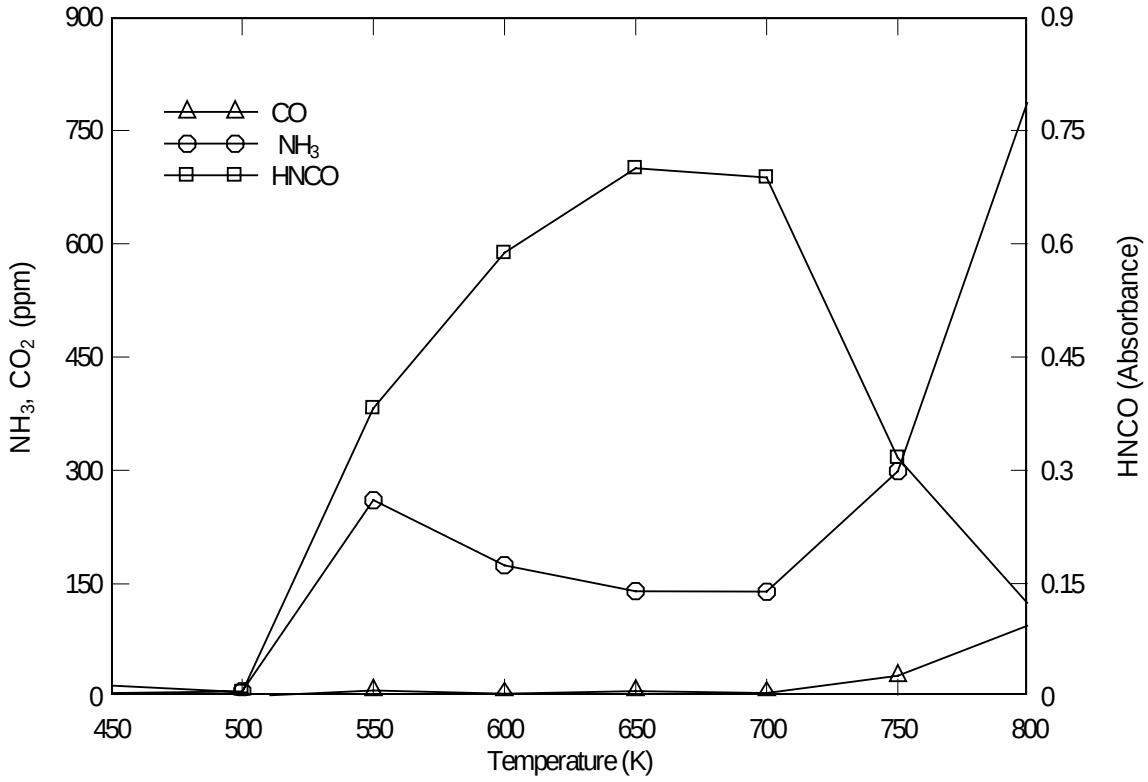

Figure 28. Urea powder decomposition experiment. 3.0 g was placed into the entrance of the reactor (Residence time 672/T(K)).

$$HNCO + H_2O \rightarrow CO_2 + NH_3 \qquad (43)$$

The major species noted in the output were NH_3, CO_2, H_2O and HNCO, because of the strong H_2O band in the FTIR spectra and interference with NH_3, other possible products such as biuret, ammelide, and ammeline could not be identified using the FTIR.

6.1.2 Urea-Water Solution Decomposition Experiment

Table 4. Injection condition of urea-water solution

Parameter	Value (Source)
Urea	Extra pure (EM Industries)
Distilled water	OmniSolv with purge gas in bottle
Temperature range	500 K to 800 K
Oxygen level	0%, 1%

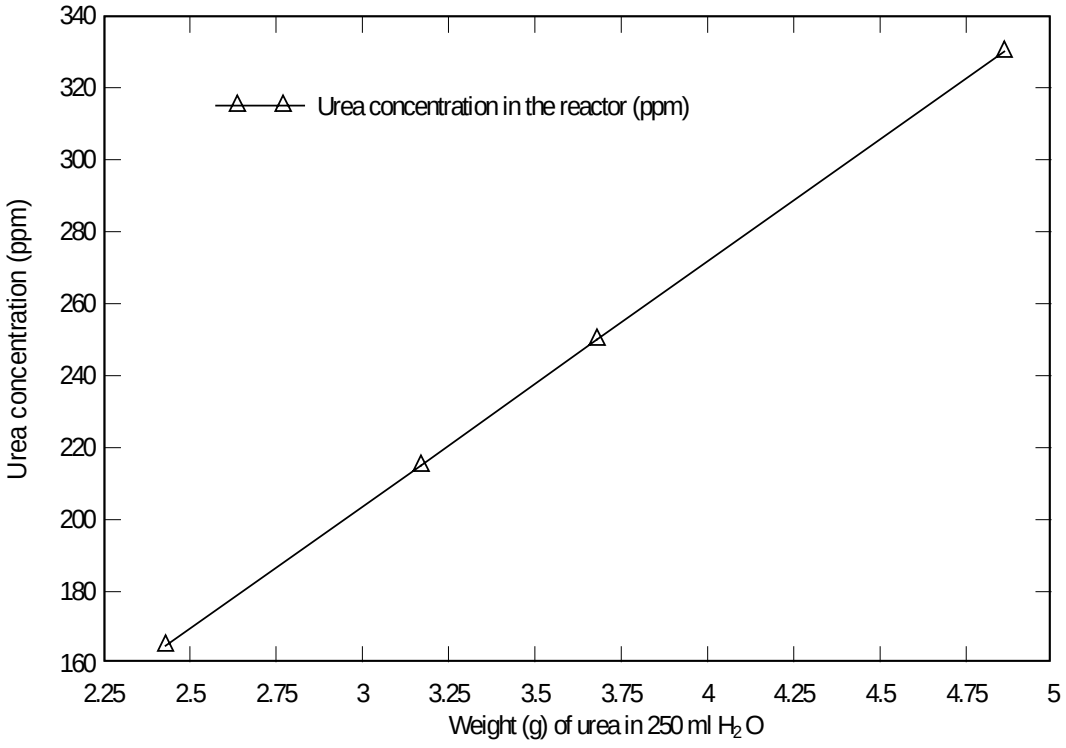

Figure 29. Concentration of urea (ppm) in the reactor as a function of the weight (g) of urea per 250 ml in a flask at a fixed 0.05 ml/minute of urea-water solution feeding rate.

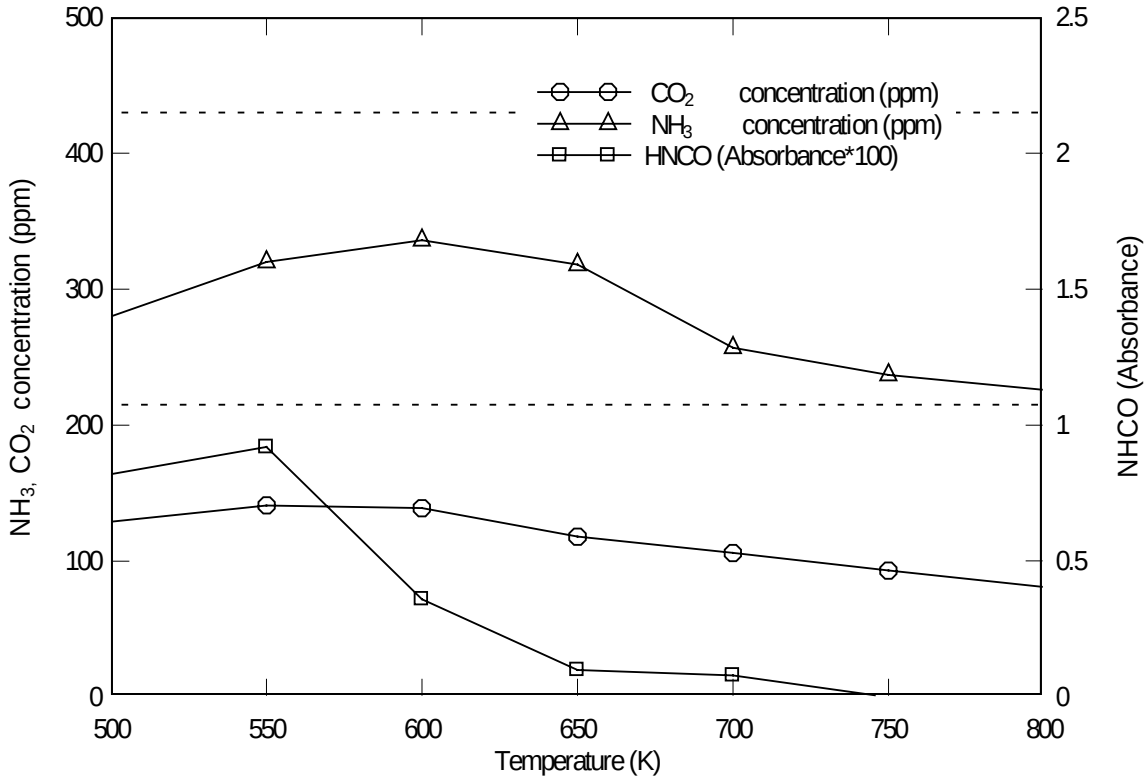

Figure 30. NH_3 and CO_2 production from 215 ppm urea. Residence time 442/T(K).

Since urea-water solution used for NO reduction, the decomposition of urea-water solution must be essential for NO removal reaction. Table 4 shows the injection condition for experimental cases.

Urea concentration in the reactor, corresponding to the weight of urea in 250 ml distilled water can be seen in figure 29. For example, the weight 3.17g of urea resulted in 215 ppm, which is 1.27 wt % (urea solution by mass). This example case was chosen for the urea-water solution decomposition experiment. Since the weight of urea is so small to compare the amount of water, the produced amount of NH_3 and CO_2. To reduce the amount of error, this experiment was repeated three times. As seen in figure 30, the

maximum production of NH_3 and CO_2 from decomposition of urea-water solution occurred around 550-600 K. After 600 K, the derived amount of NH_3 and CO_2 slightly decreased at higher temperature. But the amounts of NH_3 and CO_2 were less than amounts expected from the reaction (48), which suggests the production of other species such as biuret, ammelide, and ammeline. As with the urea powder decomposition experiment, because of the strong H_2O band in the FTIR spectra and interference with NH_3, other possible species like biuret, ammelide, ammeline could not be identified using the FTIR.

$$NH_2CONH_2+H2O \rightarrow 2NH_3+CO_2 \quad (48)$$

6.2 Nitric Oxide Removal Using Urea as the Reducing Agent

6.2.1 Nitric Oxide Removal Using Urea with 1% Oxygen

Table 5 shows the different cases examined in this study. The concentration of nitric oxide was set at 330 ppm. The concentration of urea was varied 165, 250 and 330 ppm to represent as β - ratio 1, 1.5 and 2. The concentration of oxygen was 1% for all cases.

Table 5. Experimental test cases for NO removal experiments using urea

	NO (ppm)	Urea (ppm)	β - ratio	O_2 (%)	Residence time (sec.)
1	330	165	1	1 %	102 / T(K)
2					442 / T(K)
3					672 / T(K)
4				5 %	102 / T(K)
5					442 / T(K)
6					672 / T(K)
7		250	1.5	1 %	102 / T(K)
8					442 / T(K)
9					672 / T(K)
10				5 %	102 / T(K)
11					442 / T(K)
12					672 / T(K)
13		330	2	1 %	102 / T(K)
14					442 / T(K)
15					672 / T(K)
16				5 %	102 / T(K)
17					442 / T(K)
18					672 / T(K)

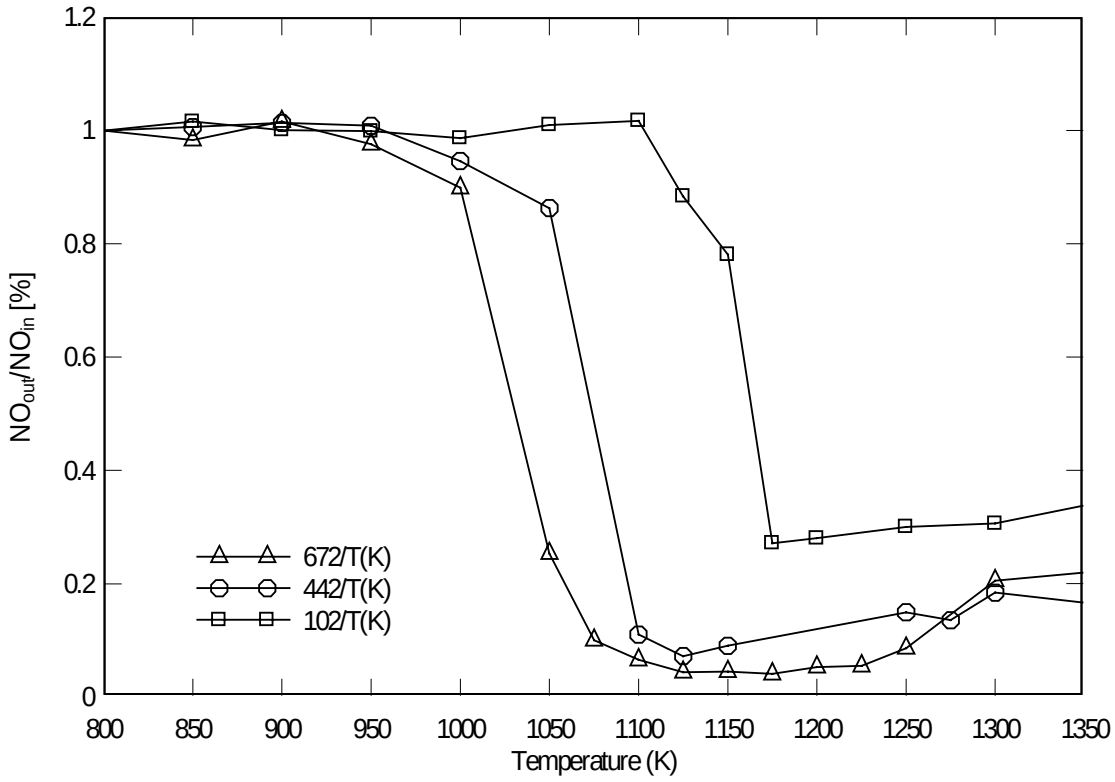

Figure 31. Nitric oxide removal as a function of temperature for changing residence time. Inital NO = 330 ppm, urea = 330 ppm, O_2 = 1%.

Figure 31 shows NO reduction as a percentage of the original NO as a function of reactor temperature for various residence times, for a β - ratio of 2.0 (NO = 330 ppm, urea = 330ppm), and 1% O_2. Up to a temperature of 950 K, NO reduction was not noted. After a temperature of about 1000 K, as temperature is increased, the NO_{out}/NO_{in} ratio decreased gradually, which means NO reduction increases, except 102/T(K) residence time case, whose NO reduction started at 1100 K. This gradual trend continues as the temperature increases to about 1100 K (672/T(K), 442/T(K)) or 1200 K(102/T(K)).

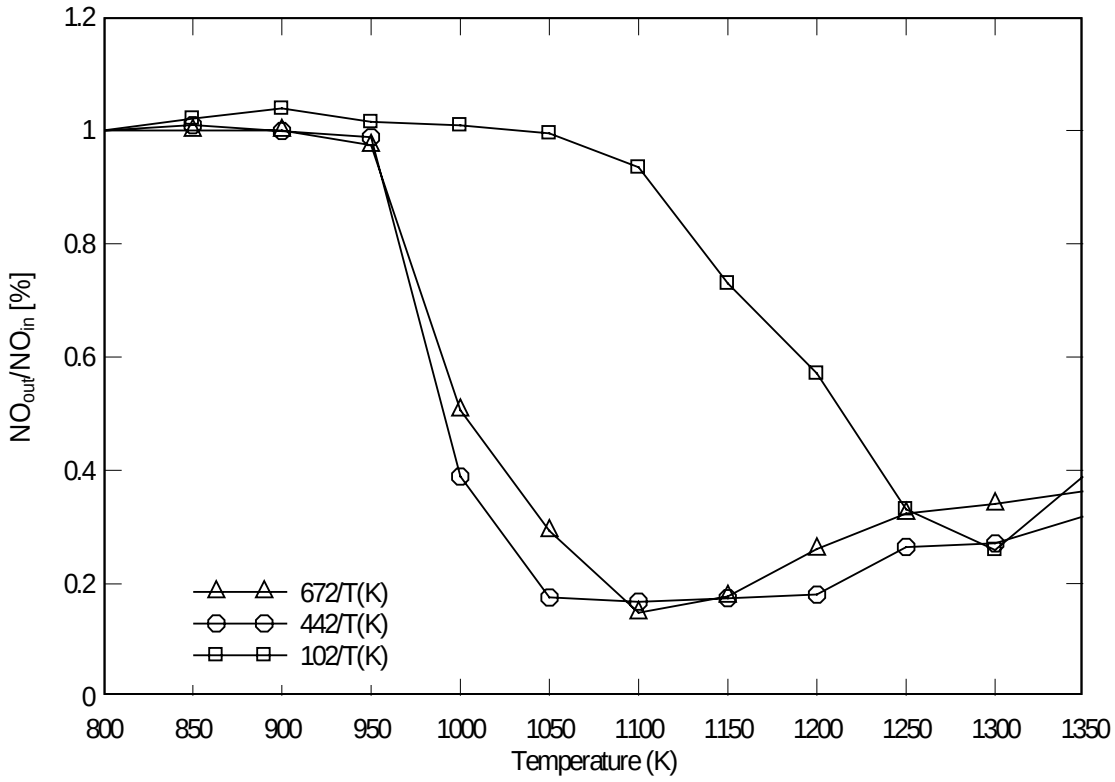

Figure 32. Nitric oxide removal as a function of temperature for changing residence time. Inital NO = 330 ppm, urea = 250 ppm, O_2 = 1%.

Figure 32 shows NO reduction as a percentage of the original NO as a function of reactor temperature for various residence times, for a β - ratio of 1.5 (NO = 330 ppm, urea = 250 ppm), and 1% O_2. Below a temperature 950 K, little NO removal was observed. For all cases, a maximum NO removal was observed for a certain temperature before the NO increased again. This trend was seen at a temperature of 1200 K (672/T(K)), 1100 K (442/T(K)), and 1300 K (102/T(K)). Longer residence time lead to higher reduction of NO and wider NO reduction "window" as well. A maximum NO reduction of around 85% occurs at 1100 K for the case with a residence time of 672/T(K).

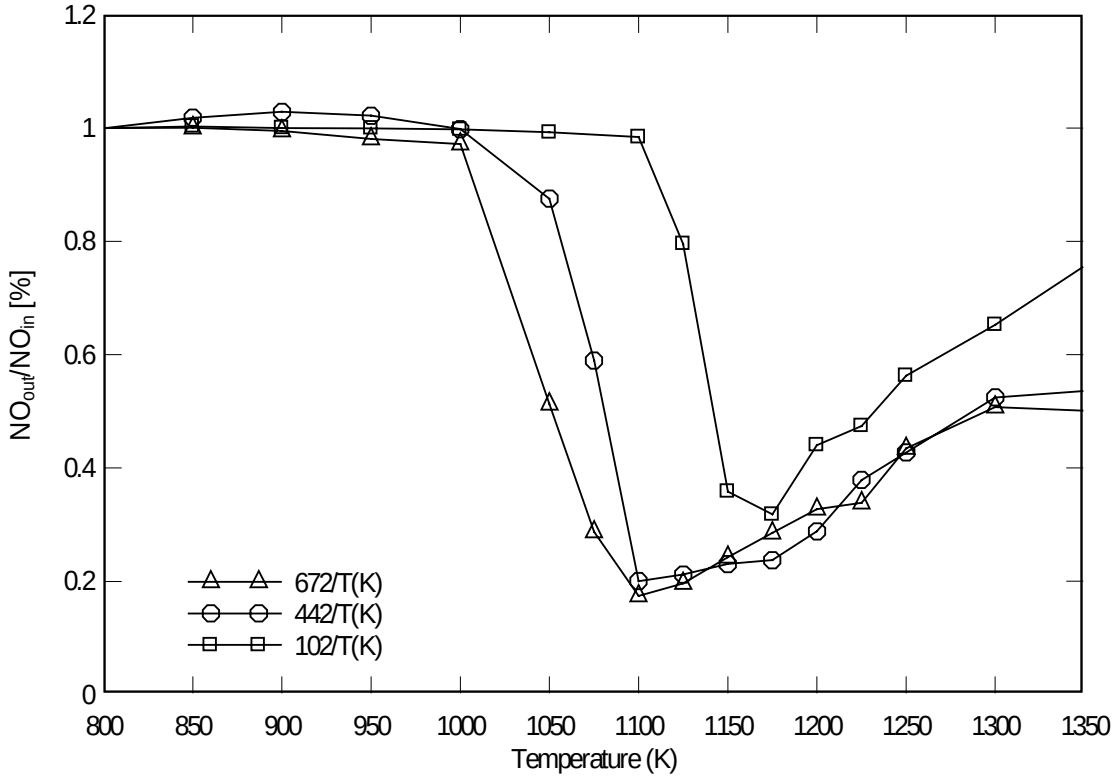

Figure 33. Nitric oxide removal as a function of temperature for changing residence time. Inital NO = 330 ppm, urea = 165 ppm, O_2 = 1%.

Figure 33 shows NO reduction as a percentage of the original NO as a function of reactor temperature for various residence times, for a β - ratio of 1.0 (NO = 330 ppm, urea = 165 ppm), and 1% O_2. The maximum removal was about 84% at 1100 K for 672/T(K) and 442/T(K), and at 1175 K for 102/T(K). Above 1200 K, production of NO was observed clearly. This trend of increasing NO concentration at higher temperature was more significant than that observed for the higher β - ratio cases. In this case, longer residence time didn't contribute to widen range of NO reduction temperature "window".

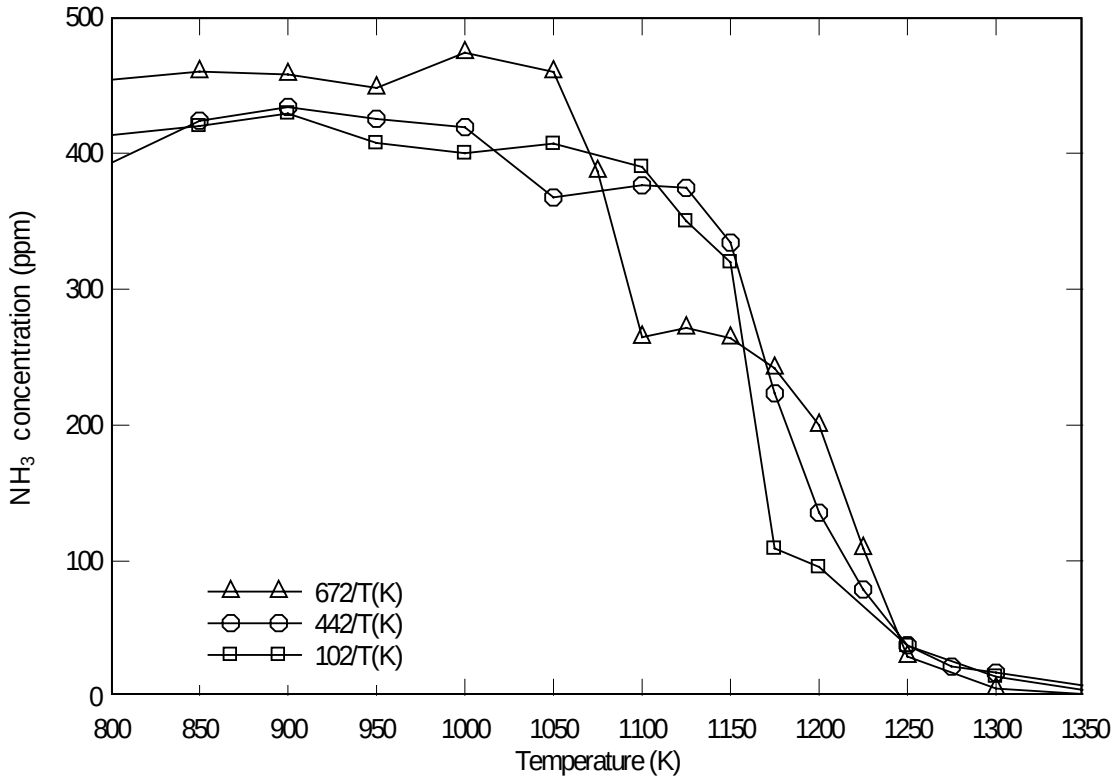

Figure 34. Ammonia concentration as a function of temperature for changing concentrations of residence time. Initial: NO = 330 ppm, urea = 330 ppm, O_2 = 1%.

Figure 34 shows the concentration of ammonia as a function of temperature. For the temperature range between 800 K and 1050 K, the ammonia concentration was about 430 ppm. For the temperature above 1050 K, the ammonia concentration decreased slightly. The trend of ammonia concentration used for NO reduction was a fluctuation in the range of occurring maximum NO reduction for the case of 672/T(K) residence time. Initial amount difference of ammonia from urea decomposition between 672/T(K) and 102/T(K) cases at 800 K was about 60 ppm.

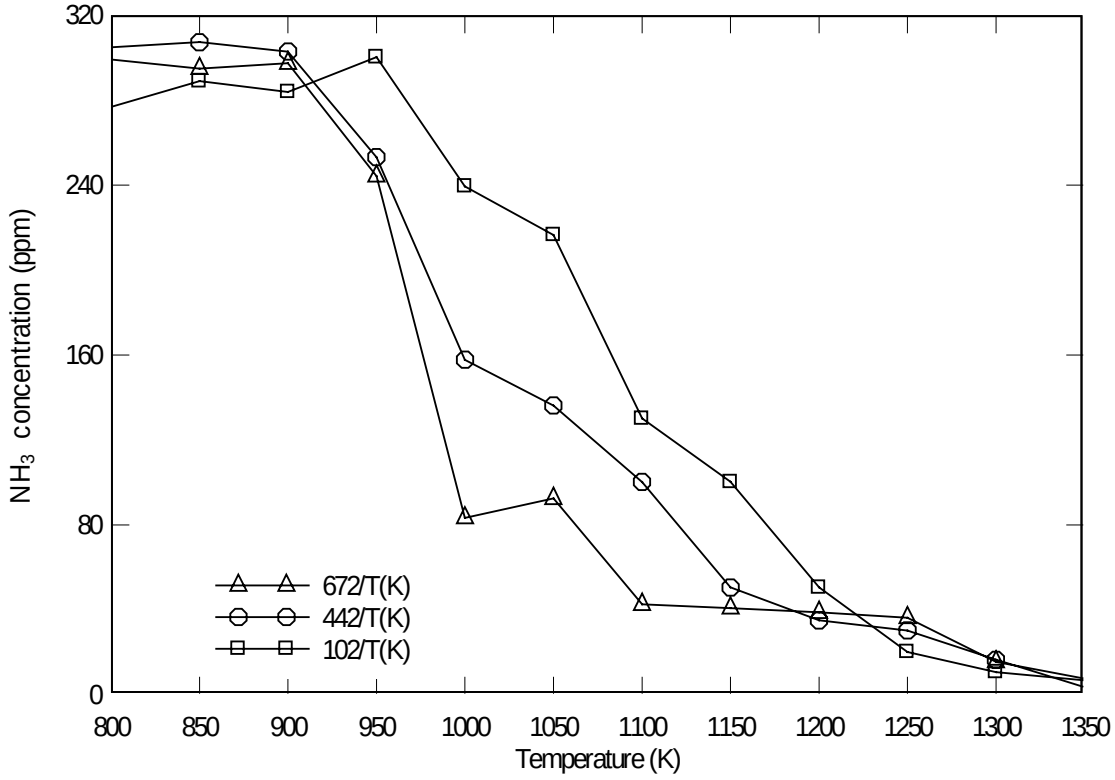

Figure 35. Ammonia concentration as a function of temperature for changing concentrations of residence time. Initial: NO = 330 ppm, urea = 250 ppm, O_2 = 1%.

Figure 35 shows the concentration of ammonia as a function of temperature. Initial amount difference of ammonia from urea decomposition between 672/T(K) and 102/T(K) cases at 800 K was about 30 ppm. For the temperature range between 800 and 950 K, ammonia concentration remained about 300 ppm. For temperatures above 950 K, the ammonia concentration decreased slightly. Depending on residence time, concentration of ammonia decreased as a function of temperature. For the 672/T(K) case, when the maximum NO reduction occurred, ammonia concentration diminished slowly.

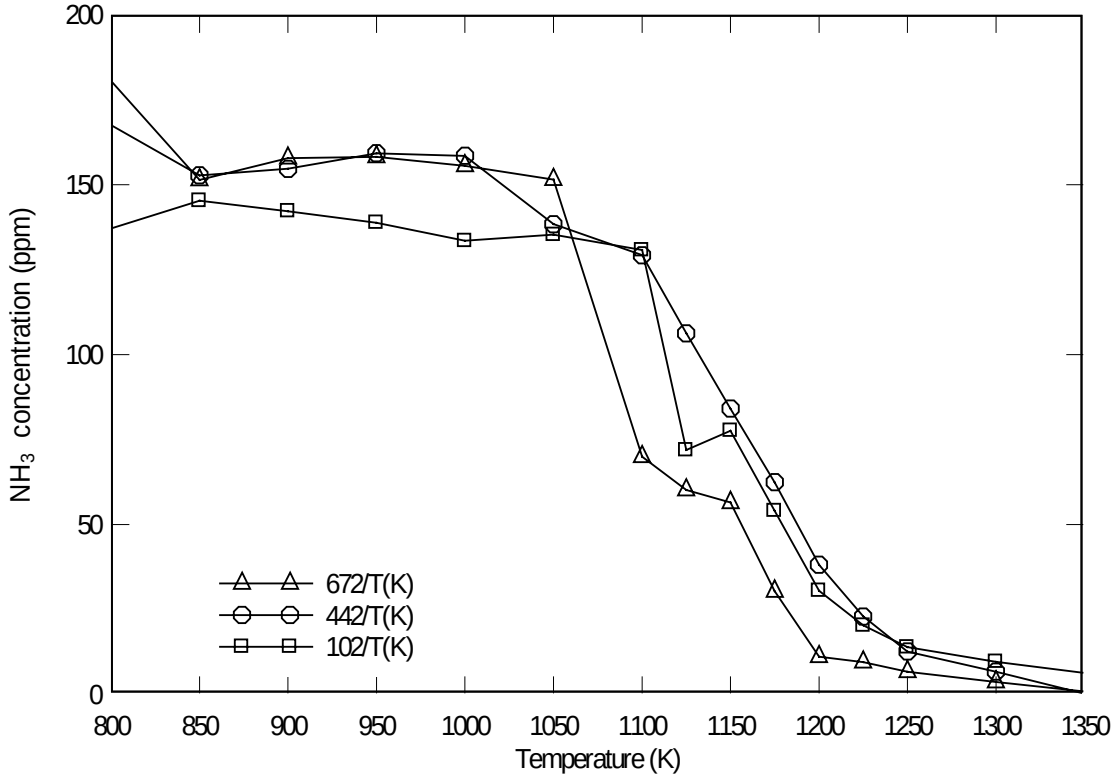

Figure 36. Ammonia concentration as a function of temperature for changing concentrations of residence time. Initial: NO = 330 ppm, urea = 165 ppm, O_2 = 1%.

Figure 36 shows the concentration of ammonia as a function of temperature. Initial amount difference of ammonia from urea decomposition between 672/T(K) and 102/T(K) cases at 800 K was about 40 ppm. For the temperature range between 800 and 1050 K, ammonia concentration remained around 150 ppm. For the temperature above 1100 K up to 1200 K, the ammonia concentration decreased rapidly. Between 1000 K and 1100 K, there was small fluctuation in the region when the maximum NO reduction occurred.

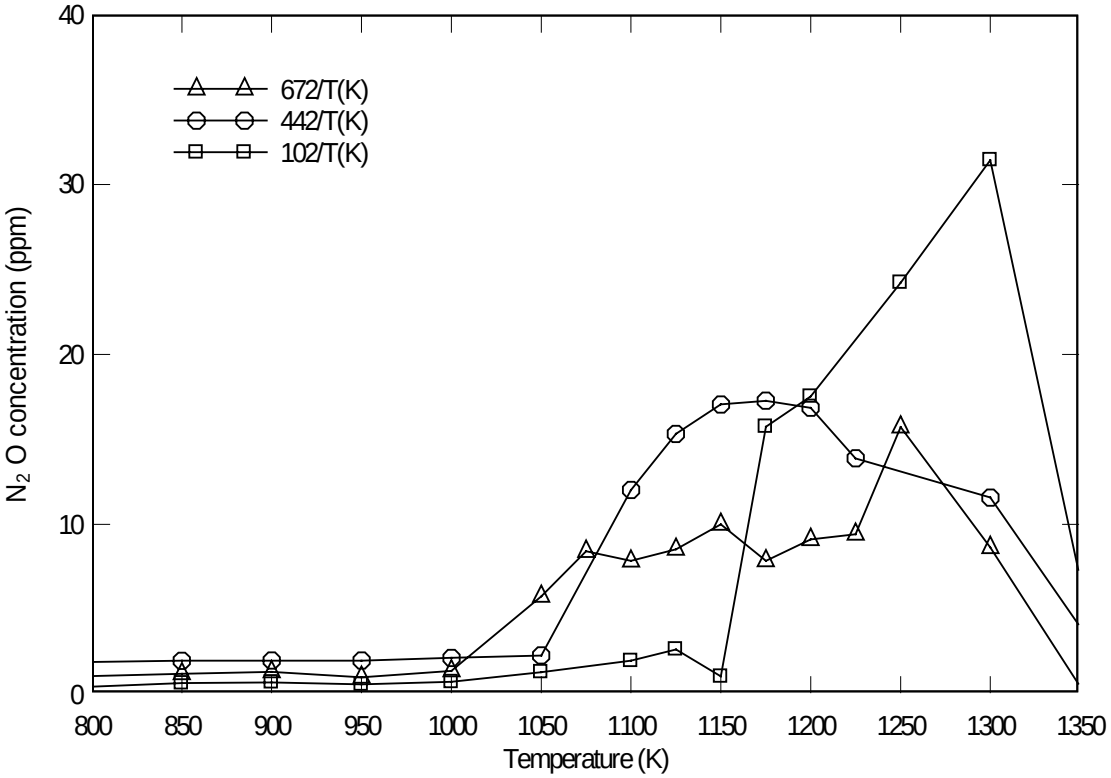

Figure 37. Nitrous oxide concentration as a function of temperature for changing concentrations of residence time. Initial: NO = 330 ppm, urea = 330 ppm , O_2 = 1%.

Figure 37 shows the concentration of nitrous oxide as a function of temperature for various residence time cases. Up to 1000 K, N_2O concentration was insignificant. For all cases, the cases with the shortest residence times resulted in the highest N_2O concentration. The maximum N_2O concentration for the 102/T(K) residence time case was at least twice the value for the other two cases. The place where the maximum N_2O concentration occurred was nearly matched with the place of the maximum NO reduction occurred.

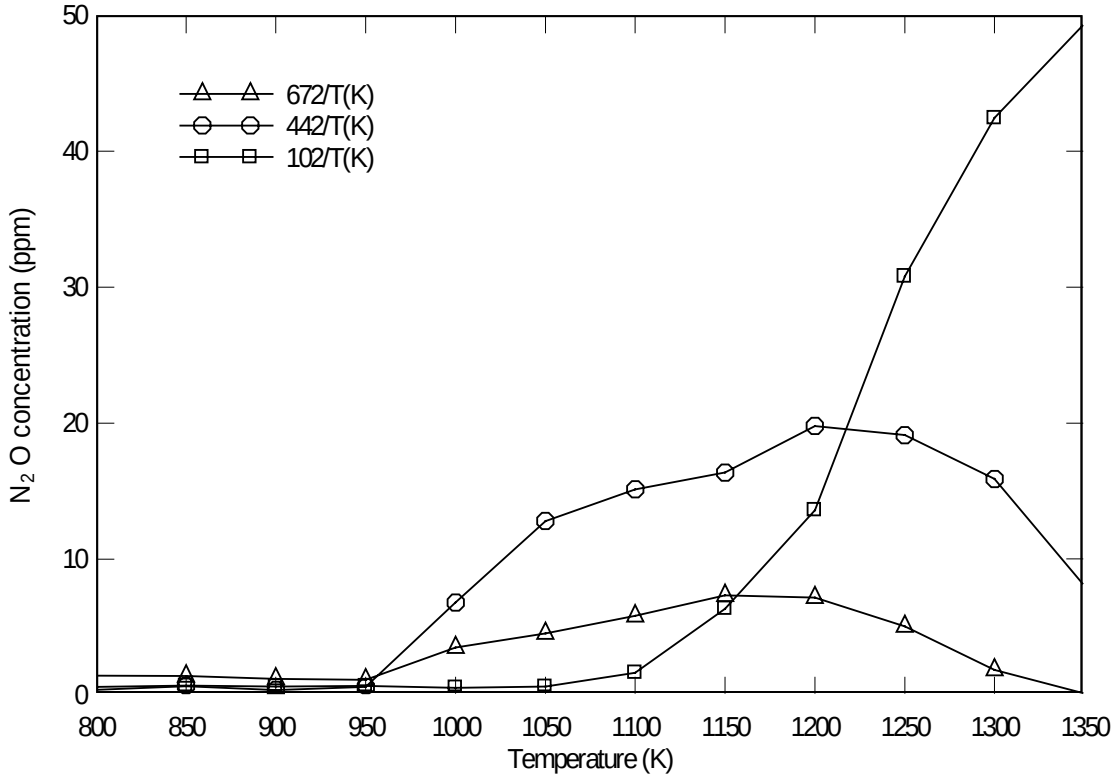

Figure 38. Nitrous oxide concentration as a function of temperature for changing concentrations of residence time. Initial: NO = 330 ppm, urea = 250 ppm, O_2 = 1%.

Figure 38 shows the concentration of nitrous oxide as a function of temperature for various residence time cases. Up to 950 K, N_2O concentration was insignificant. Again, the shortest residence time case led to the highest N_2O concentration. The maximum N_2O concentration for the 102/T(K) residence time case was at least three times the value from the other two cases. The place where the maximum N_2O concentration occurred was nearly matched with the place of the maximum NO reduction occurred for 672/T(K) and 442/T(K) cases.

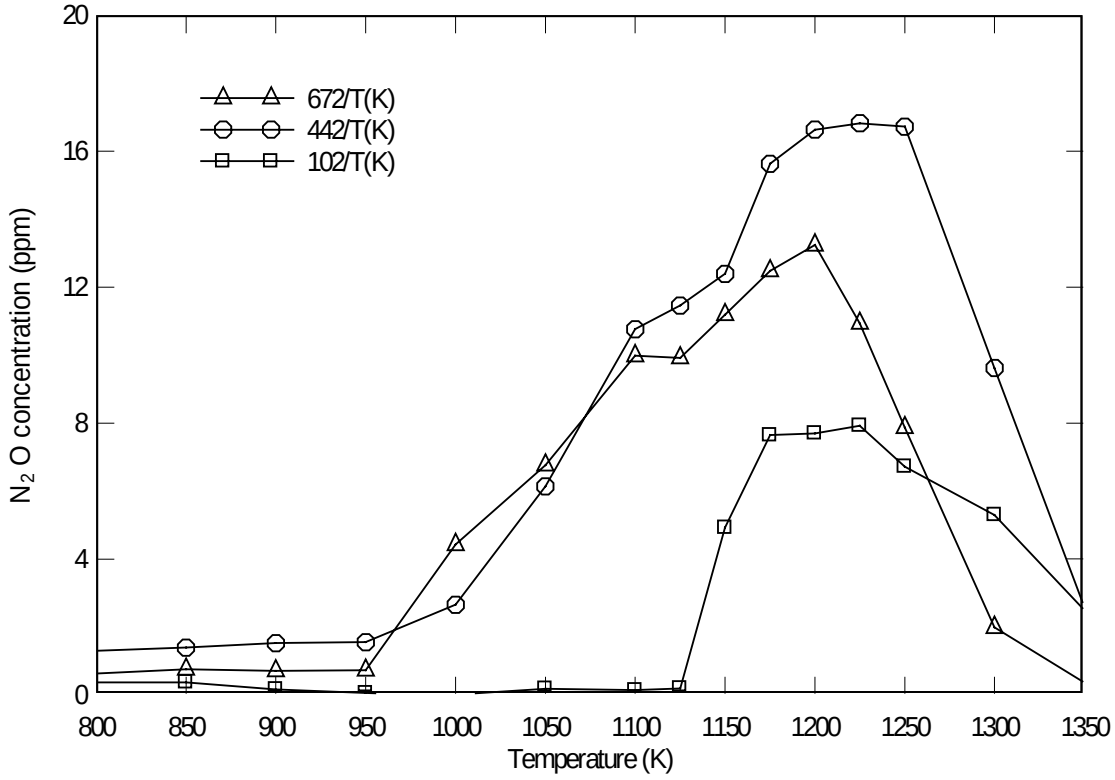

Figure 39. Nitrous oxide concentration as a function of temperature for changing concentrations of residence time. Initial: NO = 330 ppm, urea = 165 ppm, O_2 = 1%.

Figure 39 shows the concentration of nitrous oxide as a function of temperature for various residence time cases. Up to 950 K, N_2O concentration was insignificant. In this case, the shortest residence time case didn't lead to the highest nitrous oxide concentration, which could be explained because of inlet urea concentration 165 ppm. Small amount of inlet urea concentration could lead to small amount of HNCO production, which results from urea decomposition during the reaction process.

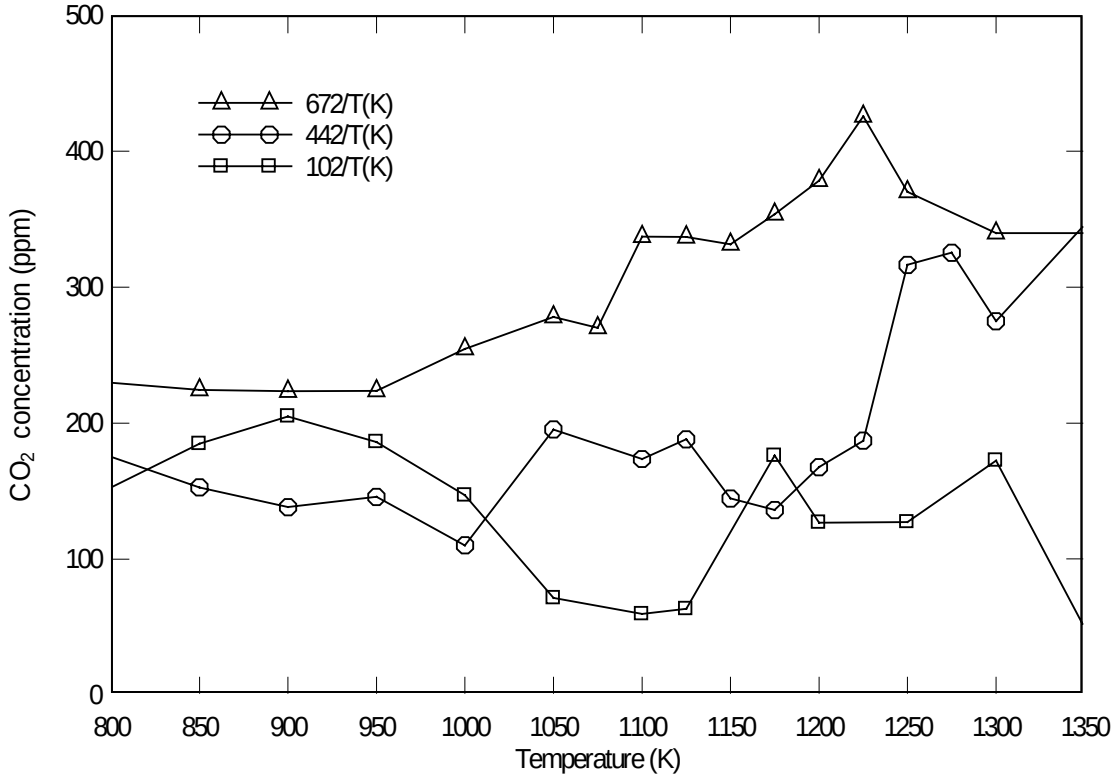

Figure 40. Carbon dioxide concentration as a function of temperature for changing concentrations of residence time. Initial: NO = 330 ppm, urea = 330 ppm, O_2 = 1%.

Figure 40 shows the concentration of carbon dioxide as a function of temperature for various residence time cases. From a constant level with a small fluctuation in concentration up to 950 K, the carbon dioxide concentration increased with temperature rise for two cases (672/T(K), 442/T(K)). While, in short residence time case, the carbon dioxide concentration nearly remained constant.

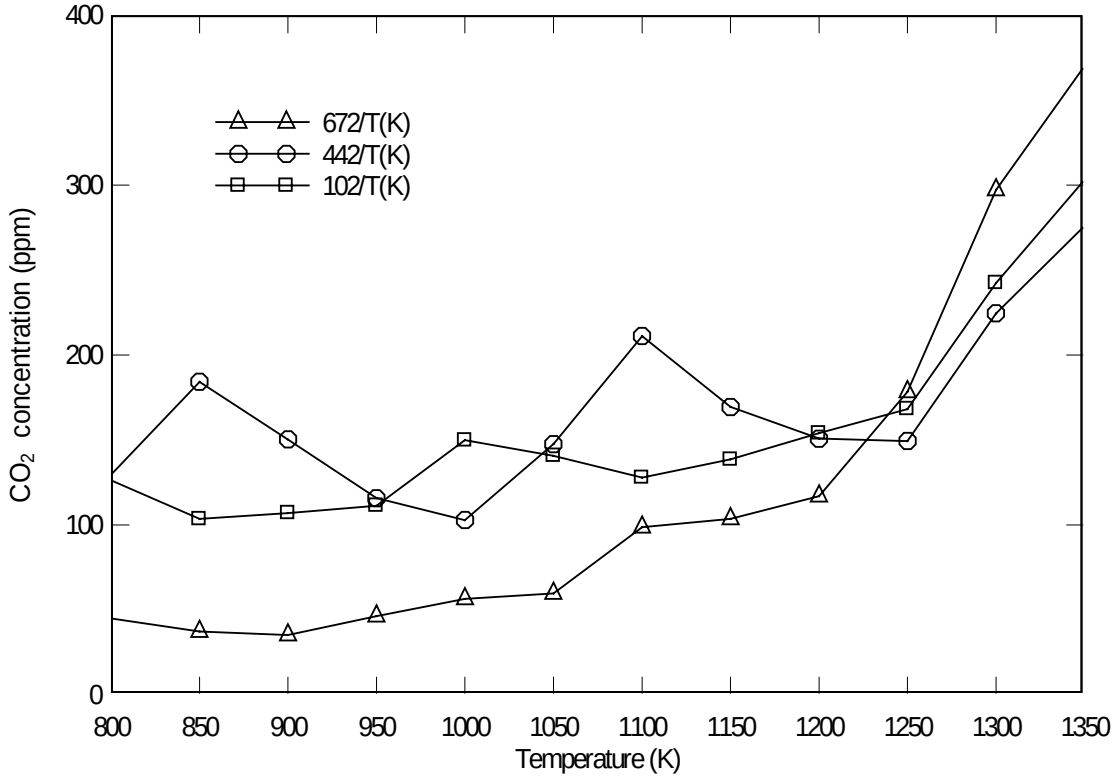

Figure 41. Carbon dioxide concentration as a function of temperature for changing concentrations of residence time. Initial: NO = 330 ppm, urea = 250 ppm, O_2 = 1%.

Figure 41 shows the concentration of carbon dioxide as a function of temperature for various residence time cases. From a constant level with a small fluctuation in concentration up to 1000 K, the carbon dioxide concentration increased with temperature rise for all cases. The concentration of carbon dioxide from urea decomposition theoretically could be made up to 250 ppm in this case, but after 1300 K, the concentration of carbon dioxide increased rapidly.

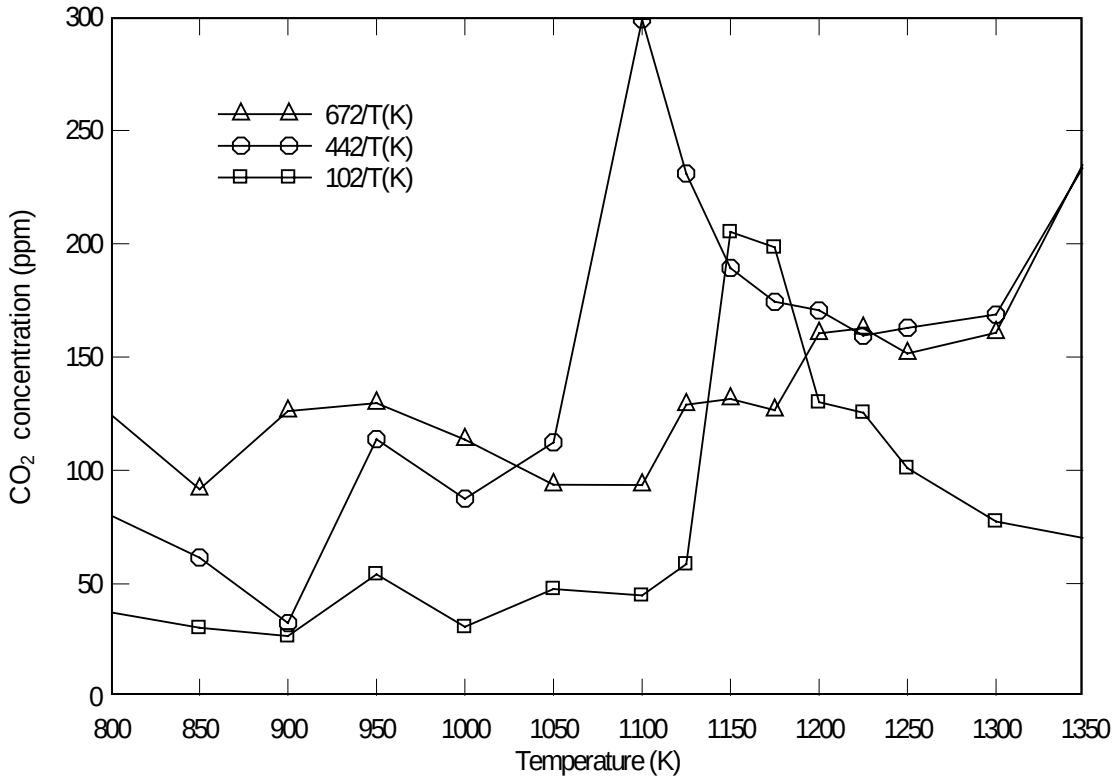

Figure 42. Carbon dioxide concentration as a function of temperature for changing concentrations of residence time. Initial: NO = 330 ppm, urea = 165 ppm, O_2 = 1%.

Figure 42 shows the concentration of carbon dioxide as a function of temperature for various residence time cases. Up to 900 K, the carbon dioxide concentration decreased with temperature rise for all cases. After 1050 K, the carbon dioxide concentration increased rapidly with temperature rise for two cases (442/T(K), 102/T(K)). This trend of sharp rise in the carbon dioxide concentration might come from urea solution mixing problem. After 1200 K, the carbon dioxide concentration increased with temperature rise for two cases (672/T(K), 442/T(K)). While, for the short residence time case, the carbon dioxide concentration nearly remained constant.

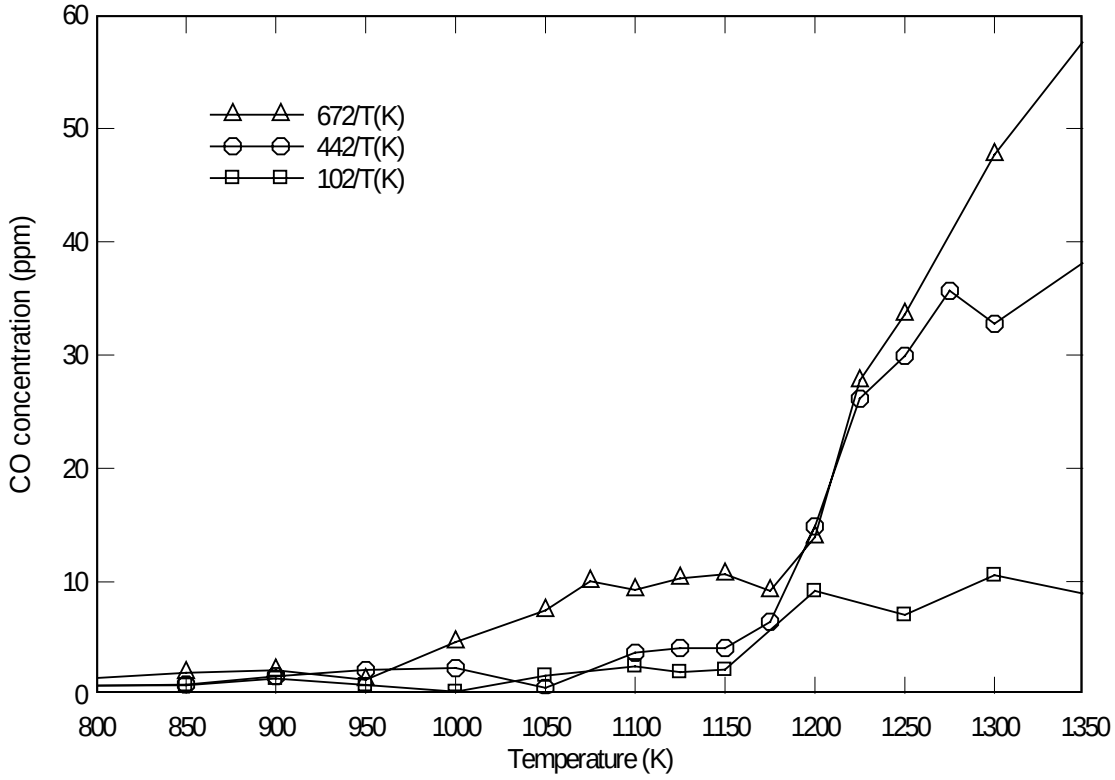

Figure 43. Carbon monoxide concentration as a function of temperature for changing concentrations of residence time. Initial: NO = 330 ppm, urea = 330 ppm, O_2 = 1%.

Figure 43 shows the concentration of carbon monoxide as a function of temperature for various residence time cases. For all three carbon monoxide concentration cases, the carbon monoxide level was low up to 950 K. Between 950 and 1175 K, the carbon monoxide concentration increased slightly with temperature for all cases. After 1175 K, the carbon monoxide concentration increased rapidly with temperature for two cases (672/T(K), 442/T(K)). While the carbon monoxide concentration of 102/T(K) remained about constant after 1200 K.

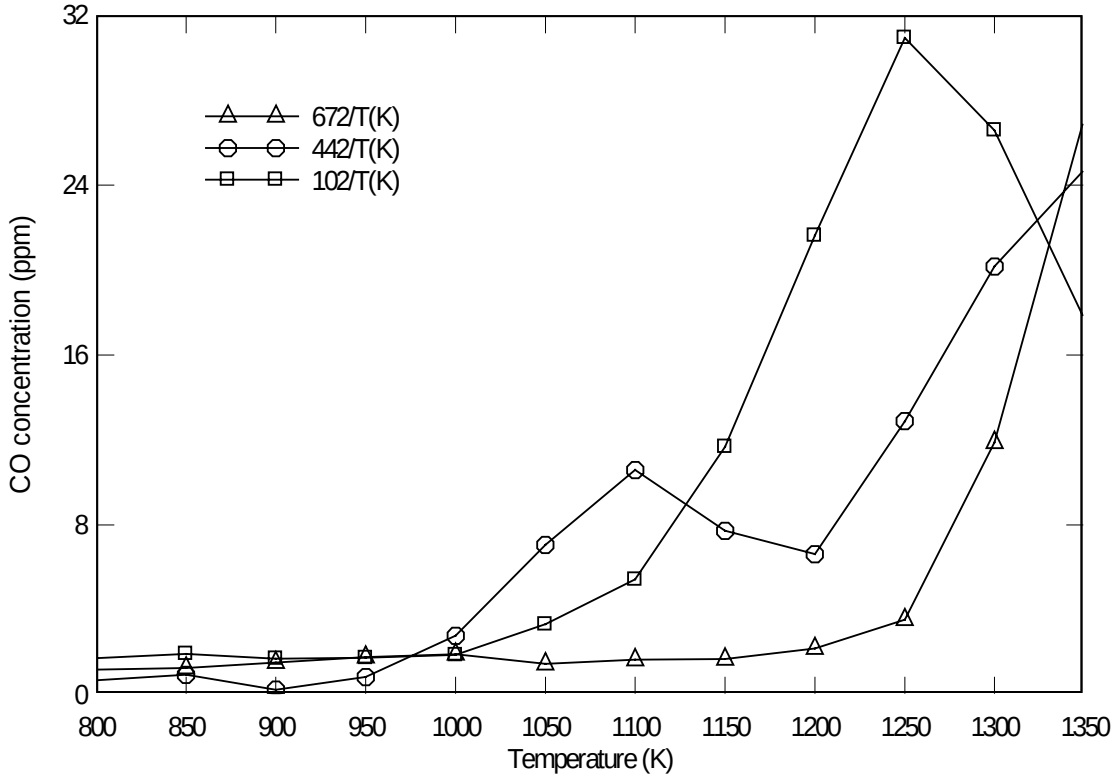

Figure 44. Carbon monoxide concentration as a function of temperature for changing concentrations of residence time. Initial: NO = 330 ppm, urea = 250 ppm, O_2 = 1%.

Figure 44 shows the concentration of carbon monoxide as a function of temperature for various residence time cases. For all three carbon monoxide concentration cases, the carbon monoxide level stayed constant up to 1000 K. Between 1000 K and 1175 K, the carbon monoxide concentration increased slightly with temperature for all cases. After 1200 K, the carbon monoxide concentration increased rapidly with temperature for two cases (672/T(K), 442/T(K)). While the carbon monoxide concentration of 102/T(K) decreased after 1200 K.

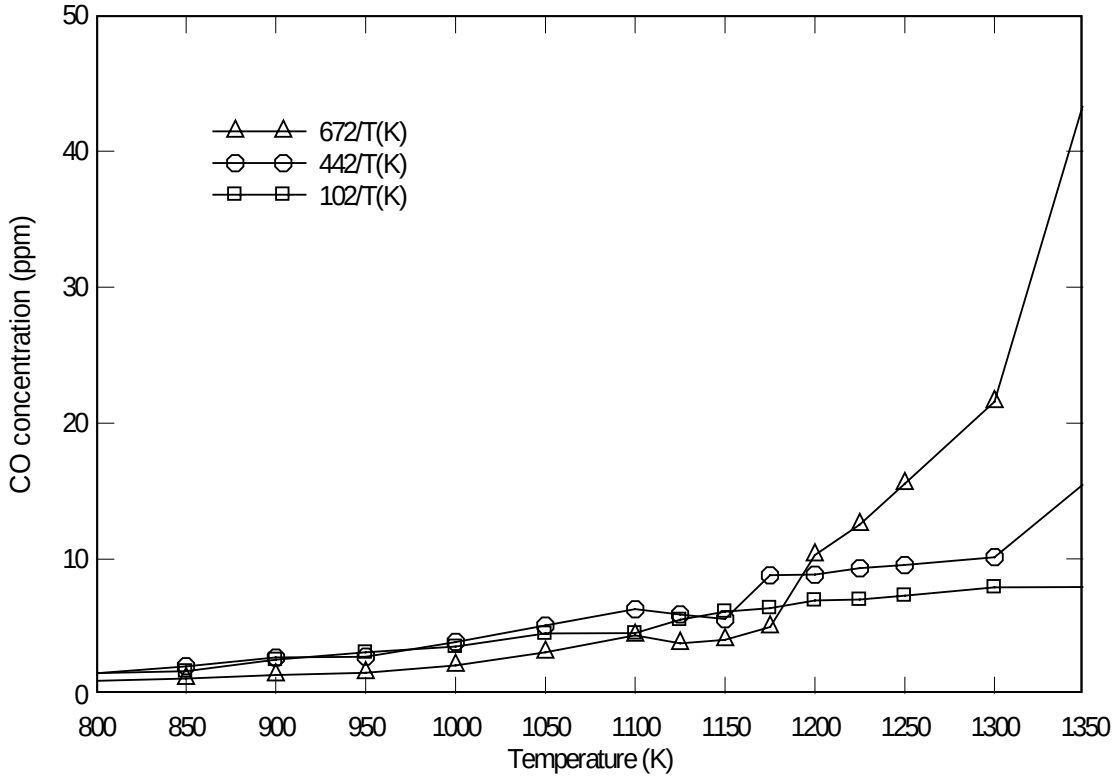

Figure 45. Carbon monoxide concentration as a function of temperature for changing concentrations of residence time. Initial: NO = 330 ppm, urea = 165 ppm, O_2 = 1%.

Figure 45 shows the concentration of carbon monoxide as a function of temperature for various residence time cases. For all three carbon monoxide concentration cases, the carbon monoxide level stayed constant up to 1150 K. Between 1000 K and 1175 K, the carbon monoxide concentration increased slightly with temperature for all cases. After 1200 K, the carbon monoxide concentration increased slightly with temperature for two cases (442/T(K), 102/T(K)). While the carbon monoxide concentration of 672/T(K) increased rapidly after 1200 K.

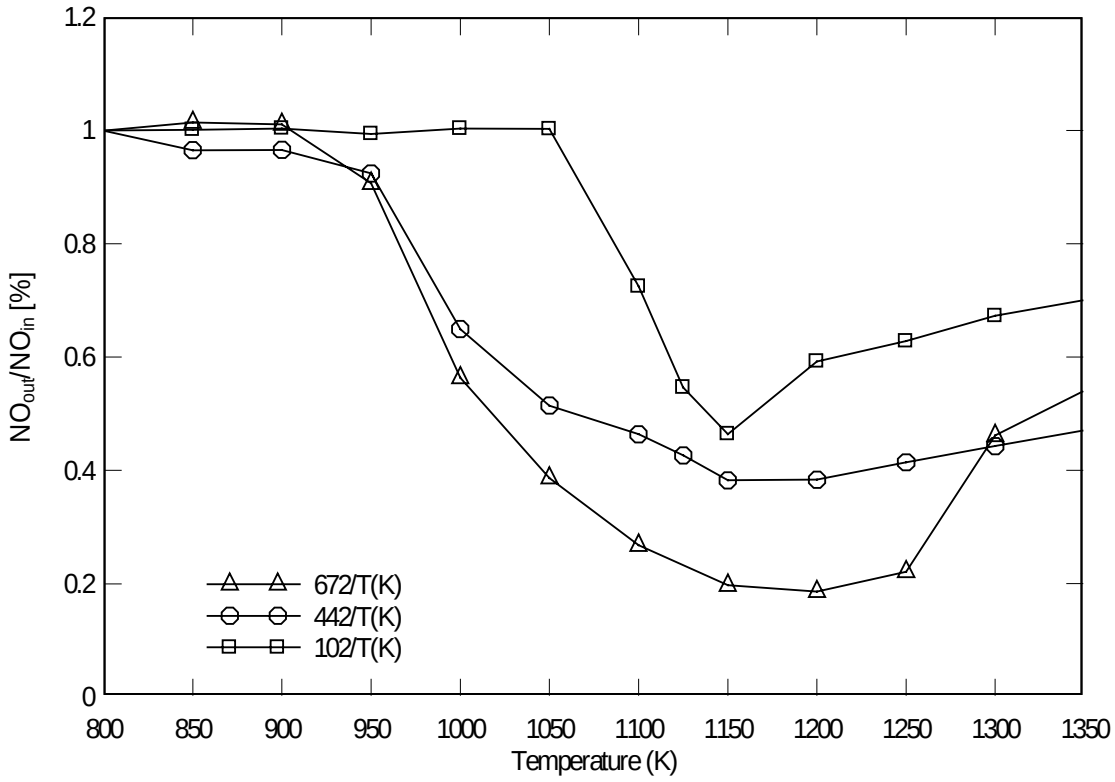

Figure 46. Nitric oxide removal as a function of temperature for changing concentrations of residence time. Initial: NO = 330 ppm, urea = 330 ppm, O_2 = 5 %.

6.2.2 Nitric Oxide Removal Using Urea with 5% Oxygen

Figure 46 shows the NO reduction as a percentage of the original NO as a function of reactor temperature for various residence times, for a β - ratio of 2.0 (NO = 330 ppm, urea = 330 ppm), and 5 % O_2. Up to a temperature of 950 K, NO was zero or small. For temperature greater than about 1000 K, as temperature increased, the NO_{out}/NO_{in} ratio decreased gradually, which means the NO reduction increases. This gradual trend continues until the temperature is to about 1200 K (672/T(K) and 442/T(K)) or 1150 K (102/T(K)).

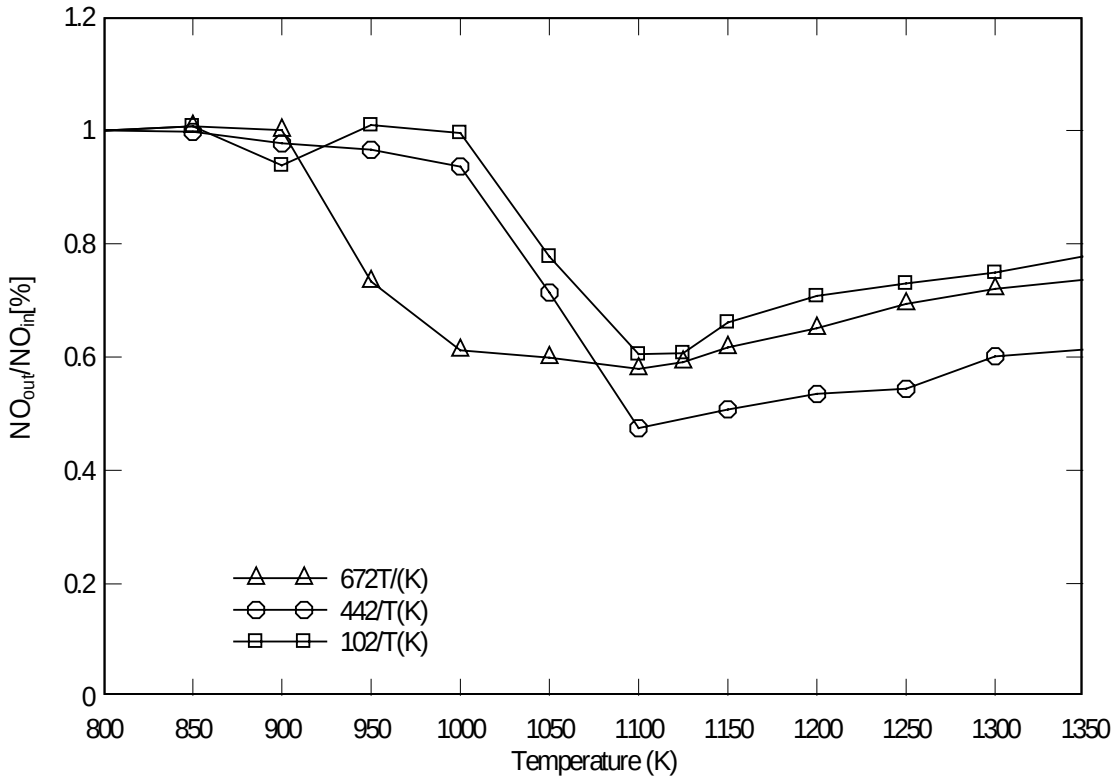

Figure 47. Nitric oxide removal as a function of temperature for changing concentrations of residence time. Initial: NO = 330 ppm, urea = 250 ppm, O_2 = 5 %.

Figure 47 shows the NO reduction as a percentage of the original NO as a function of reactor temperature for various residence times, for a β - ratio of 1.5 (NO = 330ppm, urea = 250 ppm), and 5% O_2. For all cases, a maximum NO removal was observed for a certain temperature before the NO increased again. This trend was seen at a temperature of 1100 K for all three cases. But a maximum NO reduction of around 55% occurs at 1100 K for the case with a residence time of 442/T(K). This trend is the same for the 1% O_2 concentration case, which means, in the case of a β - ratio of 1.5, the maximum NO reduction occurred for the case of 442/T(K) residence time.

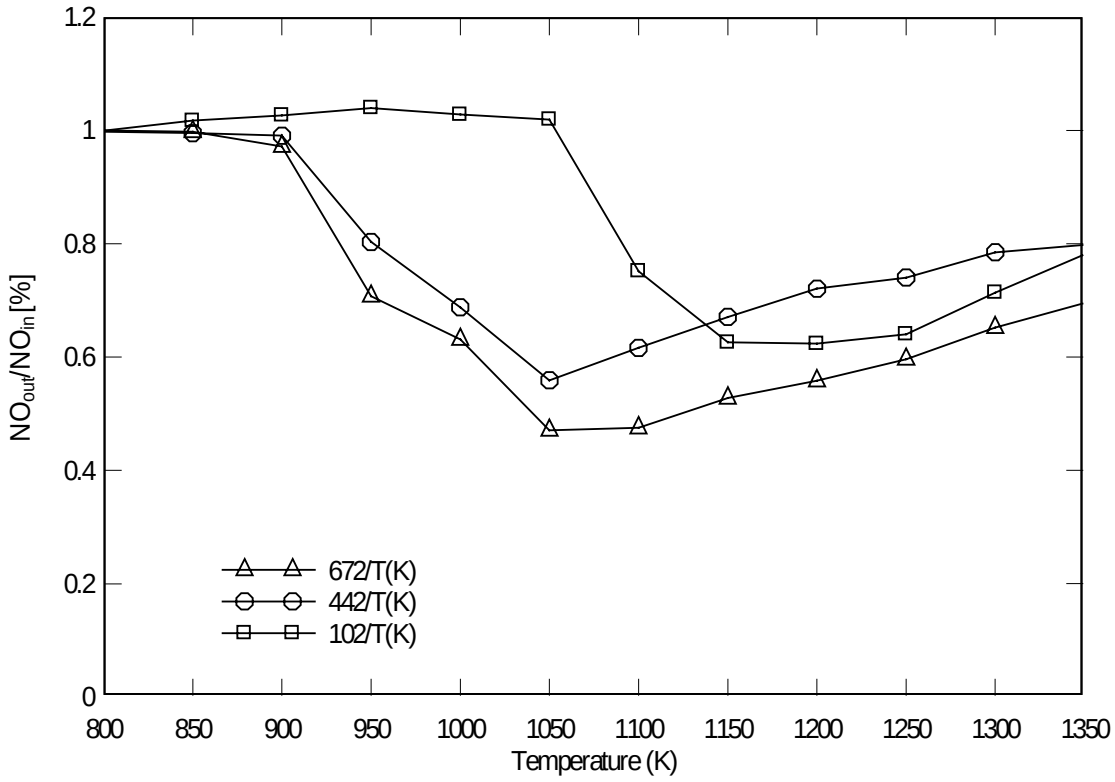

Figure 48. Nitric oxide removal as a function of temperature for changing concentrations of residence time. Initial: NO = 330 ppm, urea = 165 ppm, O_2 = 5 %.

Figure 48 shows the NO reduction as a percentage of the original NO, as a function of reactor temperature for various residence times, for a β - ratio of 2.0 (NO = 330 ppm, urea = 330 ppm), and 5 % O_2. Up to a temperature of 1050 K, NO concentration of the case of 102/T(K) residence time is slightly increased. After the temperature of 900 K, as temperature is increased, the NO_{out}/NO_{in} ratio is decreased gradually, which means NO reduction increases. This gradual trend continues as the temperature increases to about 1050 K (672/T(K) and 442/T(K)) or 1150 K(102/T(K)). The longer residence time case leads to a higher reduction of NO and a wider NO reduction "window", as well. A

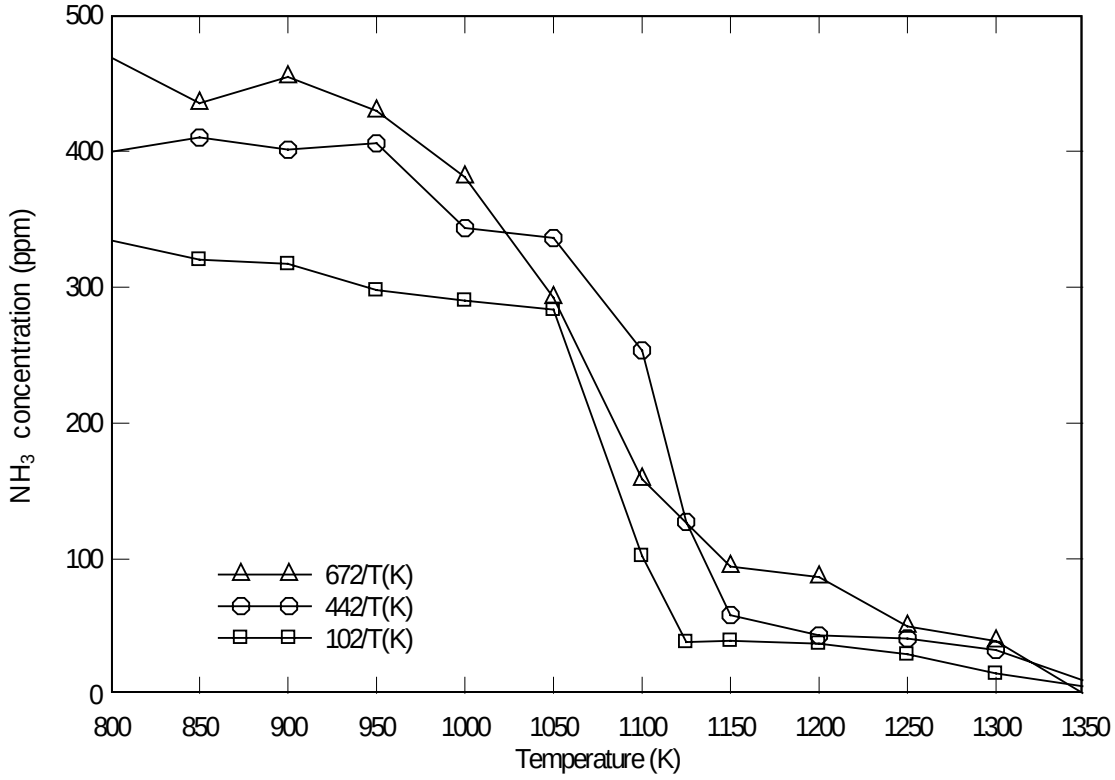

Figure 49. Concentration of ammonia as a function of temperature for changing concentrations of residence time. Initial: NO = 330 ppm, urea = 330 ppm, O_2 = 5 %.

maximum NO reduction of around 52% occurs at 1050 K for the case with a residence time of 672/T(K).

Figure 49 shows the concentration of ammonia as a function of temperature. Initial ammonia concentration from the urea decomposition was about 470 ppm, 400 ppm and 340 ppm for the residence times of 672/T(K), 442/T(K) and 102/T(K), respectively. For the temperature range between 800 and 950 K, ammonia concentration decreased slightly. For temperatures above about 1000 K, the ammonia concentration decreased

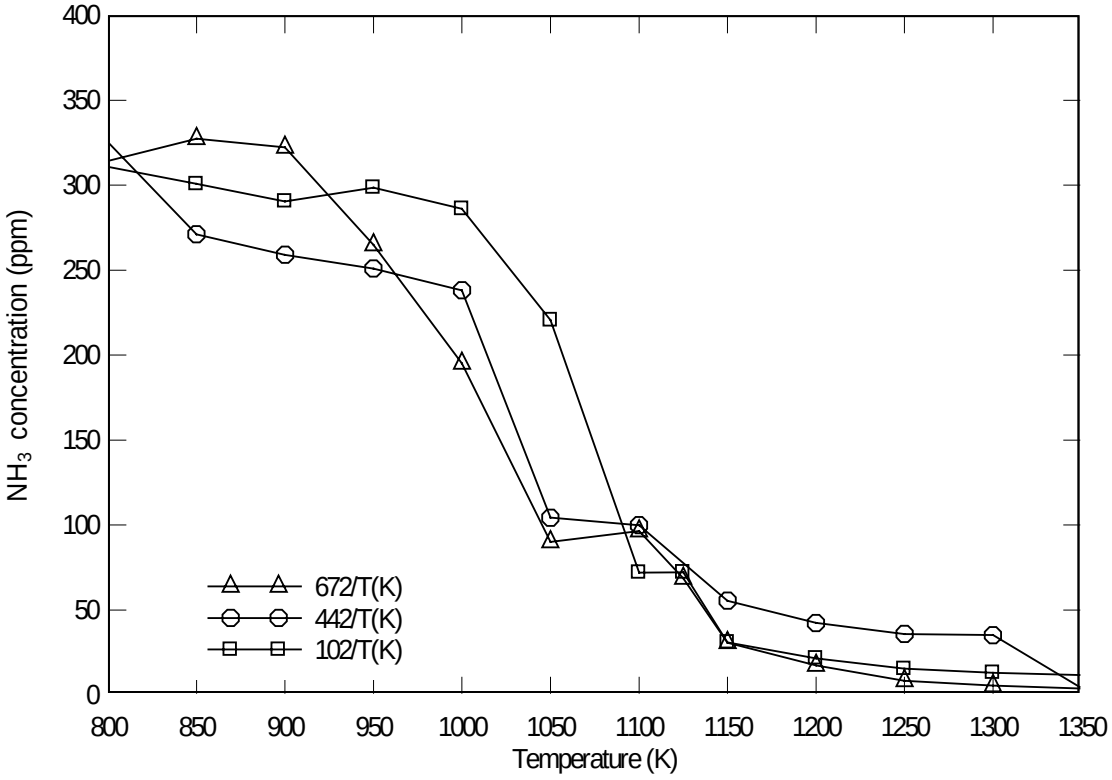

Figure 50. Concentration of ammonia as a function of temperature for changing concentrations of residence time. Initial: NO = 330 ppm, urea = 250 ppm, O_2 = 5 %.

rapidly. For all cases, when the maximum NO reduction occurred, ammonia concentration diminished slowly.

Figure 50 shows the concentration of ammonia as a function of temperature. Initial ammonia concentration from urea decomposition between 672/T(K) and 102/T(K) cases was nearly the same. For the temperatures range between 800 K and 950 K, ammonia concentration decreased slightly. For the temperature above 1000 K, the ammonia concentration decreased rapidly. For all cases, when the maximum NO reduction

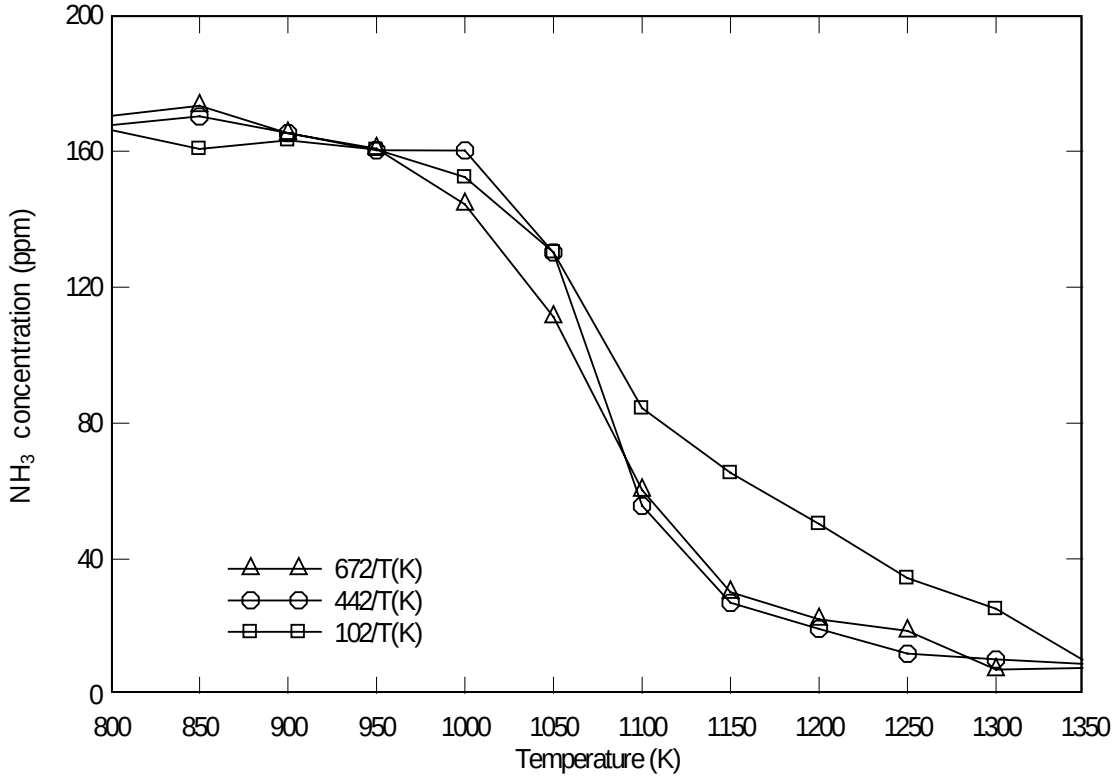

Figure 51. Concentration of ammonia as a function of temperature for changing concentrations of residence time. Initial: NO = 330 ppm, urea = 165 ppm, O_2 = 5 %.

occurred, the ammonia concentration diminished slowly or increased a little. Unreacted NH_3 (ammonia slip) was about 15 ppm for the shortest residence time case at 1350 K.

Figure 51 shows the concentration of ammonia as a function of temperature. Initial ammonia concentration from urea decomposition was nearly the same for these cases. For the temperature range between 800 and 1000 K, the ammonia concentration decreased slightly. For the temperature above 1000 K, the ammonia concentration decreased rapidly. For these cases, the unreacted NH_3 concentration (ammonia slip) was almost 10 ppm. For the cases of β = 2 or 1.5, the unreacted NH_3 was almost 3 times higher.

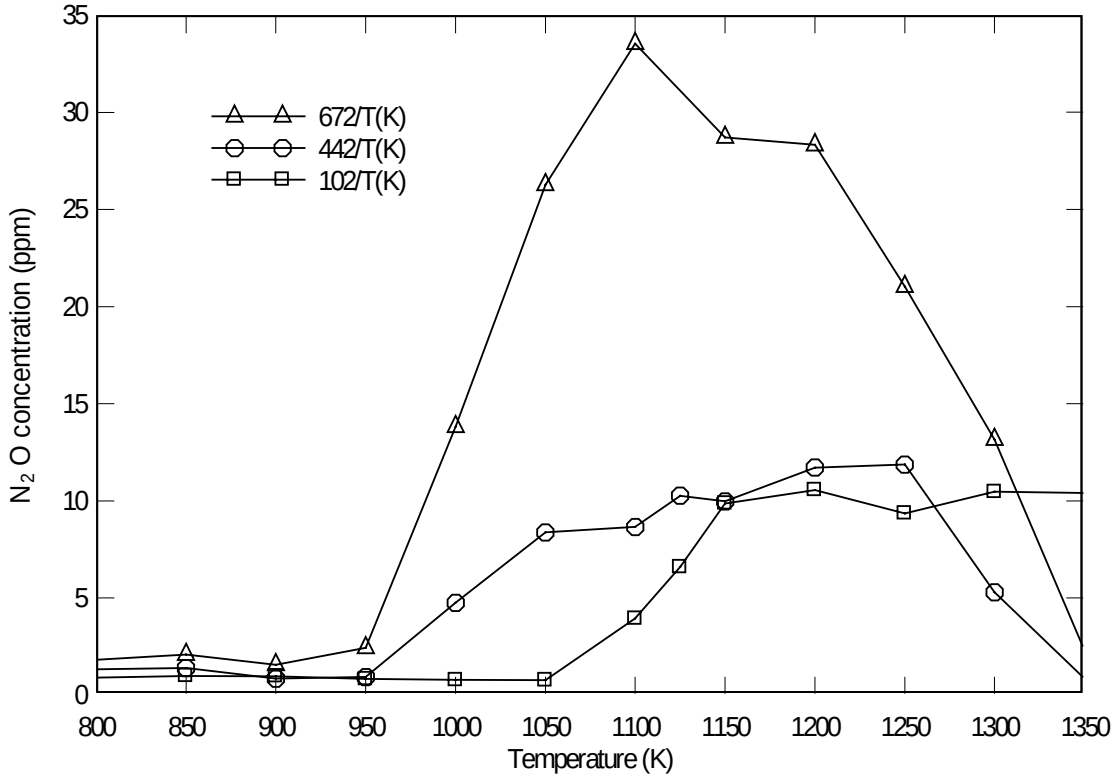

Figure 52. Concentration of nitrous oxide as a function of temperature for changing concentrations of residence time. Initial: NO = 330 ppm, urea = 330 ppm, O_2 = 5 %.

Figure 52 shows the concentration of nitrous oxide (N_2O) as a function of temperature for various residence time cases. Up to 950 K, N_2O concentration remained constant at about 2 ppm. Among all cases, the longest residence time case leads to the highest N_2O concentration. The maximum N_2O concentration for the 102/T(K) residence time case was at least three times the other two cases. The temperature for the maximum N_2O concentration was nearly the same as the temperature for the maximum NO reduction.

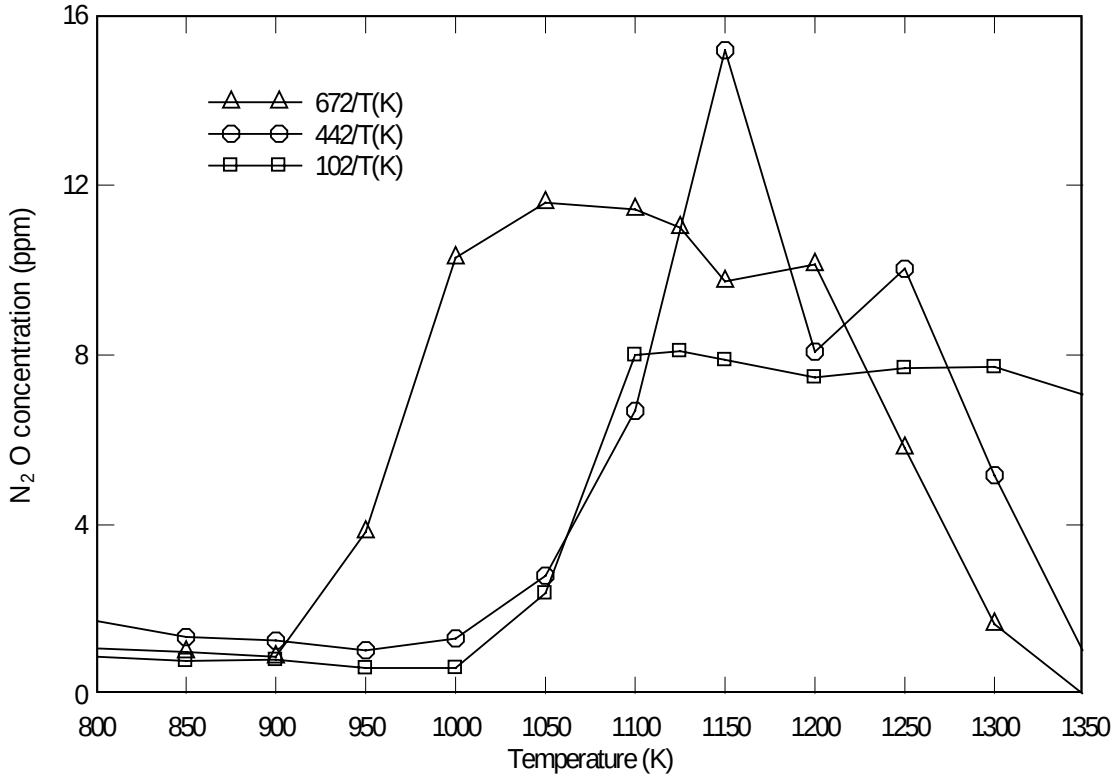

Figure 53. Concentration of nitrous oxide as a function of temperature for changing concentrations of residence time. Initial: NO = 330 ppm, urea = 250 ppm, O_2 = 5 %.

Figure 53 shows the concentration of nitrous oxide (N_2O) as a function of temperature for various residence time cases. Up to 900 K, N_2O concentration was less than 2 ppm. Among all cases, the longest residence time case leads to the production of N_2O concentration at lower temperature. The maximum N_2O concentration for the 442/T(K) residence time case produced the highest concentration (15 ppm). The temperature of the maximum N_2O concentration was nearly the same temperature for the maximum NO reduction. For the case of 5% O_2 concentration, the maximum NO reduction case leads to maximum production of N_2O.

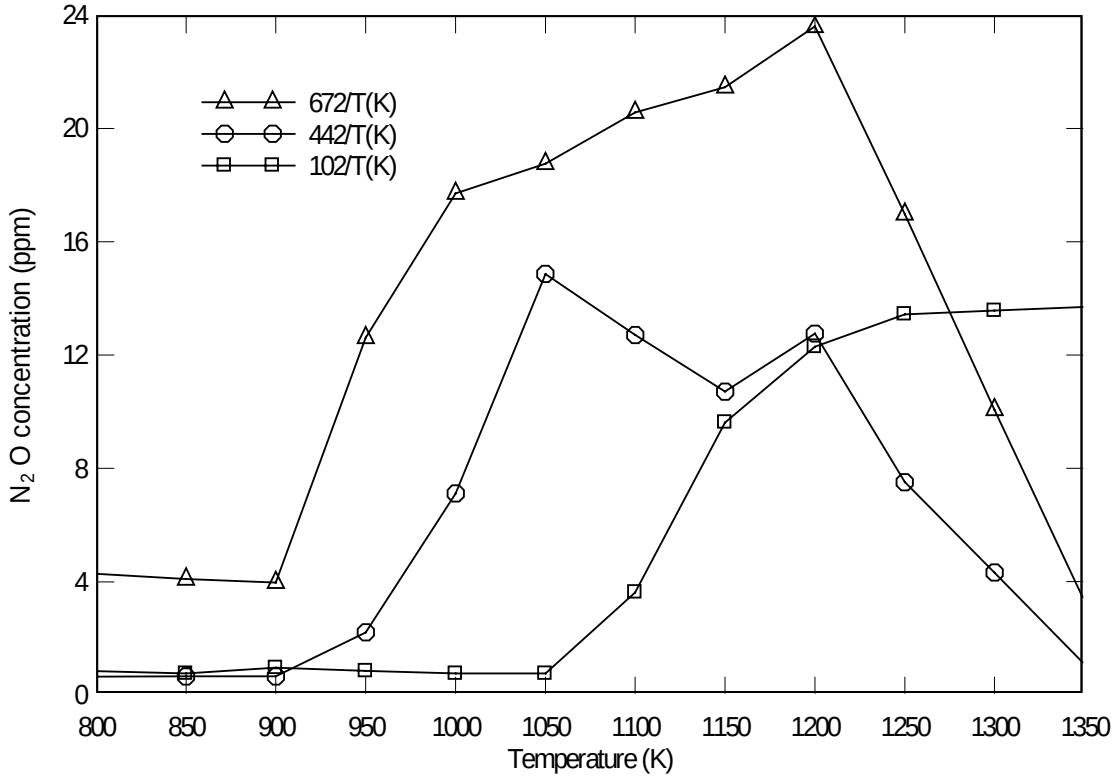

Figure 54. Concentration of nitrous oxide as a function of temperature for changing concentrations of residence time. Initial: NO = 330 ppm, urea = 165 ppm, O_2 = 5 %.

Figure 54 shows the concentration of nitrous oxide (N_2O) as a function of temperature for various residence time cases. Up to 900 K, N_2O concentration was nearly constant. Among all cases, the longest residence time case leads to the production of N_2O concentration at lower temperatures, and the largest production of N_2O. The maximum N_2O concentration of 672/T(K) residence time case was nearly twice that of the other cases (442/T(K), 102/T(K)). The temperature for the maximum N_2O concentration was nearly the same temperature as for the maximum NO reduction. For the case of

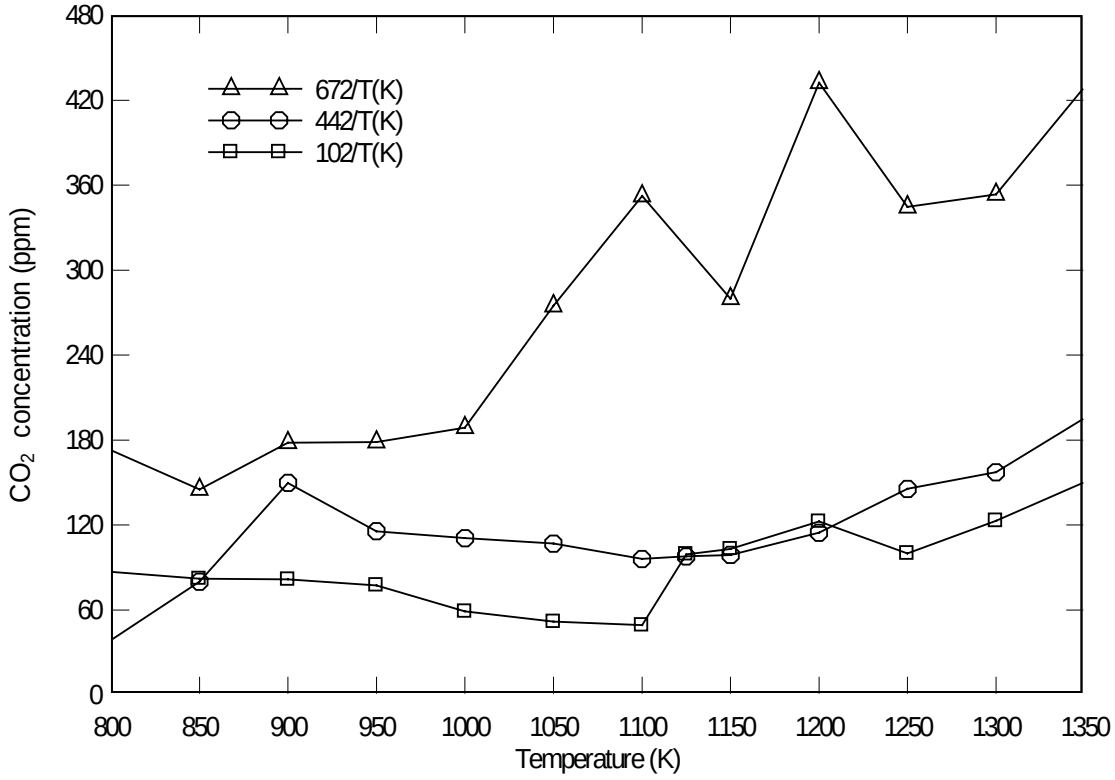

Figure 55. Carbon dioxide concentration as a function of temperature for changing concentrations of residence time. Initial: NO = 330 ppm, urea = 330 ppm, O_2 = 5%.

102/T(K) residence time, after the maximum NO reduction, N_2O concentration stayed nearly for further temperature increases.

Figure 55 shows the concentration of carbon dioxide (CO_2) as a function of temperature for various residence time cases. For the longer residence time case of 672/T(K), the carbon dioxide concentration generally increase although the results exhibited some variation. While the carbon dioxide concentration for the two shorter residence time cases (442/T(K) and 102/T(K)) remained nearly constant up to 1200 K and the CO2 concentration increased slightly for temperatures above about 1200 K.

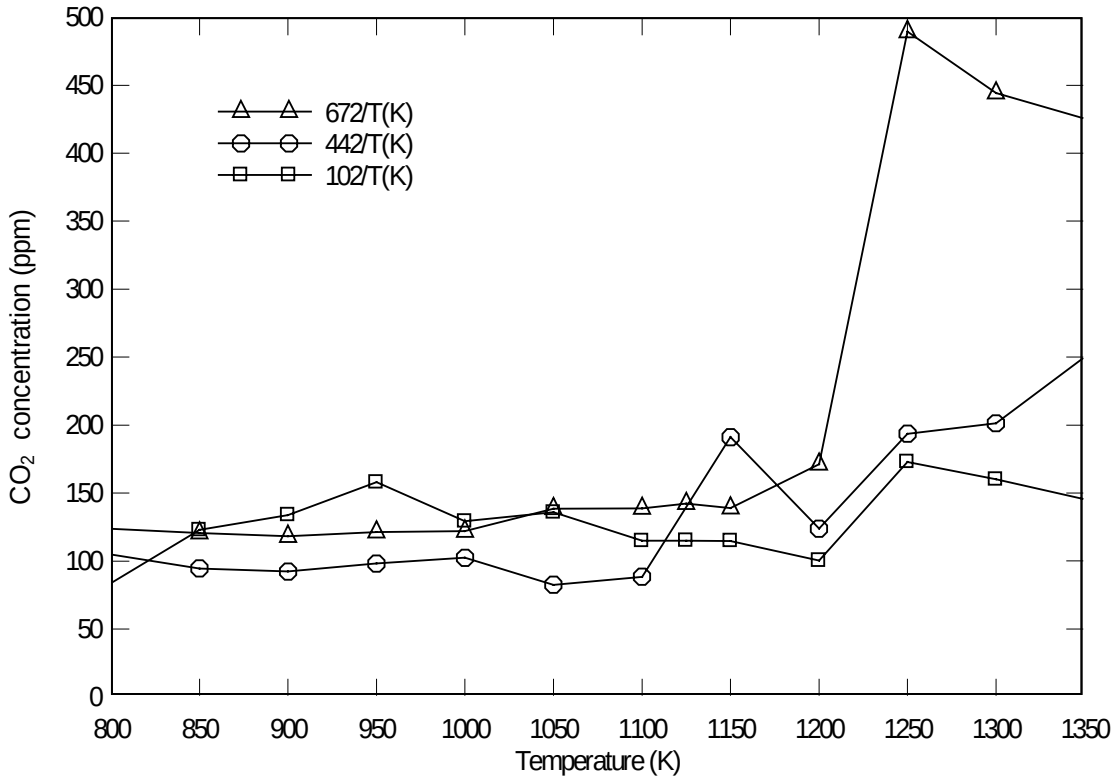

Figure 56. Carbon dioxide concentration as a function of temperature for changing concentrations of residence time. Initial: NO = 330 ppm, urea = 250 ppm, O_2 = 5%.

Figure 56 shows the concentration of carbon dioxide (CO_2) as a function of temperature for various residence times, for a β - ratio of 1.5 (NO = 330 ppm, urea = 250 ppm), and 5 % O_2. For the longer residence time case of 672/T(K), the carbon dioxide concentration remained constant up to about 1200 K, and increased with temperature increases after about 1200 K. While the carbon dioxide concentration of two short residence time case (442/T(K) and 102/T(K)) also remained constant up to about 1200 K, the CO_2 concentration increased only slightly for temperatures above almost 1200 K.

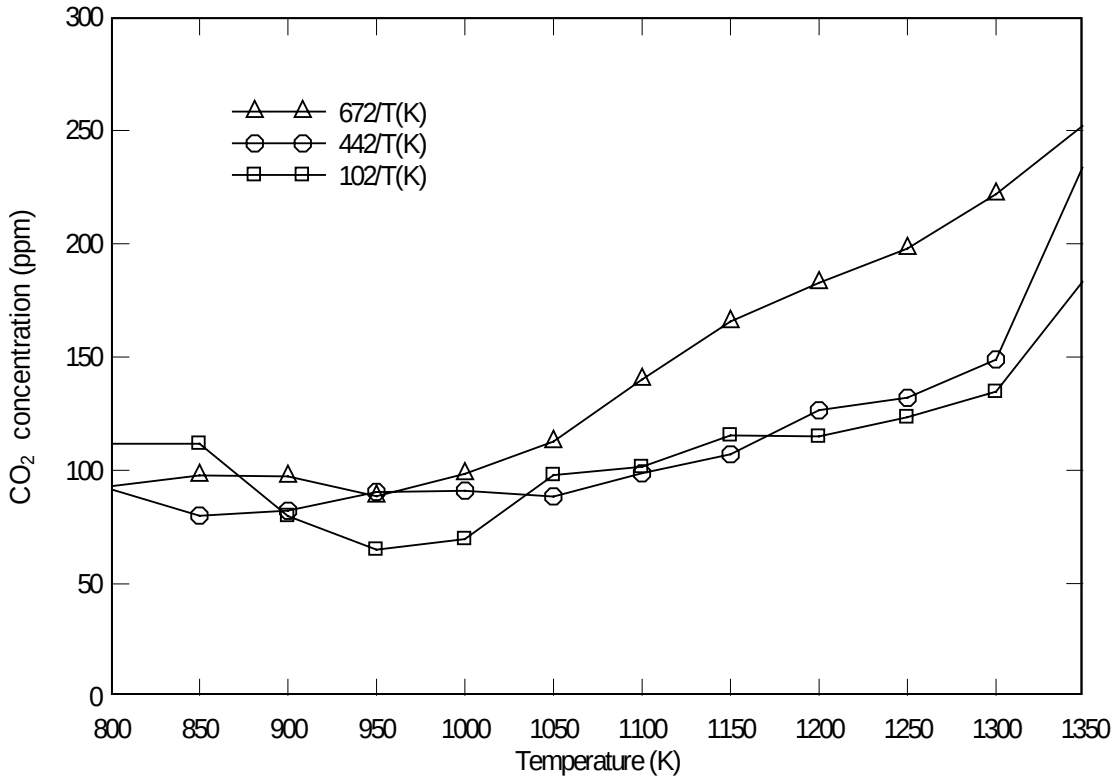

Figure 57. Carbon dioxide concentration as a function of temperature for changing concentrations of residence time. Initial: NO = 330 ppm, urea = 165 ppm, O_2 = 5%.

Figure 57 shows the concentration of carbon dioxide (CO_2) as a function of temperature for various residence time cases for a β - ratio of 1.5 (NO = 330 ppm, urea = 165 ppm), and 5 % O_2. From a nearly constant level up to 1000 K, the carbon dioxide concentration increased with further temperature increases for all these cases. The concentration of carbon dioxide from the urea decomposition theoretically could be 165 ppm. The higher value may be a result of reaction between NCO and NO.

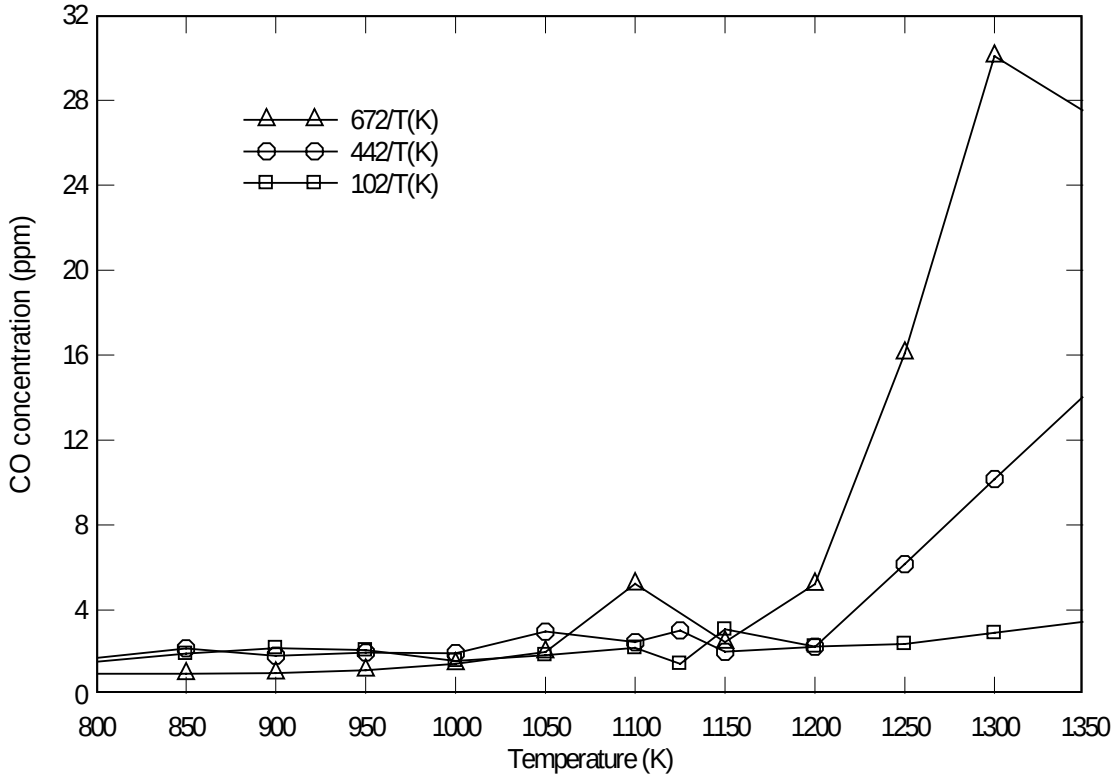

Figure 58. Carbon monoxide concentration as a function of temperature for changing concentrations of residence time. Initial: NO = 330 ppm, urea = 330 ppm, O_2 = 5%.

Figure 58 shows the concentration of carbon monoxide (CO) as a function of temperature for these residence time cases for a β - ratio of 2.0 (NO = 330 ppm, urea = 330 ppm), and 5 % O_2. For all three cases, the carbon monoxide level was nearly constant up to about 1000 K. Between 1000 K and 1175 K, the carbon monoxide concentration increased slightly with temperature rise for all cases. After 1175 K, the carbon monoxide concentration increased rapidly with temperature rise for two cases (672/T(K) and 442/T(K)). While the carbon monoxide concentration of 102/T(K) remained constant after 1200 K.

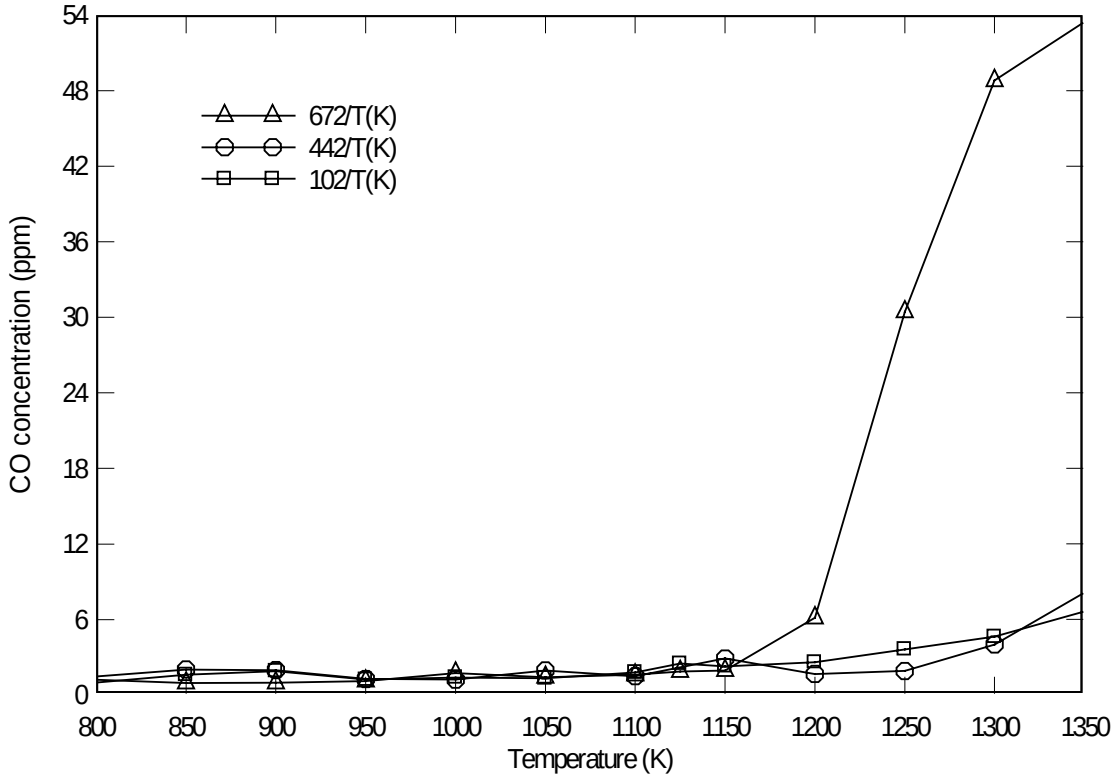

Figure 59. Carbon monoxide concentration as a function of temperature for changing concentrations of residence time. Initial: NO = 330 ppm, urea = 250 ppm, O_2 = 5%.

Figure 59 shows the concentration of carbon monoxide (CO) as a function of temperature for these residence time cases for a β - ratio of 1.5 (NO = 330 ppm, urea = 250 ppm), and 5 % O_2. For all three cases, the carbon monoxide level was nearly constant up to about 1150 K. After 1175 K, the carbon monoxide concentration increased rapidly with temperature rise for one case (672/T(K)). While the carbon monoxide concentration for two cases (442/T(K) and 102/T(K)) remained constant after 1200 K.

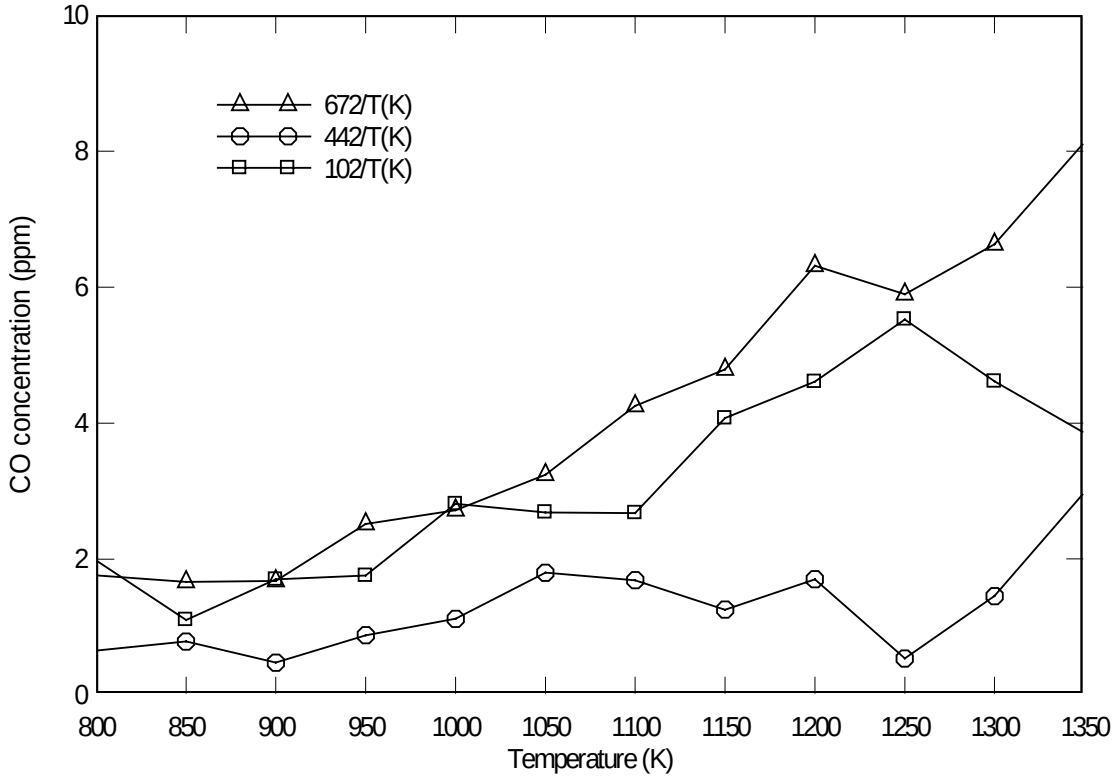

Figure 60. Carbon monoxide concentration as a function of temperature for changing concentrations of residence time. Initial: NO = 330 ppm, urea = 165 ppm, O_2 = 5%.

Figure 60 shows the concentration of carbon monoxide (CO) as a function of temperature for these residence time cases for a β - ratio of 1.0 (NO = 330 ppm, urea = 165 ppm), and 5 % O_2. For all three cases, the carbon monoxide level was nearly constant up to about 900 K. After 900 K, the carbon monoxide concentration increased slightly with temperature rise for two cases (672/T(K) and 442/T(K)). While the carbon monoxide concentration of 102/T(K) residence time case remained constant. Note that the amount of CO is very small for these cases compared to the other cases.

6.3 Nitric Oxide Removal Using Ammonia as the Reducing Agent

To compare urea as the reducing agent, ammonia was used for two cases: effect of β - ratio and O_2 concentration effect in the NO removal process. The inlet gas compositions, which were used for the experimental set, are shown in table 6.

Table 6. Experimental test cases for NO removal experiments using ammonia

NO (ppm)	NH_3 (ppm)	β - ratio	O_2 concentration (%)	Residence time (sec.)
330	660	2	0.9	87/T(K)
	495	1.5		
	330	1		
	660	2	15	
			5	
			0.9	
			0.1	

6.3.1 Effect of β - Ratio in the Removal Process with Ammonia (NO = 330 ppm, NH_3 = 660, 495, and 330 ppm, 0.9% O_2 concentration, Residence time: 87/T(K))

Using the 3.6 mm diameter quartz tube and heating three heat zones resulted in a residence time of 87/T(K). This study was performed for the same conditions that are used for the nitric oxide removal process using urea.

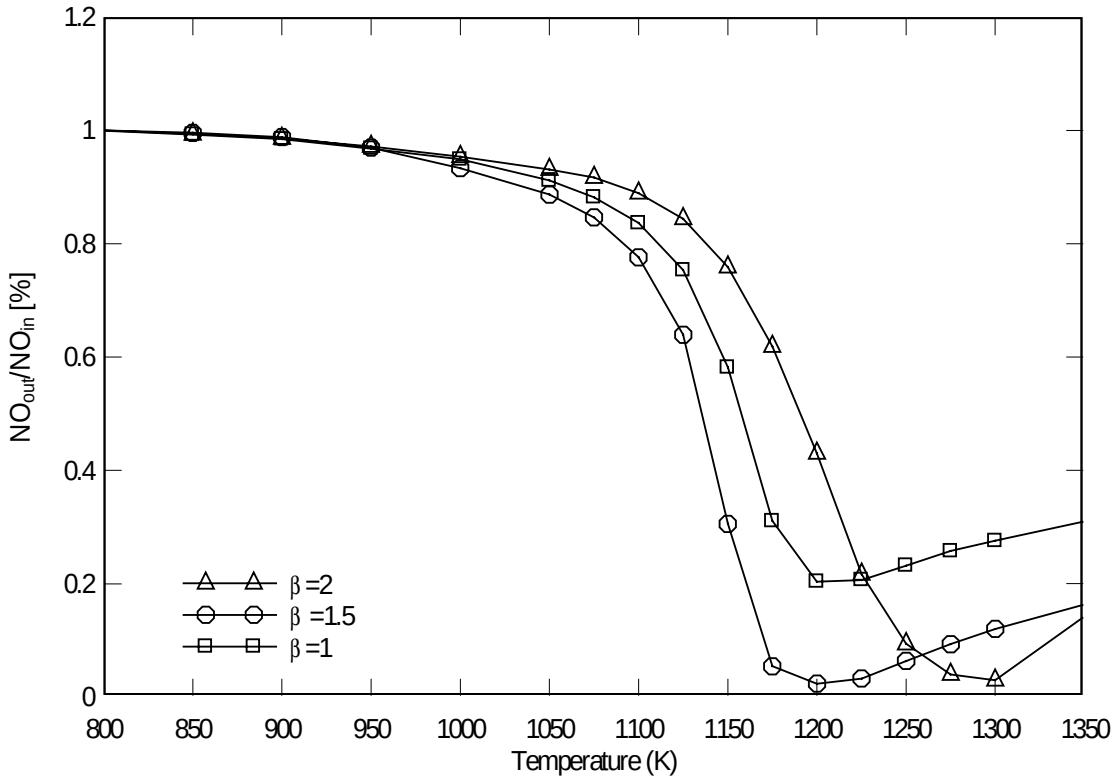

Figure 61. Nitric oxide removal as a function of temperature for 87/T(K) residence time. Inital NO = 330 ppm, NH_3 = 660, 495 and 330 ppm, O_2 = 0.9%.

Figure 61 shows NO reduction as a percentage of the original NO, as a function of reactor temperature for these β - ratios (NO = 330 ppm, NH_3 = 660, 495 and 330 ppm), 87/T(K) residence time and 0.9% O_2. For all three cases, for temperatures below about 1000 K, the NO removal was between 0 and 5% with a decreasing tendency. For further increasing temperature, the maximum removal was around 95% at about 1200 K for the β=1.5 case, and 1300 K for the β=2 case. For the case of β=1, the maximum removal was around 80% at about 1200 K. In addition to this, the NO removal decreased for temperatures higher than for the temperature of optimum removal.

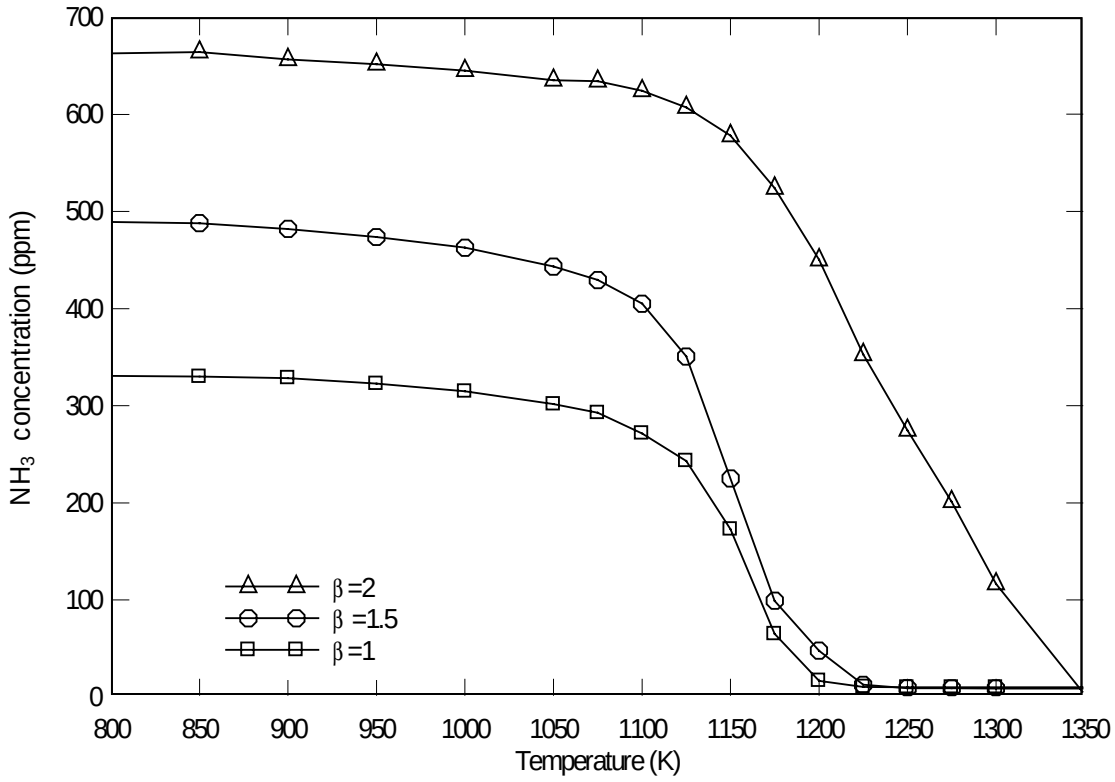

Figure 62. Concentration of ammonia as a function of temperature for 87/T(K) residence time. Inital NO = 330 ppm, NH_3 = 660, 495 and 330 ppm, O_2 = 0.9%.

Figure 62 shows the ammonia (NH_3) concentration as a function of reactor temperature for these β - ratios (NO = 330 ppm, NH_3 = 660, 495 and 330 ppm), 87/T(K) residence time and 0.9% O_2. For all three cases, for temperature below 1075 K, the amount of decreasing ammonia was between 0 and 5% with a rise of temperature. For further increasing temperature, the ammonia concentration decreased rapidly up to the region where the maximum NO removal occurred was at 1225 K for β=1.5 and 1 cases. For the case of β=2 case, the ammonia was used completely after reaching 1350 K.

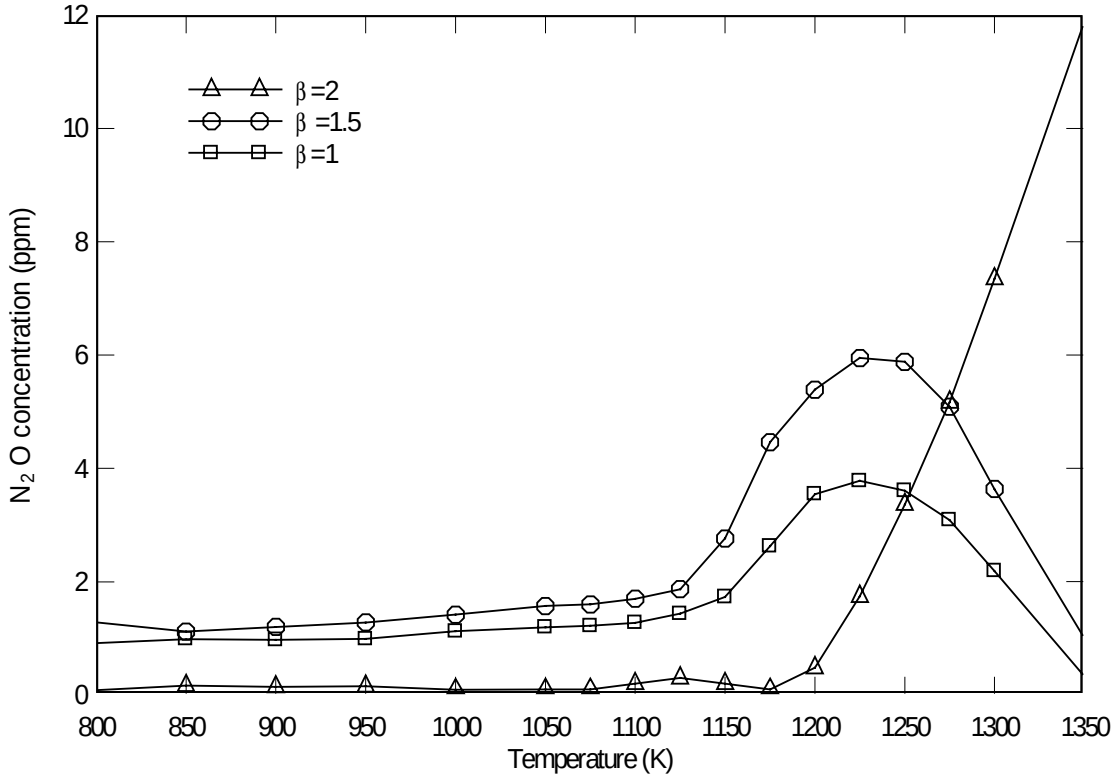

Figure 63. Concentration of nitrous oxide as a function of temperature for 87/T(K) residence time. Inital NO = 330 ppm, NH_3 = 660, 495 and 330 ppm, O_2 = 0.9%.

Figure 63 shows nitrous oxide (N_2O) concentration as a function of reactor temperature for these β - ratios (NO = 330 ppm, NH_3 = 660, 495 and 330 ppm), 87/T(K) residence time and 0.9% O_2. For all three cases, for temperatures below about 1125 K, the amount of nitrous oxide was below about 1 ppm. For further increasing temperature, nitrous oxide concentration increased up to the region where the maximum NO removal occurred was at 1225 K for β=1.5 and 1 cases. For the case of β=2, the nitrous oxide concentration continued to increase with temperature after 1175 K.

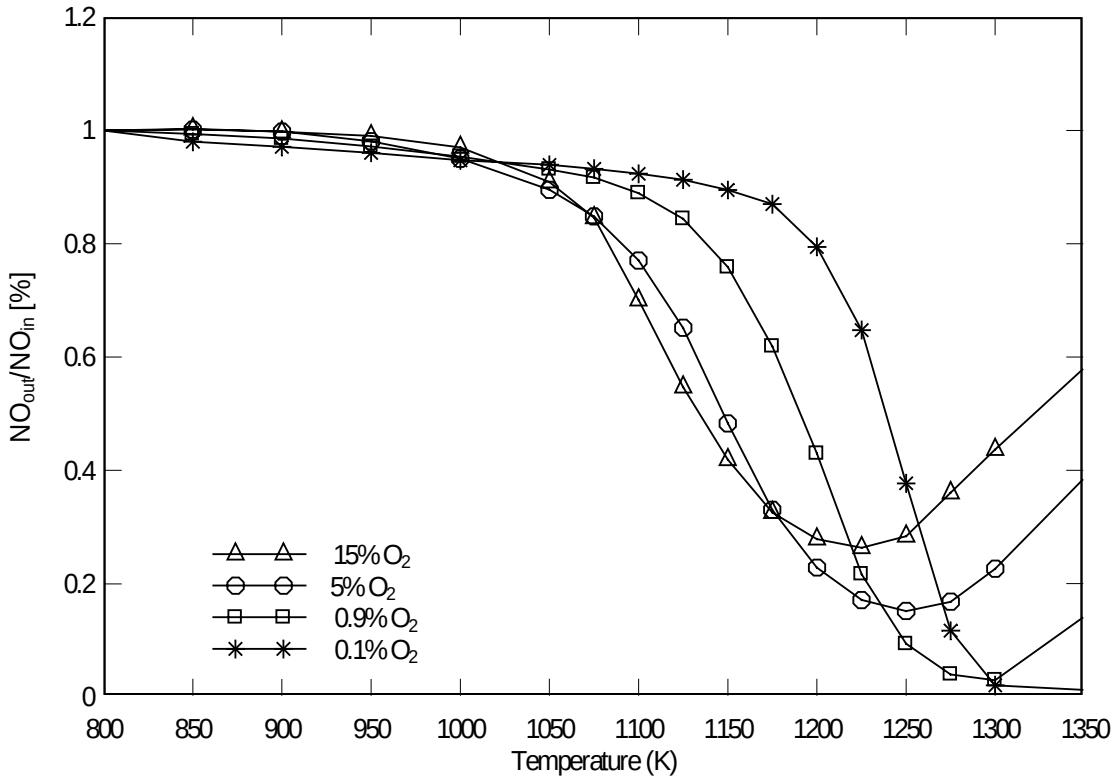

Figure 64. Nitric oxide removal as a function of temperature for 87/T(K) residence time. Inital NO=330 ppm, NH_3 = 660 ppm, O_2 = 15, 5, 0.9 and 0.1%.

6.3.2. Effect of O_2 Concentration in the Removal Process with Ammonia (NO = 330 ppm, NH_3 = 660 ppm, 15, 5, 0.9 and 0.1 % O_2 concentration, Residence time: 87/T(K))

Figure 64 shows NO reduction as a percentage of the original NO as a function of reactor temperature for four O_2 concentrations (15, 5, 0.9 and 0.1 %), 87/T(K) residence time and a β-ratio of 2.0 (NO = 330 ppm, NH_3 = 660 ppm). For all four cases, for temperatures below about 1050 K, the NO removal was between 0 and 5% with a decreasing tendency. For further increasing temperature, the maximum removal was around 95% at 1300 K for the 0.9 % O_2 case, and at 1350 K for the 0.1 % O_2 case. For

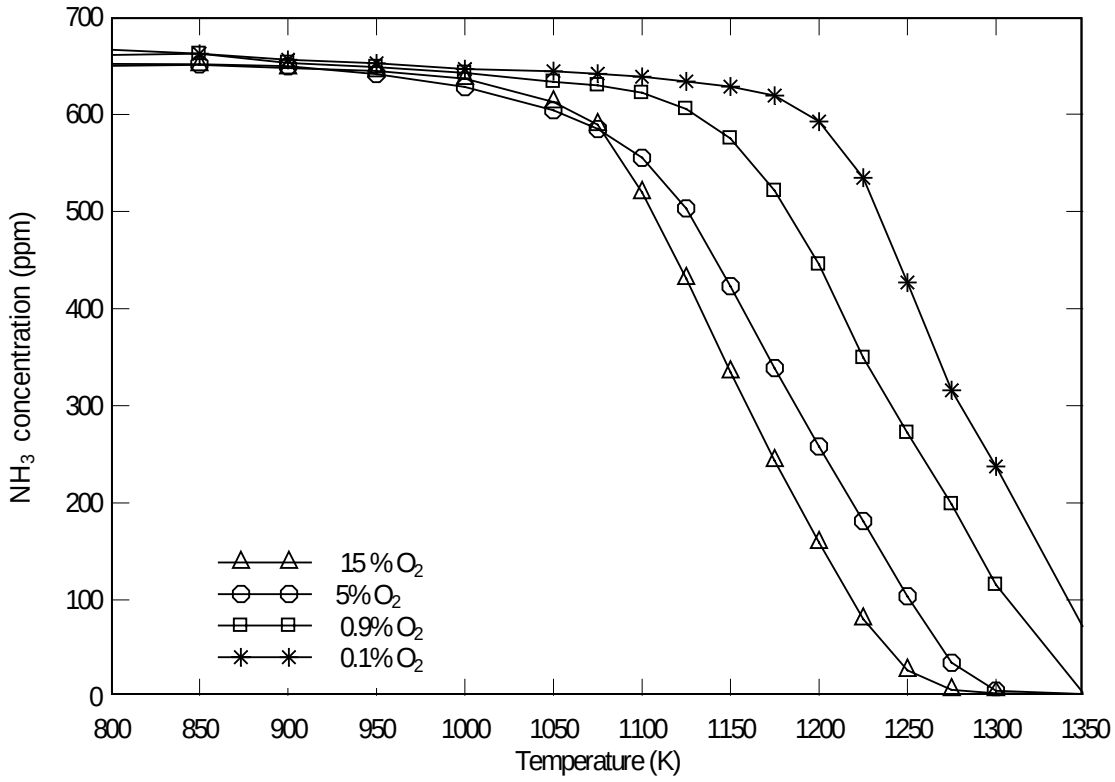

Figure 65. Concentration of ammonia as a function of temperature for 87/T(K) residence time. Inital NO=330 ppm, NH_3 = 660 ppm, O_2 = 15, 5, 0.9 and 0.1%.

the case of 5 % O_2, the maximum removal was around 85% at 1250 K. While for the 15 % O_2 case, the maximum NO reduction was about 70% at 1250 K.

Figure 65 shows the ammonia (NH_3) concentration as a function of reactor temperature for four O_2 concentrations (15, 5, 0.9 and 0.1 %), a 87/T(K) residence time and a β-ratio of 2.0 (NO = 330 ppm, NH_3 = 660 ppm). For all four cases, for temperatures below about 1000 K, the ammonia concentration was nearly constant. For further increasing temperature, the ammonia concentration decreased rapidly up to the region where the maximum NO removal occurred at about 1300 K for the 15 and 5% O_2

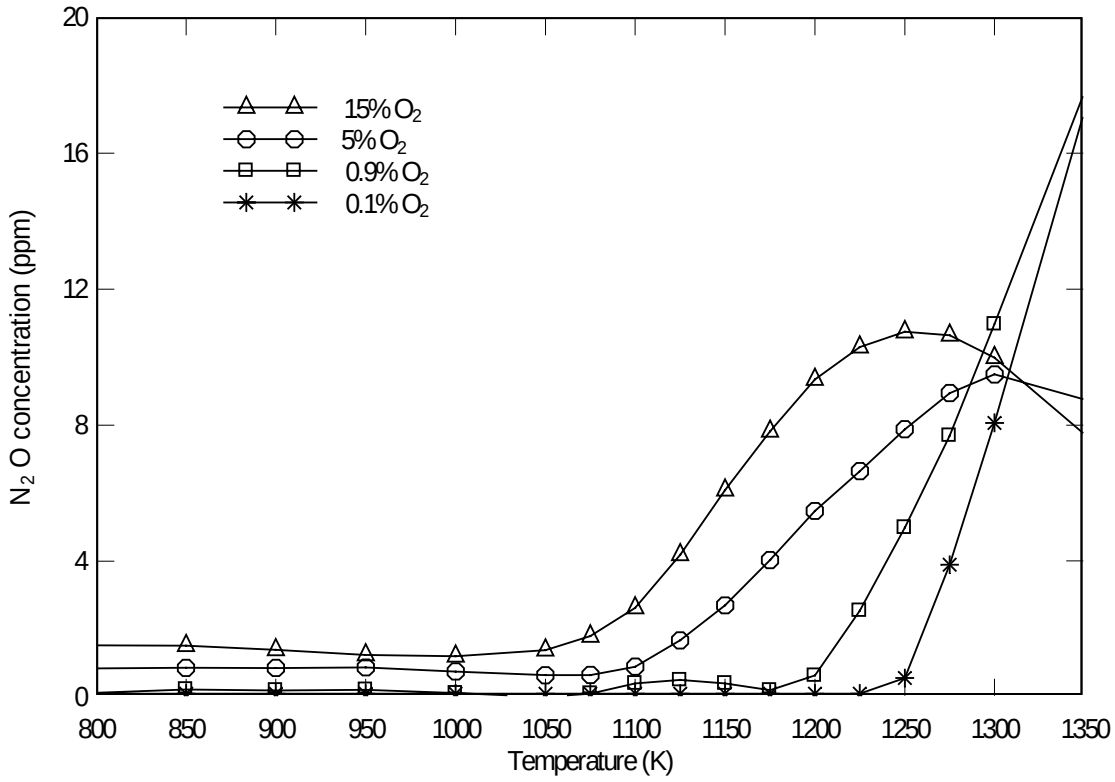

Figure 66. Concentration of nitrous oxide as a function of temperature for 87/T(K) residence time. Inital NO=330 ppm, NH_3 = 660 ppm, O_2 = 15, 5, 0.9 and 0.1%.

concentrations cases. For the case of the 0.9 and 0.1 % O_2 concentration, the ammonia was used completely at 1350 K.

Figure 66 shows nitrous oxide concentration (N_2O) as a function of reactor temperature for four O_2 concentrations (15, 5, 0.9 and 0.1 %), a 87/T(K) residence time and a β-ratio of 2.0 (NO = 330 ppm, NH_3 = 660 ppm). For all four cases, for temperatures below about 1075 K, the amount of nitrous oxide remained nearly constant. For further increasing temperature, the nitrous oxide concentration increased up to the region where the maximum NO removal occurred at about 1250 K for the 15% O_2 case, and at 1300 K

for the 5% O_2 case. For the case of 0.9 and 0.1% O_2, the nitrous oxide concentration increased continuously with temperature rise after 1175 K.

6.4 Comparison of the Results Between NH_3 and Urea in the NO Removal

To compare the cases using urea as a reducing agent, ammonia was used for the NO removal process. The results in the process section (6.3) were for a 87/T(K) residence time. To compare with urea results at 672/T(K), this section will examine NH_3 at 672/T(K) and 1% O_2. The inlet gas compositions, which were used for the experimental set, are shown in table 7. This study was performed for the same conditions that used for the nitric oxide removal process using urea.

Table 7. Experimental test cases for NO removal experiments using ammonia

NO (ppm)	NH_3 (ppm)	β - ratio	O_2 concentration (%)	Residence time (sec.)
330	660	2	1%	672/T(K)
	495	1.5		
	400	1.21		
	330	1		
	250	0.75		
	165	1		

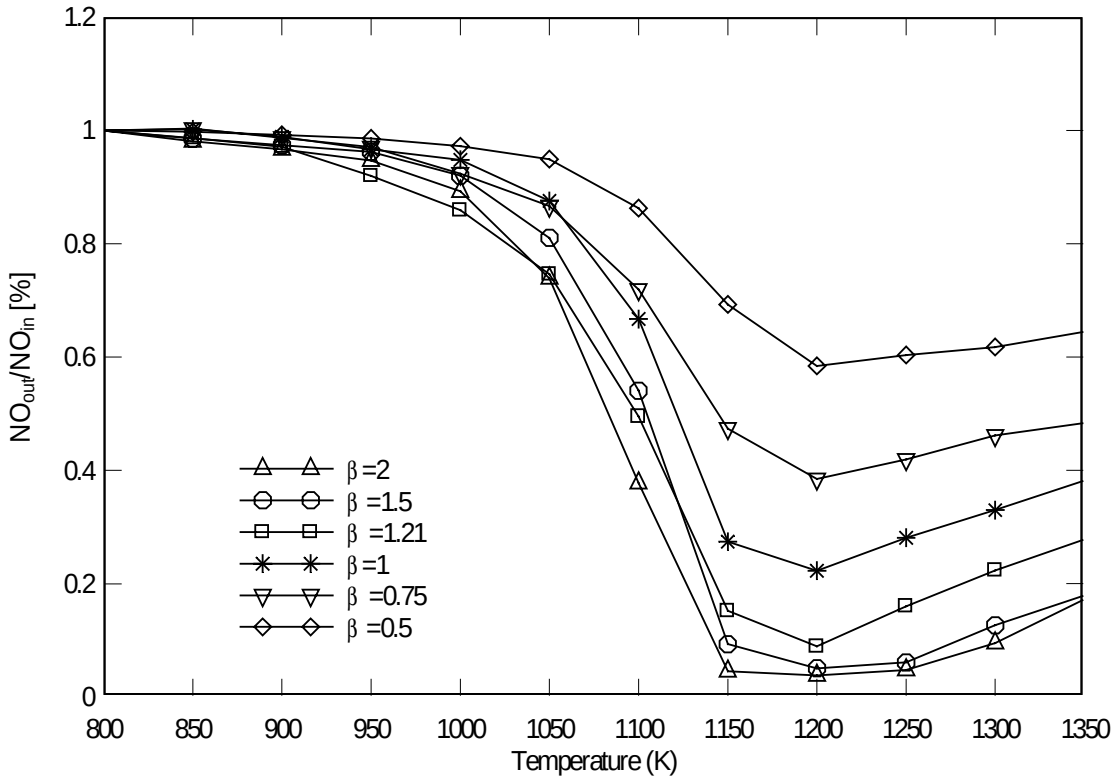

Figure 67. Nitric oxide removal as a function of temperature for 672/T(K) residence time. Inital NO = 330 ppm, NH_3 = 660, 495, 400, 330, 250 and 165 ppm, 1 % O_2.

Figure 67 shows the exit NO as a percentage of the original NO as a function of reactor temperature for various β-ratios (2, 1.5, 1.21, 1, 0.75 and 0.5), 672/T(K) residence time and 1% O_2 concentration. For all cases, higher β-ratio case leads to NO reduction earlier, NO removal "window" widen. Up to 1050 K, NO reduction increase slightly. For further increasing temperature, after 1050 K, the NO reduction increased rapidly, the maximum removal for all cases was at 1200 K. The maximum NO reduction depends on initial β-ratio.

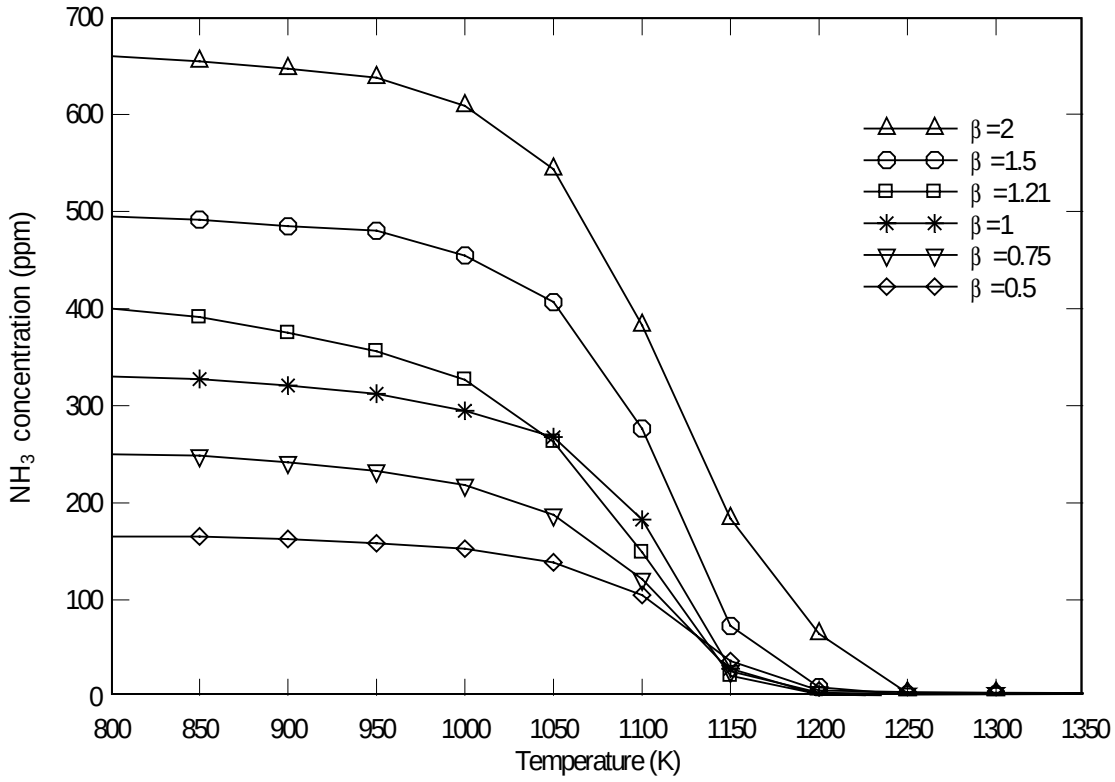

Figure 68. Concentration of ammonia as a function of temperature for 672/T(K) residence time. Inital NO = 330 ppm, NH_3 = 660, 495, 400, 330, 250 and 165 ppm, 1 % O_2.

Figure 68 shows the ammonia (NH_3) concentration as a function of reactor temperature for various β-ratios (2, 1.5, 1.21, 1, 0.75 and 0.5), a 672/T(K) residence time and the 1% O_2 concentration. For all four cases, for temperatures below about 1000 K, the amount of decreasing ammonia was between 0 and 5% with temperature. For further increasing temperature, the ammonia concentration decreased rapidly up to the region where the maximum NO removal occurred at about 1200 K for all cases except two β-ratio case.

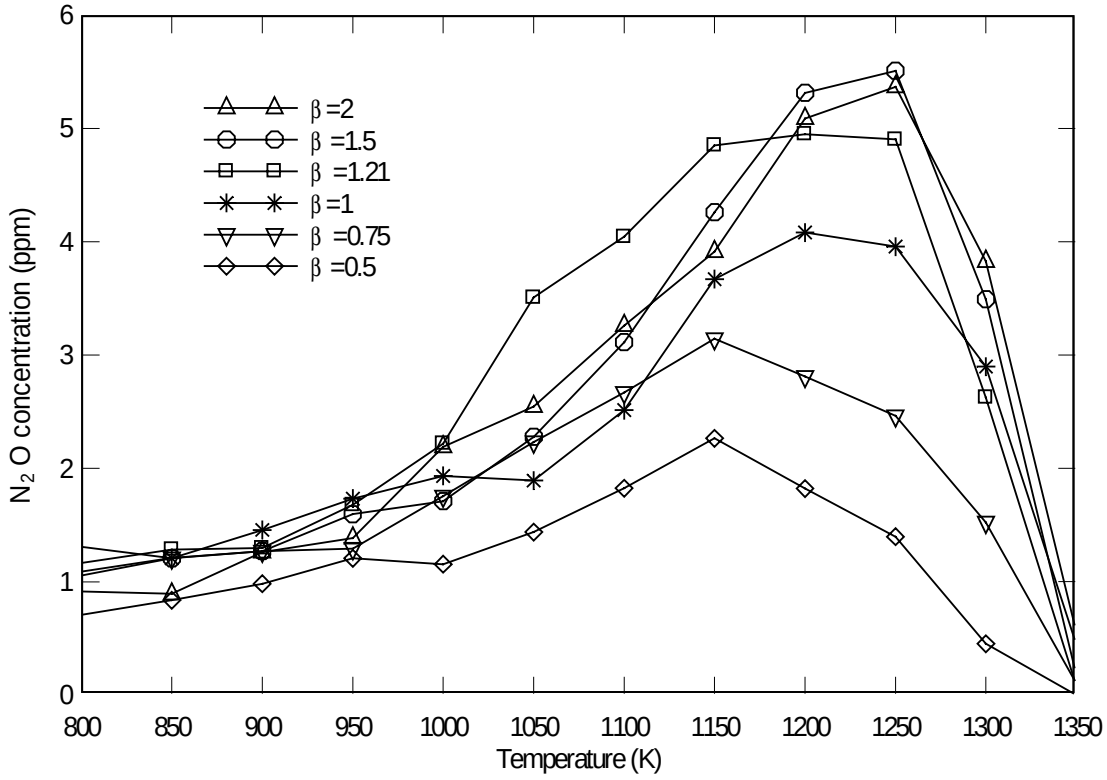

Figure 69. Concentration of nitrous oxide as a function of temperature for 672/T(K) residence time. Inital NO = 330 ppm, NH_3 = 660, 495, 400, 330, 250 and 165 ppm, 1 % O_2.

Figure 69 shows nitrous oxide (N_2O) concentration as a function of reactor temperature for various β-ratio (2, 1.5, 1.21, 1, 0.75 and 0.5), a 672/T(K) residence time and the 1% O_2 concentration. For all cases, for temperatures below about 1000 K, the amount of nitrous oxide increased a little with temperature. For further increasing temperature, nitrous oxide concentration increased up to the region where the maximum NO removal occurred at 1150 K for the cases (β-ratio: 0.75 and 0.5), at 1200 K for the cases (β-ratio: 1 and 1.21) for the 15% O_2 case, at 1250 K for the cases (β-ratio: 1.5 and 2).

6.5 Nitric Oxide Removal Using Ammonia as the Reducing Agent with H_2O and CO_2

To better simulate the urea experiments, both H_2O and CO_2 are needed in the exhaust gases. The water is present due to the urea-water solution, and CO_2 is present as a product of the urea decomposition. To explain the difference between urea and ammonia as the reducing agent, therefore, another three cases were conducted. The first case is with 5% H_2O but without CO_2, the second case is with 5% H_2O and 330 ppm CO_2, and the third cases is with 10% H_2O case without CO_2. All these cases are based on the use of ammonia as the reducing agent.

The inlet gas compositions, which were used for these experimental sets are shown in table 8. This study was performed for the same conditions that are used for the nitric oxide removal process using urea.

Table 8. Experimental test cases for NO removal experiments using ammonia with H_2O and CO_2

NO (ppm)	NH_3 (ppm)	O_2 (%)	H_2O (%)	CO_2 (ppm)	Residence time (sec.)
330	660	1	5	0	672/T(K)
			5	330	
			10	0	

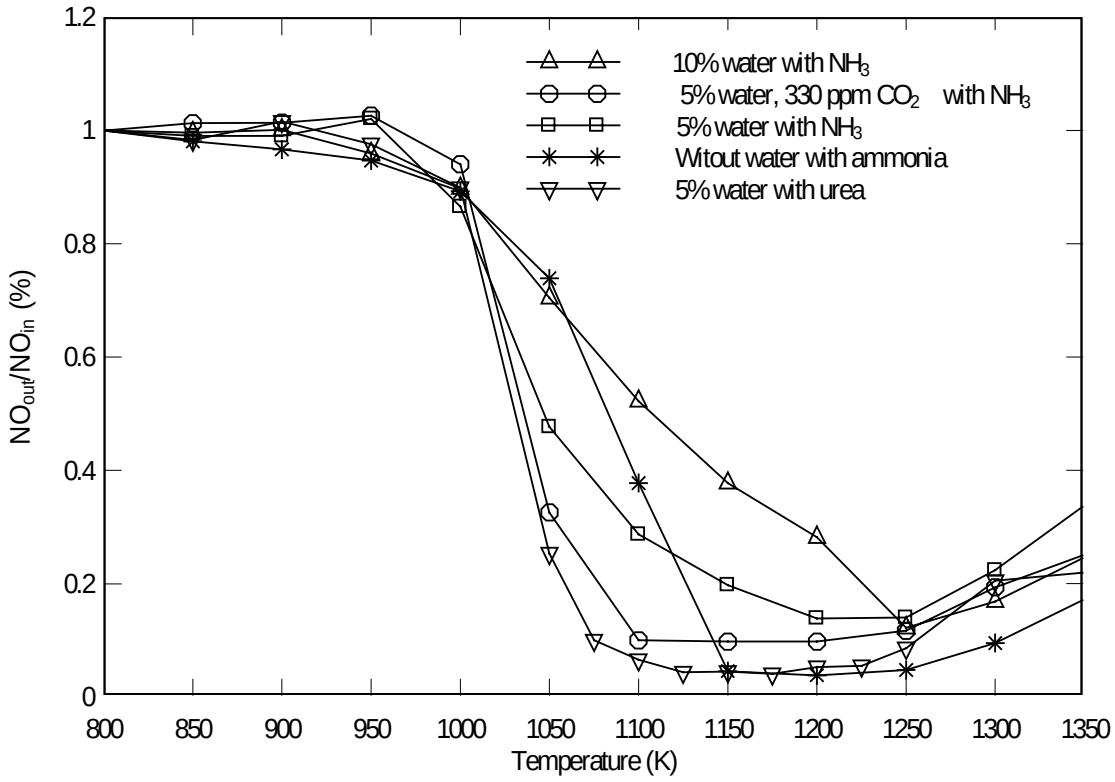

Figure 70. Nitric oxide removal as a function of temperature for 672/T(K) residence time. Inital NO=330 ppm, O_2 = 1%. Symbols Δ: 10% H_2O with NH_3, O: 5% H_2O and 330 ppm CO_2 with NH_3, : 5% H_2O with NH_3, *: without H_2O, CO_2 with NH_3, ∇: urea 330 ppm (5% H_2O).

Figure 70 shows NO reduction as a percentage of the original NO as a function of reactor temperature for a 672/T(K) residence time and the 1% O_2 concentration. Increasing H_2O concentration, for example from 0%, 5% to 10%, degraded the NO reduction. The trend of NO reduction when using 330 ppm urea with 5% H_2O was close to the case with ammonia using 5% H_2O and 330 ppm CO_2. The maximum NO reduction was achieved 95% at between 1100 K and 1200 K when using urea, and was almost the same between 1150 K and 1250 K when using ammonia.

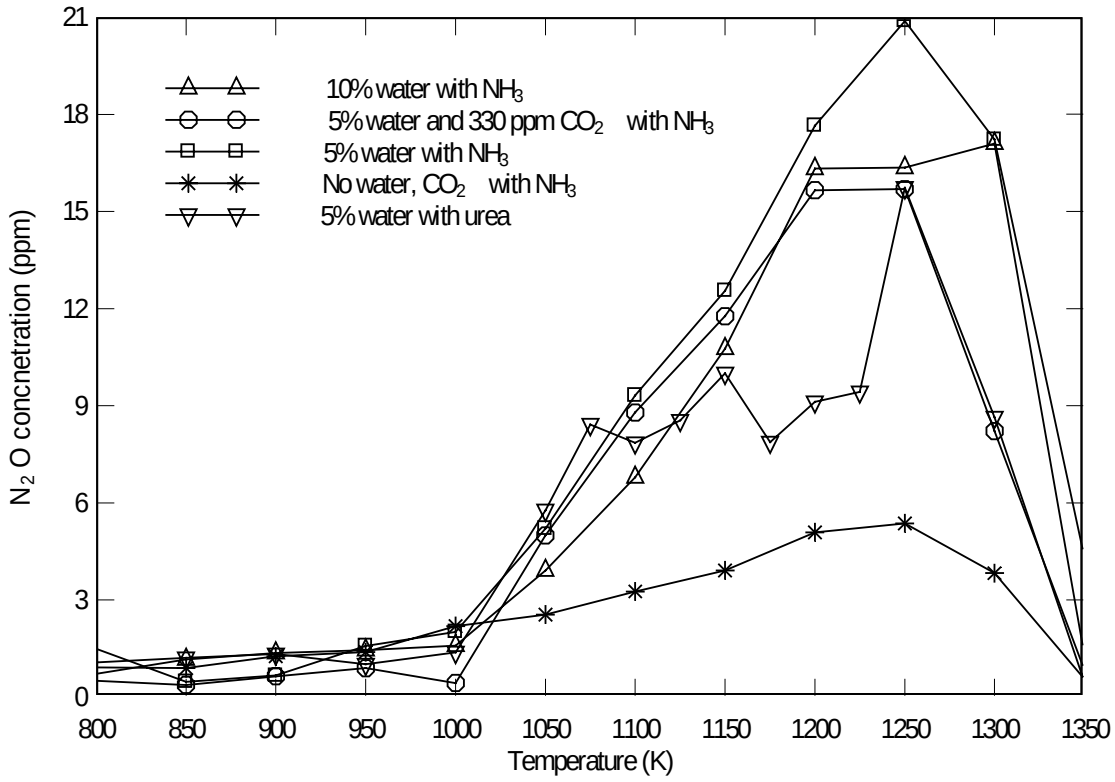

Figure 71. Concentration of nitrous oxide as a function of temperature for 672/T(K) residence time. Inital NO=330 ppm, O_2 = 1%. Symbols Δ: 10% H_2O with NH_3, O: 5% H_2O and 330 ppm CO_2 with NH_3, : 5% H_2O with NH_3, *: without H_2O, CO_2 with NH_3, ∇: urea 330 ppm (5% H_2O).

Figure 71 shows nitrous oxide (N_2O) concentration as a function of reactor temperature for a 672/T(K) residence time and 1% O_2 concentration. For all cases, for temperatures below 1000 K, the amount of nitrous oxide remained nearly constant. For further increasing temperature, nitrous oxide concentration increased up to the region where the maximum NO removal occurred at about 1250 K for all cases. The case of using only ammonia got the lowest nitrous oxide concentration.

7. SUMMARY AND CONCLUSIONS

The use of urea (NH_2CONH_2) and ammonia (NH_3) to remove nitric oxide (NO) from exhaust streams was investigated using a laboratory laminar-flow reactor. The experiments used a number of gas compositions to simulate different combustion gases. The urea was injected into the gases as a urea solution. For the nitric oxide removal (SNCR) experiments, the gas mixture was heated to temperatures between 800 K and 1350 K.

The primary species from urea powder decomposition were HNCO, NH_3, and CO_2. Below 700 K, the species HNCO and NH_3 were dominant. The highest concentration of HNCO was found around 650 K, while NH_3 and CO_2 were detected increasingly after 700 K as HNCO decreased.

The primary species from the decomposition of the urea-water solution were NH_3 and CO_2. The amount of HNCO was small compared to the decomposition of urea powder, but the highest amount of HNCO was found at about 550 K. The NH_3 and CO_2 concentration reached their maximum amount around 600 K. After 600 K, the amount of NH_3 and CO_2 decrease with a temperature rise. From these results, once water was injected, CO_2 started to be produced, while the amount of HNCO decreased rapidly.

The selective non-catalytic reduction (SNCR) process using urea reduced NO over a wide range of oxygen and residence time conditions. This reduction is significantly greater at longer residence time and higher β-ratios. Depending on the temperature, gas composition, residence time, and urea feed rate, removal levels of up to 95% were obtained.

The amount of N_2O is typically 2-3 times higher when using urea compared to the use of ammonia. When using ammonia, the formation of N_2O wasn't much affected by inlet NH_3 concentration. But when using urea, the N_2O increased for higher β-ratio. The higher N_2O values for the urea cases suggest, that HNCO was a product of the urea decomposition.

For an increase of the O_2 concentration from 1% to 5%, the temperature "window" for NO removal was slightly narrowed, shifted toward lower temperature regions and the maximum of NO reduction was decreased.

The higher urea/NO ratio (β-ratio) and longer residence time increased the temperature region of NO reduction and led to higher NO reduction.

Compared to NH_3 as a reducing agent for NO reduction, the urea solution was found to decrease the temperatures (by about 50 K) for maximum NO reduction. Increasing the H_2O percentage to 10% caused the maximum NO reduction to occur at higher temperatures (about 1250 K).

8. RECOMMENDATIONS

- The effect of pressure on NO reduction is needed with different experimental conditions. It is worthwhile to investigate the effect of pressure variation on NO reducing with urea and ammonia.

- The combination of NO and NO_2 should be tested in a NO reducing experiment. There may be interactions between the two species in the NO removal process.

- The production of CO_2 and CO above 1300 K for the NO removal process should be explained.

REFERENCES

1. Rosenberg, H. S., Curran, L. M., Slack, A. V., Ando, J., and Oxley, J. H., 1980, "Post Combustion Methods for Control of NO_x Emissions," Energ. Combust. Sci., **6**, pp. 287–302.

2. Bowman, C. T., 1992, "Control of Combustion-Generated Nitrogen Oxide Emissions; Technology Driven by Regulation," Twenty-Fourth Symposium (International) on Combustion, The Combustion Institute, Pittsburgh, PA, pp. 859–878.

3. Innes, W. B., 1978, *Effect of Nitric Oxide Emissions on Photochemical Smog*, Purad Inc., Upland, CA.

4. Albanese, V., Kellogg, G., and Eisenmann, D.R., 1994, "The Clean Air Advisor," Nalco/Fuel Tech, **3**(2), pp.1–6.

5. Sanyal, A., Light, M., Hong, C. C., Sommer, T. M., and Folsom, B.E., 1993, "Advanced NO_x Control Technologies," Power-Gen Americas 93, Energy and Environmental Research Corporation, Dallas, TX.

6. University of California at Los Angles, Department of Atmospheric Sciences, Photochemical Smog, [www.atmos.ucla.edu/AS2/scrns/12smog.pdf] (02/08/2003).

7. Mincy, J. E., 1992, "Controlling NO_x to Obtain Offsets of Meet Compliance," Fourteenth National Industrial Energy Technology Conference, Houston, TX. pp. 173-176.

8. National Aeronautics and Space Administration (NASA) Facts, 1998 "Ozone: What is it, and why do we care about it " Cape Girardeau, MO, NF–198.

9. Prediction of NOx Emissions in Recovery Boilers – An Introduction to NOx Module, [http://www.psl.bc.ca/downloads/ftp/kilns/Model-NOx.pdf] (02/08/2003).

10. Glarborg, P., Miller, J. A. and Kee, R. J., 1986, "Kinetic Modeling and Sensitivity Analysis of Nitrogen Oxide Formation in Well-Stirred Reactors," Combust. Flame, **65,** pp. 177-202.

11. Miller, J. A. and Bowman, C. T., 1989, "Mechanisms and Modeling of Nitrogen Chemistry in Combustion," Prog. Energy Combust. Sci., **15**, pp**.** 287–338.

12. NO_X Formation Literature Review and Research Project, [http://ecosse.org/jack/Projects/proj2000/degussa/degussa.html], (02/08/2003).

13. Houser, T. J., McCarville, M. E., and Zhou-Ying, G., 1988, " Nitric Oxide Formation from Fuel – Nitrogen Model Compound Combustion," Fuel, **67**, pp. 642–650.

14. Lyon, R. K., and Hardy, J. E., 1986, "Discovery and Development of the Thermal DeNO$_x$ Process," Ind. Eng. Chem. Fundam., **25**, pp. 19–24.

15. Hurst, B. E., 1985, "Thermal DeNOx Technology Update," presented at the Joint Symposium on Stationary Combustion, NO$_x$ Control Proceedings, Boston, MA.

16. Caton, J. A., and Siebers, D.L., 1989, "Comparison of Nitric Oxide Removal by Cyanuric Acid and by Ammonia," Combustion Science and Technology, **65**, pp. 277–293.

17. Perry, R.A., 1989, "System for NO Reduction Using Sublimation of Cyanuric Acid," U.S. Patent No. 4,800,068.

18. Nowroozi-Isfahani, T., 2001, "Theoretical Study on the Mechanism of Removing Nitrogen Oxides Using Isocyanic Acid," M.S. Thesis, East Tennessee State University, Johnson, TN.

19. Arand, J. K., Verdes, R. P., Muzio, L. J., Nigel, L., and Sotter, J. G., 1980, "Urea reduction of NO$_x$ in combustion effluents," U.S. Patent No. 4,208,386.

20. Koebel M. and Elsener M., 1992, "Nitrogen Removal from Waste Gases by Selective Non-Catalytic Reduction Processes (SNCR), Ammonia or Urea as Reducing Agent?" Chemical Engineering and Technology **64**, pp. 934–947.

21. Itaya, Y., Deguchi, S., Takei, M., Yoshino, M., and Matsuda, H., 1997 " NO Reduction Behavior by Urea Solution Injection in the Tubular Reactor" 4th International Conference on Technologies and Combustion for a Clean Environment, Lisbon, Portugal, **II**, pp. 7–12.

22. Lyon, R. K., 1975, "Method for the Reduction of the Concentration of NO in Combustion Effluents Using Ammonia," U.S. Patent No. 3,900,554.

23. Saliman, S., and Hanson, R. K., 1980, "A Kinetic Study of NO Removal from Combustion Gases by Injection of NHi-Containing Compounds," Combustion Science and Technology, **23**, pp. 225–230.

24. Miller, J. A., and Bowman, C. T., 1989, "Mechanism and Modeling of Nitrogen Chemistry in Combustion," Prog. Energy Combustion Sci., **15**, pp. 287–338.

25. Dooren, V. J., Bian, J., and Tiggelen, P. J., 1994, "Comparison of Experimental and Calculated Structures of an Ammonia-Nitric Oxide Flame: Importance of the NH_2 + NO Reaction," Combustion and Flame, **98**, pp. 402–410.

26. Smith, T., 1995, "Experiments on the Selective Non-Catalytic Reduction of Nitric Oxide," Ph.D. Dissertation, Texas A&M University, College Station, TX.

27. Kasuya, F., Glarborg, P., Johnsson, J. J. and Kim, D., 1995, "The Thermal DeNOx Process: Influence of Partial Pressures and Temperature," Chemical Engineering Science, **50**(9), pp. 1455–1466.

28. Caton, J. A., Narney, II, J. K., Cariappa, C., and Laster, W. R., 1995, "The Selective Non-Catalytic Reduction of Nitric Oxide Using Ammonia at up to 15% Oxygen," Canadian Journal of Chemical Engineering, **73**(3), pp. 345–350.

29. Kjaergaard, K., Glarborg, P., Dam-Johansen, K., 1996, "Pressure Effects on the Thermal DeNOx Process," 26th Symposium on Combustion, The Combustion Institute, Naples, Italy, pp. 2067–2074.

30. Glarborg, P., Dam-Johansen, K., and Miller, J. A., 1995, "The Reaction of Ammonia with Nitrogen Dioxide in a Flow Reactor: Implications for the NH_2 + NO_2 Reaction," International Journal of Chemical Kinetics, **27**, pp. 1207–1220.

31. Alzueta, M., Rjel, H., Kristensen, P., Glarborg, P. and Dam-Johansen, K., 1997, "Laboratory Study of the $CO/NH_3/NO/O_2$ System: Implications for Hybrid Reburn/SNCR Strategies," Energy & Fuels, **11**, pp. 716–723.

32. Rota, R., Éverton, F. Dorota, Z., Morbidelli, A., and Carra, S., 2000, "Analysis of the Thermal $DeNO_x$ Process at High Partial Pressure of Reactants," Chemical Engineering Science, **55**, pp. 1041–1051.

33. Dill, J. W., and Sowa, W. A., 1992, "Nitric Oxide Reduction Using Ammonia Injection: Numerical Modeling Comparisons," 1992 Spring Meeting of the Western States Section of the Combustion Institute, Corvallis, OR, paper no. 92–89.

34. Smith, T. S., and Caton, J. A., 1995, "Reductions and Conversions of Nitrogen Compounds Using Ammonia in a Selective Non-Catalytic Process for Exhaust Streams at Pressures up to 515 kPa," *Proceedings of the 1995 Central States Section/Combustion Institute Spring Technical Meeting*, San Antonio, TX, Paper No. 95S–015, pp. 69–74.

35. Wendt, J., Linak, W., Groff, P., and Srivastava, R., 2001, "Hybrid SNCR-SCR Technologies for NO_x Control: Modeling and Experiment," AIChE Journal, **47**(11), pp. 2603–2617.

36. Schaber, P. M., Colson, J., Higgins, S., Dietz, E., and Thielen, D.,"Study of the Urea Thermal Decomposition (pyrolysis) Reaction and Importance to Cyanuric Acid Production," [www.iscpubs.com/articles/al/a9908sch.pdf], (accessed on Jan. 10, 2003).

37. Fang, H., and DaCosta, H., 2002, "Thermolysis Characterization of Urea–SCR," presented at the DEER Workshop, San Diego, CA.

38. Caton, J. A., and Siebers, D. L., 1989, "Comparison of Nitric Oxide Removal by Cyanuric Acid and by Ammonia," Combustion Science and Technology, **65**, pp. 277–293.

39. Jødal, M., Nielsen, C., Hulgaard, T., and Dam-Johansen, K., 1990, "Pilot-Scale Experiments with Ammonia and Urea as Reductants in Selective Non-Catalytic Reduction of Nitric Oxide," The Twenty-Third Symposium (International) on Combustion, The Combustion Institute, Pittsburgh, PA, pp. 237–243.

40. Alzueta, M. U., Bilbao, R., Millera, A., Oliva, M., and Ibanez, J. C., 1998, "Interactions Between Nitric Oxide and Urea Under Flow Reactor Conditions," Energy and Fuels, **12**, pp. 1001–1007.

41. Itaya, Y., Deguchi, S., Takei, M., Yoshino, M., and Matsuda, H., 1997, "NO Reduction Behavior by Urea Solution Injection in the Tubular Reactor," 4th International Conference on Technologies and Combustion for a Clean Environment, Lisbon, Portugal, **II**, pp. 7–12.

42. Srivatsa, S., and Caton, J. A., 1998, "Selective Non-Catalytic Reduction of Nitric Oxides by Urea: Effects of Oxygen and Carbon Monoxide," *Proceedings of the 1998 Central States Section, Combustion Institute Spring Technical Meeting*, Lexington, KY, Paper No. 98–53, pp. 273–278.

43. Teixeira, D. P., Muzio, L. J., and Montgomery, T. A., 1991, "Effect of Trace Combustion Species on SNCR Performance," presented at the 1991 AFRC/JFRC International Conference on Environmental Control of Combustion Processes, Honolulu, HI, paper no. 20.

44. Chen, S. L., Ho, L., Maly, P. M., Payne R., and Seeker, W. R.,1993, "Methods for controlling N_2O emissions and for the reduction of NO_x emissions in combustion systems while controlling N_2O emissions," presented at the Joint EPRI/EPA Symposium on Stationary NOx Control, Bal Harbor, FL.

45. Brouwer, J., Heap, M. P., Pershing D. W., and Smith, P. J., "A Model for Prediction of Selective Non-Catalytic Reduction of Nitrogen Oxides by Ammonia, Urea, and Cyanuric Acid with Mixing Limitations in the Presence of CO," [http://opus.utah.edu/~smith/ResearchPapers/CIitaly/CIitaly.html#title] (accessed on Feb. 8, 2003).

46. Rota, R, Antos, D., Éverton, F., and Morbidelli, M., 2002, "Experimental and Modeling Analysis of the NO_xOUT Process," Chemical Engineering Science, **57**(1), pp. 27–38.

47. Glarborg, P., Kristensen, P. G., Jensen, S. H., and Dam-Johansen, K., 1994, "A Flow Reactor Study of HNCO Oxidation Chemistry," Combustion and Flame, **98**, pp. 241–258.

48. Gentemann, A., 2001, "Flow Reactor Experiments on the Selective Non-Catalytic Removal of Nitrogen Oxides," M.S. Thesis, Texas A&M University, College Station, TX.

49. Mangan, J., 2000, "The Calibration and Use of Mass Flow Controllers for Use in NO_x Reduction Experiments," MEEN 485 Report, Texas A&M University, College Station, TX.

50. Srivatsa, S., 1998, "The Selective Non-Catalytic Reduction of NO_x Using Urea as the Chemical Agent: An Experimental Approach," M.S. Thesis, Texas A&M University, College Station, TX.

51. Baek. K., 2003, "Selective Non-Catalytic Reduction (SNCR) of NO_x by Ammonia Injection: A Collective Study through Experiments and Numerical Models," Ph.D. Dissertation, Texas A&M University, College Station, TX.

APPENDIX 1

MASS FLOW CONTROLLERS CALIBRATION PROCEDURE

To calibrate mass flow controllers, a thermometer to measure water and ambient temperature, a ruler to measure the height of water level, a timer to measure time, flasks and a basin to contain H_2O were prepared. As a first step for preparing the calibration, MFC should turn on and let it warm and add water to the basin. After above pre-setup was made, checked the MFC reading value and confirmed no gas flowing at zero set. Then, chose the value that planned to measure, which was selected five or six flow measurements.

As a first step of calibration, a flask was filled with water completely, and covered the top of the flask securely. A flask, which was overturned, was secured by a

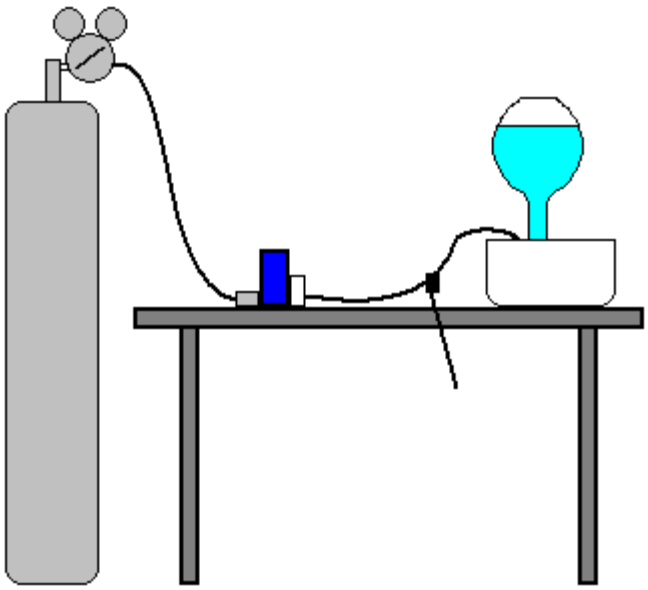

Figure 72. Calibration setup of the mass flow controllers.

holding device as shown in figure 72. After set the desired MFC value, let the gas flow until reaching the steady state. After reaching steady state, the tube of gas flowing placed at the bottom of the flask. Inserting the tube to the flask, holding a clock on at the same time. While filling gas into the flask, the output value was recorded to compare the set flow rate. Once a reasonable amount of gas was in the flask, taking out the tube from the flask and stop the timer simultaneously. Measured the height of the column of water in the flask. Weighted the flask to obtain the weight left after filling out gas.

With all data from above procedure, the calibration produced a linear curve where the slope of the trend line is nearly one.

APPENDIX 2

UREA-WATER SOLUTION FEEDING SYSTEM CALIBRATION PROCEDURE

1. Experiment Setup

The urea solution was placed in a 250 ml plastic flask and using a calibrated pressure control gauge was pressurized with N_2 gas as shown below. The urea solution flowed out due to the nitrogen gas pressure and then flowed through an injection pipette. The solution was vaporized by wrapped heating tape and then injected into the

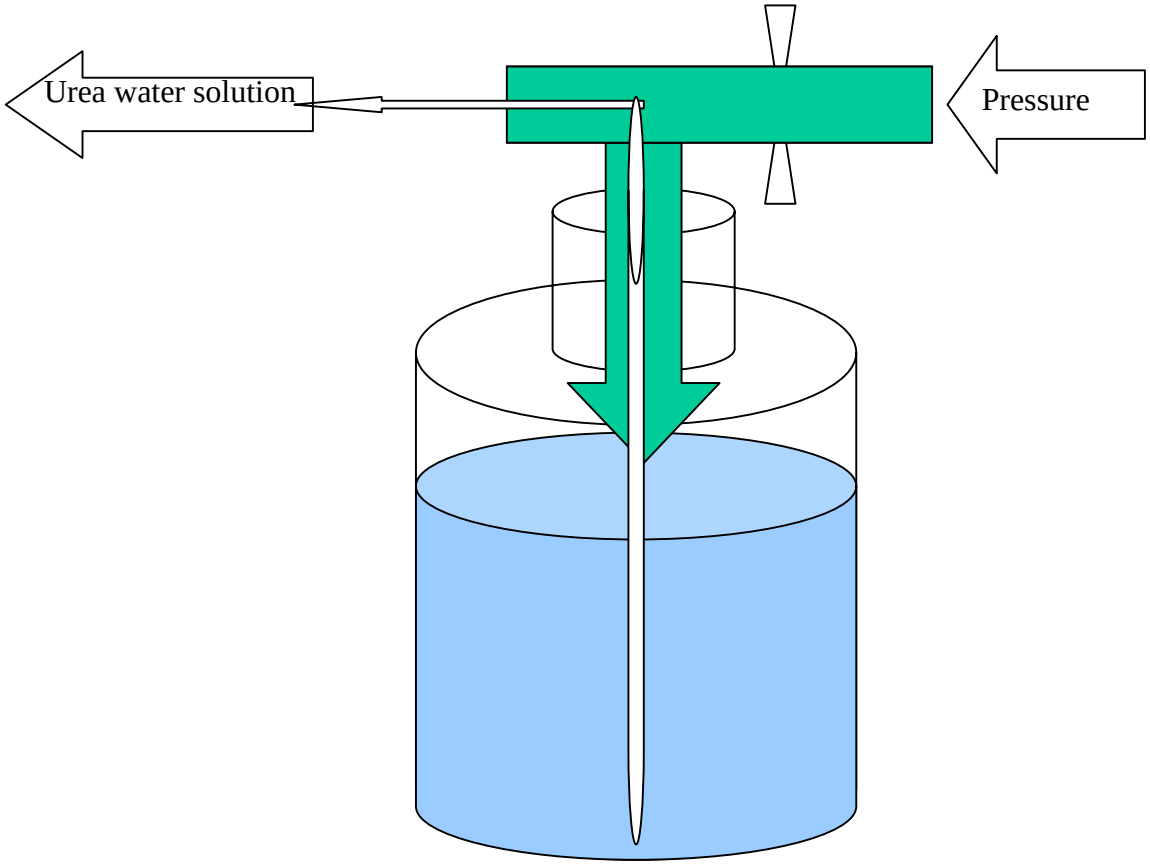

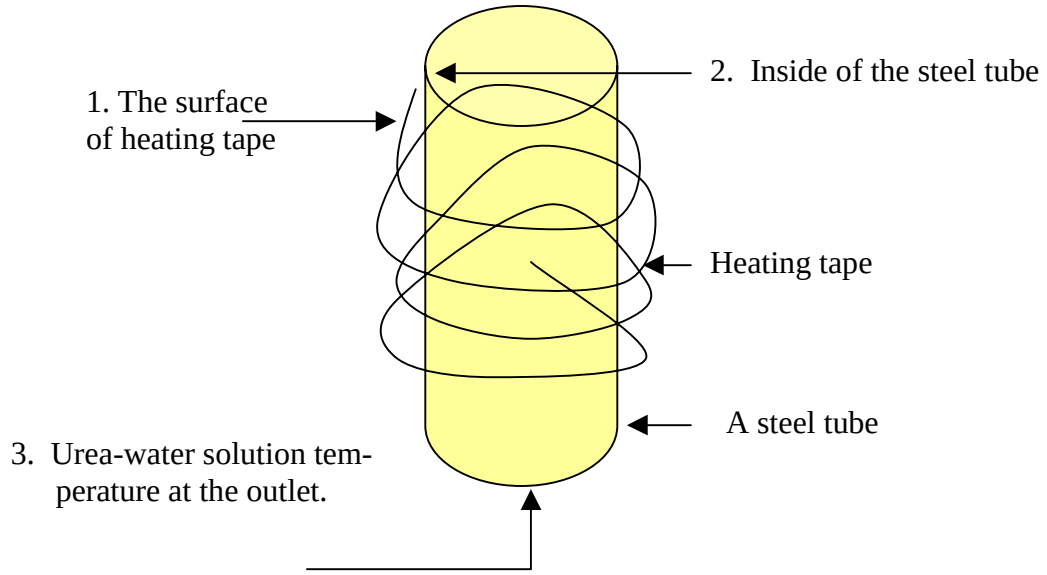

Figure 73. A steel tube wrapped by heating tape.

simulated exhaust gas stream in the pre-heat section before entering the reactor unit. Figure 73 shows a steel tube wrapped by the heating tape.

2. Calibration Procedure

The pressure regulator, connected with the N_2 gas cylinder, which controls the urea-solution feeding rate. Using the pressure regulator, which has range 0 to 5 psi, made possible of controlling low feeding rate as seen in table 9. Using the pressure regulator, outlet pressure of regulator set from 4 psi to 0.05 psi. Setting 0.05 psi as the pressure regulator resulted in 0.0046ml/min. After flowing through an injection pipette, before entering the reactor, urea-water solution should be vaporized. Inserted a steel tube (length: 30 cm), between an injection pipette and the reactor, which wrapped the steel tube by heating tape. Calibrated the temperature of heating tape, namely, the surface of

the steel tube, inside of the steel tube, and urea solution temperature in the outlet in table 10.

Table 9. Calibration of feeding rate using N_2 gas

Set pushing pressure (psi)	Time (min.)	Amount of water (ml.)	Feeding rate (liter/min.)
4	127.2	250	1.965
3	164.48	250	1.520
1.2	85.5	125	1.462
0.7	133.4	71	0.532
0.2	164.3	48	0.292
0.15	318.2	29	0.091
0.1	188.04	14	0.074
0.08	377.5	25	0.066
0.05	430.27	20	0.046

Table 10. Calibration of temperature in the heating tape, inside of the tube, and in the outlet of the tube

Heating tape controller (set point).	1. Temperature of heating tape (^{O}C).	2. Inside of steel tube temp. (^{O}C).	3. Water/vapor temperature (^{O}C).
15	55.3	49.1	42.9
20	65.6	62.7	55.8
25	80.3	75	68.8
30	90.6	86.2	80.2
35	101.6	99	95.9
40	113.3	109.5	100.3
45	123.7	120.1	100.3
50	138.6	126	100.3
55	154.6	133.6	100.3
60	166.9	139.9	101.6

.

The temperatures of the heating tape and inside surface of the steel tube increased with higher set point, but the output temperature of the water solution remained steady after reaching 100^{o}C as shown in figure 74.

After deciding a feeding rate and set point of heating tape controller from table 9 and 10, calculated how much urea powder should be mixed with some amounts of water. For example, contained 200 ml of H_2O in a flask, to give desired urea concentration (330 ppm) at a fixed feed rate 0.05ml/min, the 4.863g mixed with 200ml of water. To check the percentage of H_2O in the reactor, calculated H_2O percentage corresponded with feeding rate (ml/min.) in table 11, which shows in figure 75.

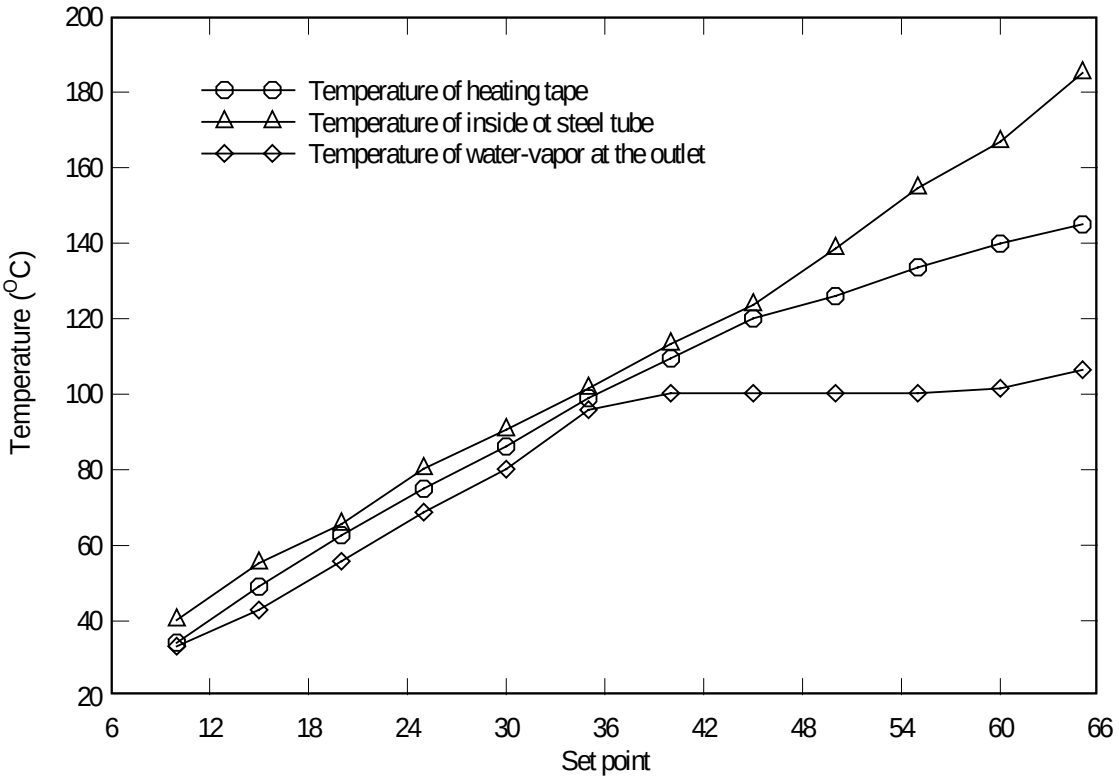

Figure 74. Temperatures in the heating tape, inside of the tube, and in the outlet of the tube Vs set of heating tape controller.

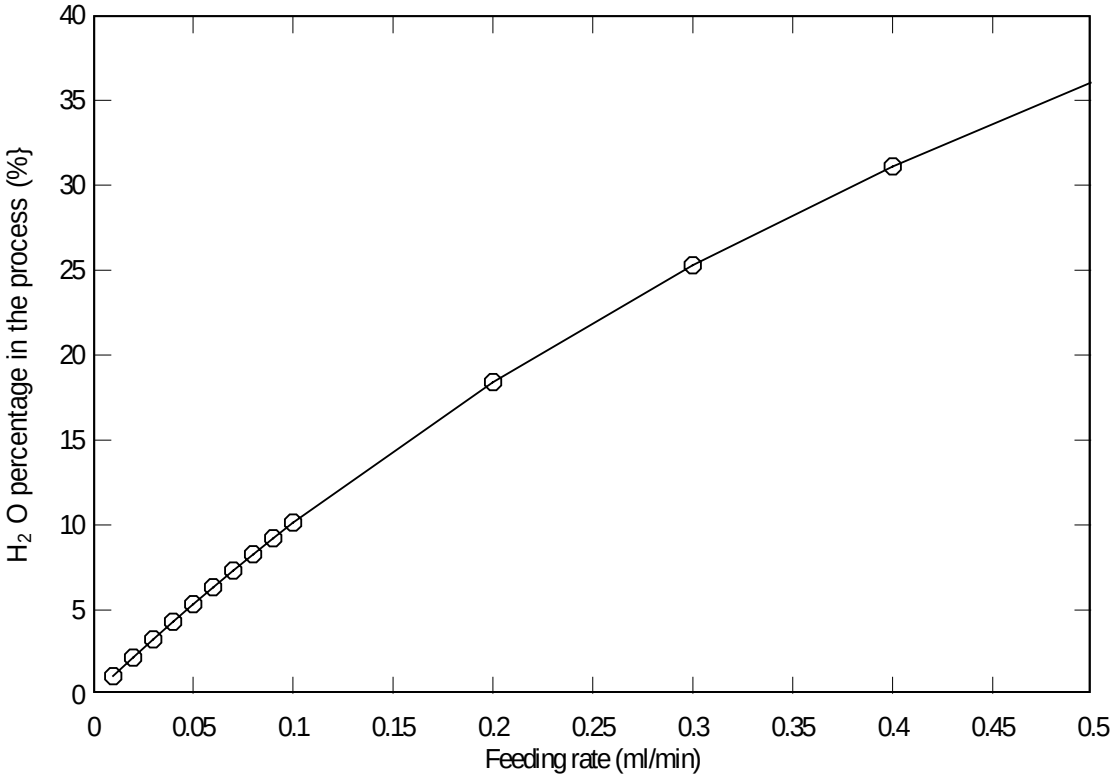

Figure 75. H_2O perecentage vs feeding rate (ml/min) in the reactor

Table 11. H_2O percentage in the reactor vs feeding rate (ml/min.)

ml/min	Mole Flow	Total Mole Flow	Mole Fra.H_2O	H_2O (%)	Concentration (ppm)
0.01	5.540E-07	4.908E-05	0.0111	1.116	11161
0.02	1.108E-06	4.908E-05	0.0220	2.208	22076
0.03	1.661E-06	4.908E-05	0.0327	3.275	32752
0.04	2.216E-06	4.908E-05	0.0430	4.320	43198
0.05	2.770E-06	4.908E-05	0.0530	5.342	53421
0.1	5.539E-06	4.908E-05	0.1010	10.142	101424

APPENDIX 3

THE FURNACE TEMPERATURE DISTRIBUTION AND RESIDENCE TIME CALCULATION

MFC (Mass Flow Controller) allowed 1100 sccm to flow. The furnace was turned on and set at the elevated temperature and waited until the steady state was reached. The temperature distribution was taken at 2 cm increments. The K-type thermocouple was inserted inside of the furnace from the inlet to the outlet side. To determine the heating length, three different tests were run with section 1 of the furnace

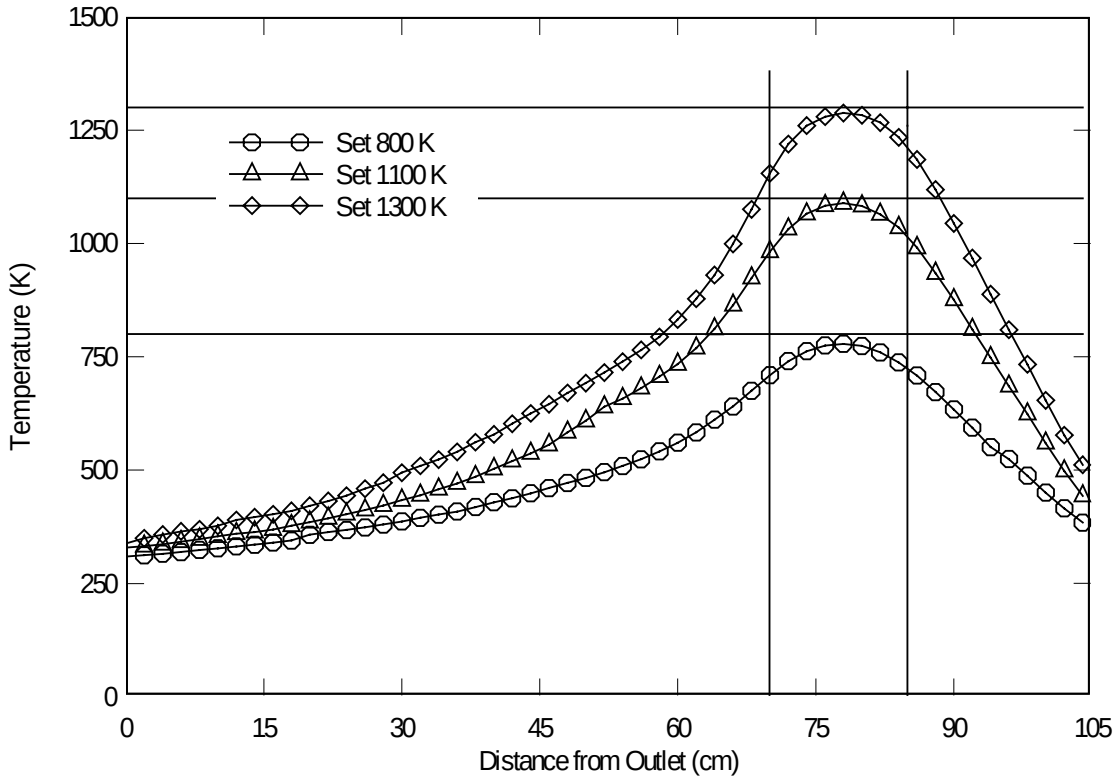

Figure 76. Axial temperature distribution with zone 1 heated at 800, 1100 and 1300 K.

activated, sections 1 and 2, and sections 1,2, and 3 at a low temperature (800 K), mid temperature (1100 K) and high temperature (1300 K). These three temperature profiles were compared to determine the heating length.

1. Zone 1 Activated Result

Figure 76 shows the temperature distributions resulting from zone 1 being activated. The measured temperature compared to the set temperature for the heating zone was a little lower since the furnace was not sealed up perfectly, which could be affected by ambient temperature. Table 12 shows the calculation of residence time. The term "accuracy" was used as acceptance level. So, with 95% accuracy, the residence time for 1 heating zone was 102/T(K). This term was used for NO removal urea to investigate the effect of residence time.

Table 12. Residence time calculation for zone 1 activated

	Total Flow (sccm)	Set Temp.(K)	Accuracy (%)	Length (cm)	Diameter (cm)	Area (cm^2)	Volume (cm^3)	Residence Time (sec.)
1 HZ	1100	800	85	16	1.0	0.79	12.57	204 /Temp.
	1100	800	90	12	1.0	0.79	9.42	153 /Temp.
	1100	800	95	8	1.0	0.79	6.28	102 /Temp.
	1100	1100	85	16	1.0	0.79	12.57	204 /Temp.
	1100	1100	90	12	1.0	0.79	9.42	153 /Temp.
	1100	1100	95	8	1.0	0.79	6.28	102 /Temp.
	1100	1300	85	18	1.0	0.79	14.14	230 /Temp.
	1100	1300	90	14	1.0	0.79	11.00	179 /Temp.
	1100	1300	95	8	1.0	0.79	6.28	102 /Temp.

2. Zones 1 and 2 Activated Result

Figure 77 shows the temperature distributions resulting from zone 1 and 2 being activated. The measured temperature compared to the set temperature for the heating zone was a little higher at the center and a little lower at both end of heating zones.

Table 13 shows the calculation of residence time. The term “accuracy” was used as acceptance level. So, with 95% accuracy, the residence time for 1 and 2 heating zone was 442/T(K), which came from (460+407+460)/3 of 95% accuracy in table 14. This term was used for NO removal urea to investigate the effect of residence time.

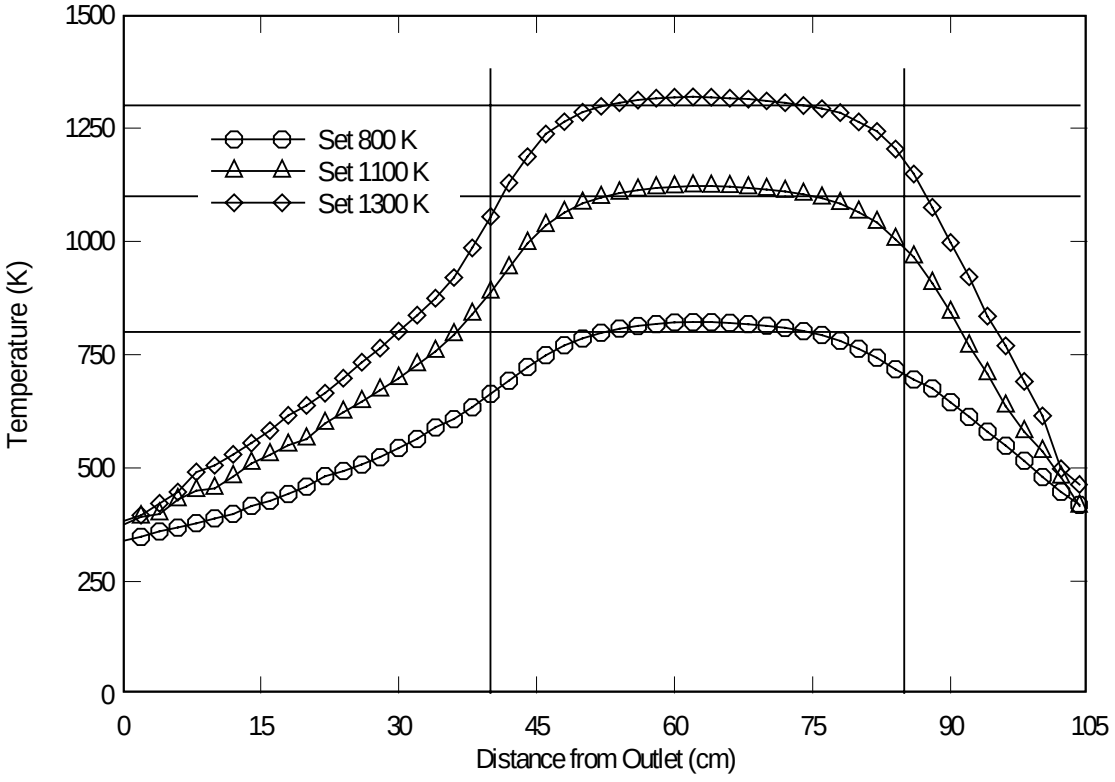

Figure 77. Axial temperature distribution with zones 1 and 2 heated at 800, 1100 and 1300 K.

Table 13. Residence time calculation for zones 1 and 2 activated

	Total Flow (sccm)	Set Temp.(K)	Accuracy (%)	Length (cm)	Diameter (cm)	Area (cm^2)	Volume (cm^3)	Residence Time (sec.)
1, 2 HZ	1100	800	85	44	1.0	0.79	34.56	562 /Temp.
	1100	800	90	38	1.0	0.79	29.85	485 /Temp.
	1100	800	95	36	1.0	0.79	28.27	460 /Temp.
	1100	1100	85	44	1.0	0.79	34.56	562 /Temp.
	1100	1100	90	40	1.0	0.79	31.42	511 /Temp.
	1100	1100	95	32	1.0	0.79	25.13	407 /Temp.
	1100	1300	85	44	1.0	0.79	34.56	562 /Temp.
	1100	1300	90	40	1.0	0.79	31.42	511 /Temp.
	1100	1300	95	36	1.0	0.79	28.27	460 /Temp.

3. Zones 1, 2 and 3 Activated Result

Figure 78 shows the temperature distributions resulting from zone 1, 2 and 3 being activated. The measured temperature compared to the set temperature for the heating zone was a little higher at the center and a little lower at both end of heating zones.

Table 14 shows the calculation of residence time. The term “accuracy” was used as acceptance level. So, with 95% accuracy, the residence time for 1, 2 and 3 heating zone was 672/T(K), which came from (638+689+689)/3 of 95% accuracy in table 15. This term was used for NO removal urea to investigate the effect of residence time.

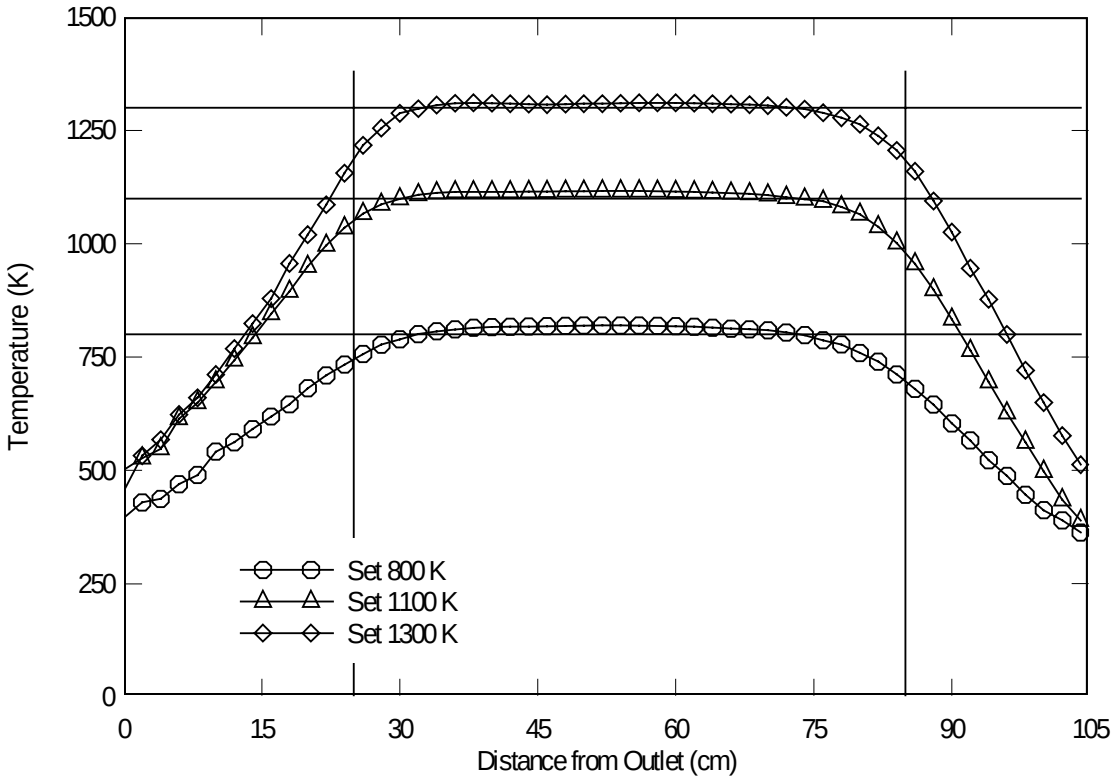

Figure 78. Axial temperature distribution with zones 1, 2 and 3 heated at 800, 1100 and 1300 K.

Table 14. Residence time calculation for zones 1, 2 and 3 activated

	Total Flow (sccm)	Set Temp.(K)	Accuracy (%)	Length (cm)	Diameter (cm)	Area (cm^2)	Volume (cm^3)	Residence Time (sec.)
1,2,3 HZ	1100	800	85	60	1.0	0.79	47.12	766 /Temp.
	1100	800	90	58	1.0	0.79	45.55	740 /Temp.
	1100	800	95	50	1.0	0.79	39.27	638 /Temp.
	1100	1100	85	66	1.0	0.79	51.84	843 /Temp.
	1100	1100	90	62	1.0	0.79	48.69	792 /Temp.
	1100	1100	95	54	1.0	0.79	42.41	689 /Temp.
	1100	1300	85	62	1.0	0.79	48.69	792 /Temp.
	1100	1300	90	58	1.0	0.79	45.55	740 /Temp.
	1100	1300	95	54	1.0	0.79	42.41	689 /Temp.

APPENDIX 4

THE FTIR CALIBRATION DATA FOR THE DIFFERENT SPECIES

1. **Introduction**

FTIR is used primarily for qualitative and quantitative analysis of organic compounds, and also for determining the chemical structure of many inorganic. It can be utilized to quantify some components of an unknown mixture. It can be applied to the analysis of solids, liquids, and gases. The term Fourier Transform Infrared Spectroscopy (FTIR) refers to a fairly recent development in the manner in which the data is collected and converted an intensity vs. time spectrum into an intensity vs. frequency spectrum. Today's FTIR instruments are computerized which makes them faster and more sensitive than the older disperse instruments.

1.1 Principle of Operation

1. Absorption in the infrared region results in changes in vibrational and rotational status of the molecules.
2. The absorption frequency depends on the vibrational frequency of the molecules, whereas the absorption intensity depends on how effectively the infrared photon energy can be transferred to the molecule, and this depends on the change in the dipole moment that occurs as a result of molecular vibration.
3. A molecule will absorb infrared light only if the absorption causes a change in the dipole moment.

4. All compounds, except for elemental diatomic gases such as N_2, H_2 and O_2, have infrared spectra and most components present in a flue gas can be analyzed by their characteristic infrared absorption.
5. For quantification of several components absorbing in the midinfrared region (400 - 5000 cm-1), either conventional disperse infrared analysis or Fourier transform infrared (FTIR) spectroscopy can be used.

2. Experiment Facilities: FTIR and Software

2.1 FTIR:

BioRad FTS- 60A has provided an especially effective alternative to generating time-resolved spectra in a point by point fashion in the infrared region. Briefly, the mirrors of the interferometer in the FTIR spectrometer are moved in a periodic fashion as to effect steps in the path length difference between the arms of the interferometer. At each step a transient is collected with a sampling interval of typically 200 ns. Thus an array of interferograms is generated from which transient spectra from 1250 cm-1 to 2250 cm-1 for selected time intervals are extracted.

2.2 Software: Digilab Win-IR Pro 3.3

This software supports export to the thermo galactic SPC Format. Imaging experiments using focal plane array detectors are made possible by Win-IR Pro's ability to handle large arrays of data efficiently. Win-IR Pro allows to view the stack of infrared images as a movie, as "flat view" or as a 3D display.

3. Calibration Method

The first step of a quantitative analysis problem is to “make-up” the standards to be used for the calibration of the quantitative analysis method. Ideally, the standards should come directly from the production facility so that they reflect the actual processing conditions. But, in most cases this is not feasible, so the selection of samples to be used for a calibration must adequately cover the expected range variation.

The standards must be composed of linearly independent concentration data. When selecting samples to be used for calibration standards in a system composed of multiple species. All component concentrations should be represented the same number of times in the calibration standards. Finally, the analysis should be tested frequently as part of a normal operating procedure to verify its validity.

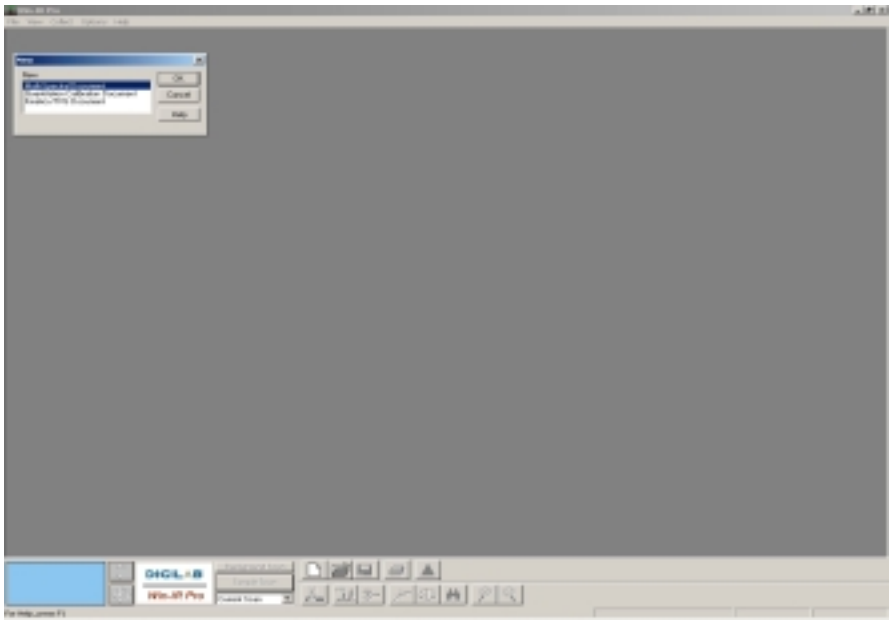

Figure 79. A window after clicking “ New” on the “File” menu.

3.1 Calibration procedure using WIN-IR pro software

(1) Go to “ File” then click “New” as shown in figure 79.

(2) There are three section to click (Multi–spectral document, Quantification Calibration Document, Kinetics/TRS Document).

(3) When a new quantification document is opened as shown in figure 80: displaying a standard spectrum (on the upper left part), for displaying calibration curve (on the upper right part), and displaying spreadsheet of the spectra (on the bottom).

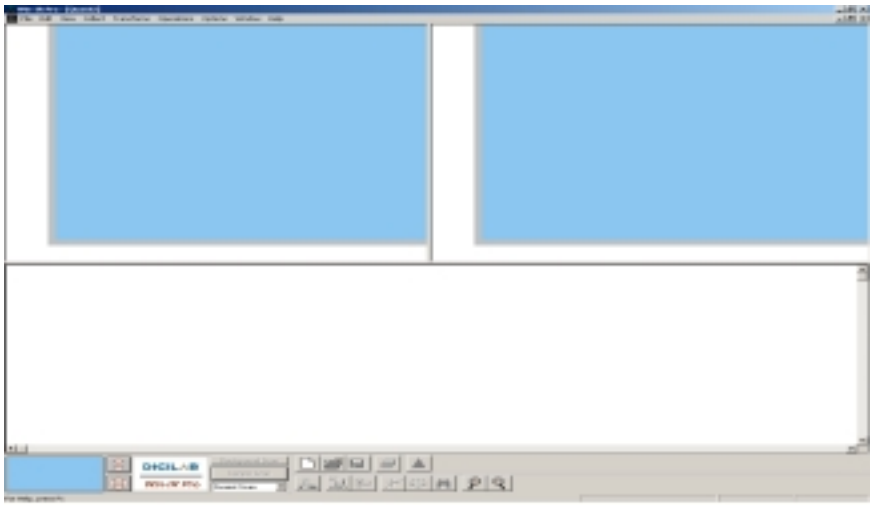

Figure 80. A window when a new quantification document is opened.

(4) Open previous saved. Copy all spectra by clicking from the spreadsheet window. Paste these documents to the quantitative document as shown in figure 81.

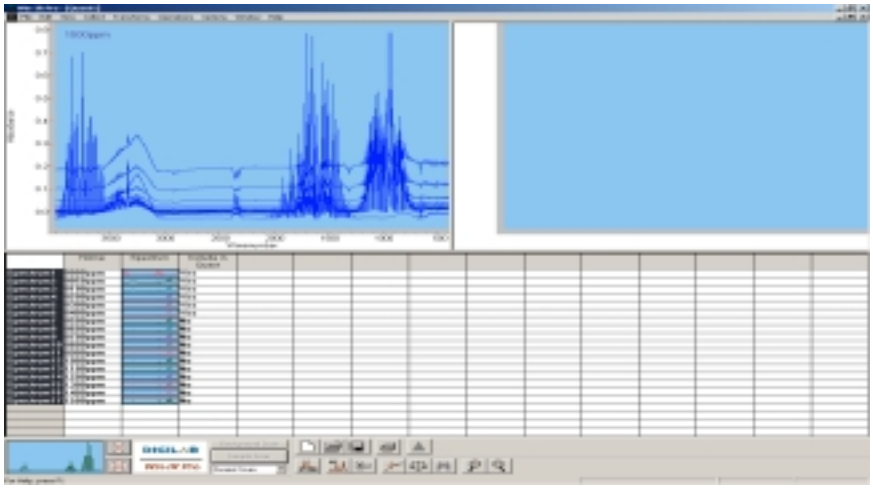

Figure 81. A window after pasting all documents to the quantification document.

(5) Click right mouse button in a peak of the trace spectrum at a certain wavenumber in the spectrum window, select “New” and click “ Component” as shown in figure 82.

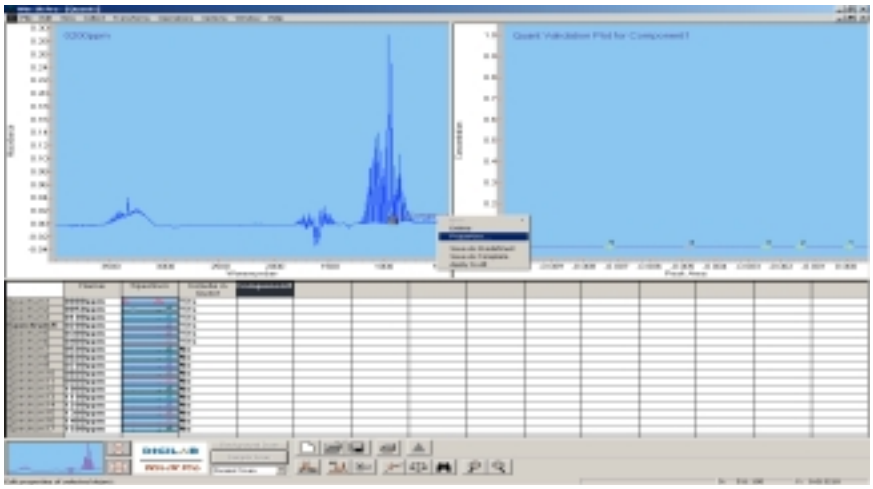

Figure 82. A window shown after clicking “Component”, after selecting “New” at a certain wavenumber.

(6) To produce a calibration document with peak heights versus concentrations, click the right mouse button in the name of the peak of spectrum, select “Properties” as shown in figure 83.

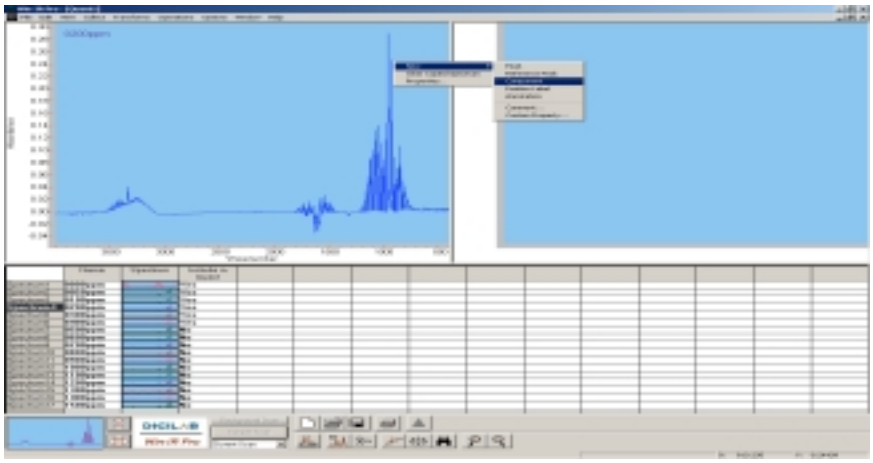

Figure 83. A window shown after selecting “Properties” after clicking “New”.

(7) After clicking “Properties”, a dialog box pop up as shown in figure 84.

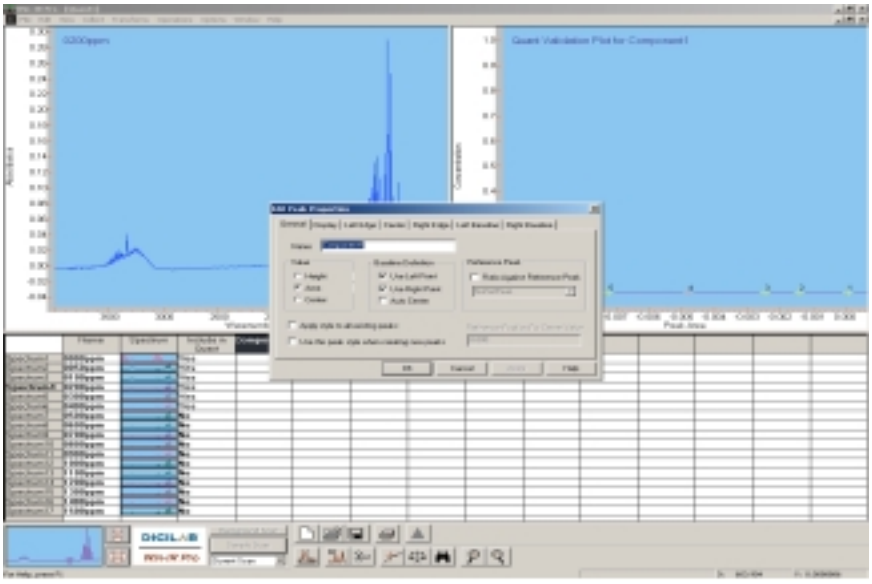

Figure 84. A window shown after clicking “ Properties”.

(8) In the “General” tap page of the box shown below, mark for “height” under “value” group, and uncheck for all items under “baseline definition and click “ OK” as shown in figure 85.

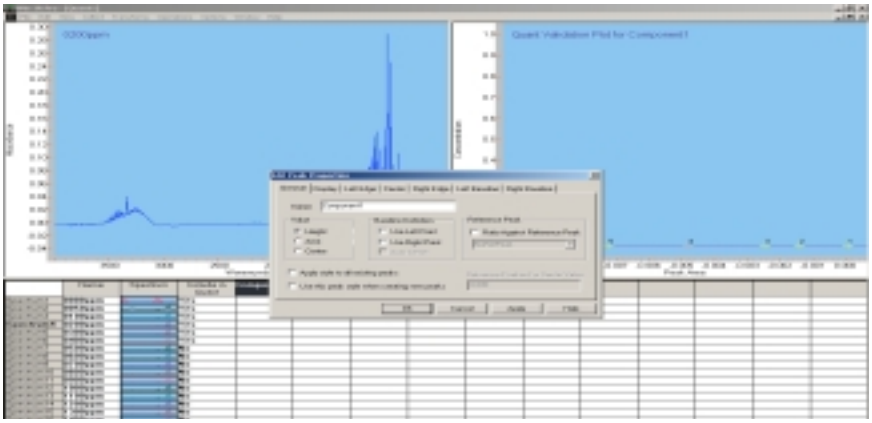

Figure 85. A window shown after marking “height” under “Value” group.

(9) This operation allows to calibrate for the chosen peak height from the zero base line as shown in figure 86.

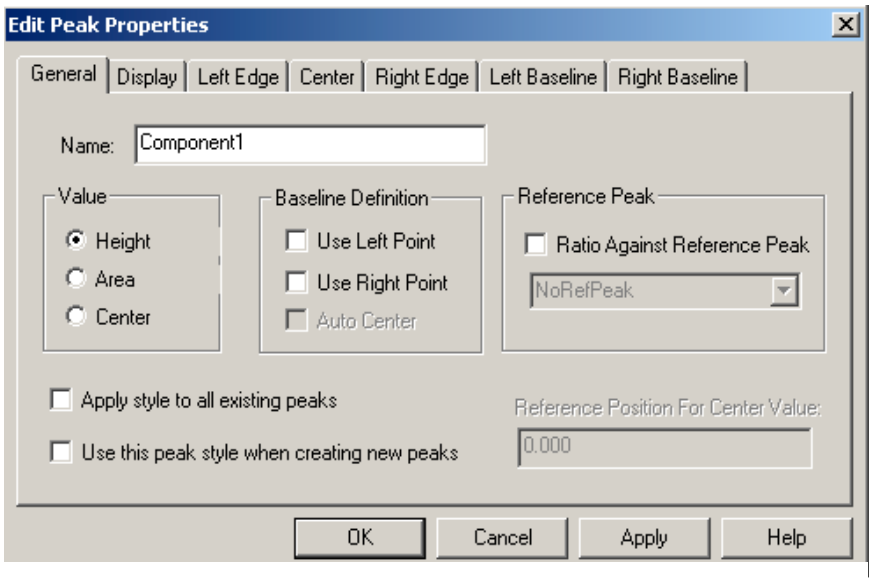

Figure 86. Edit peak properties window.

(10) To select the spectrum desired to be included in the quantitative analysis, double-click " Include in Quant (Analysis) cells". This will change the values from "No" to "Yes". Double-click on "Yes" value whenever it needed to be changed to "NO" so that it would be excluded from the analysis as shown in figure 87.

	Name	Spectrum	Include in Quant	CO(2166.030)	CO(2169.605)	CO(2158.747)
Spectrum1	0		Yes	0	0	0
Spectrum2	50ppm		No	50	50	50
Spectrum3	100ppm		Yes	100	100	100
Spectrum4	150ppm		Yes	150	150	150
Spectrum5	200ppm		Yes	200	200	200
Spectrum6	250ppm		Yes	250	250	250
Spectrum7	300ppm		No	300	300	300
Spectrum8	400ppm		No	400	400	400
Spectrum9	500ppm		No	500	500	500
Spectrum10	600ppm		No	600	600	600
Spectrum11	700ppm		No	700	700	700
Spectrum12	800ppm		No	800	800	800
Spectrum13	900ppm		No	900	900	900
Spectrum14	1100ppm		No	1100	1100	1100
Spectrum15	1300ppm		No	1300	1300	1300
Spectrum16	1600ppm		No	1600	1600	1600

Figure 87. A table showing how to include quantification cells.

(11) Enter concentrations of species, for example 50, 100. 200 ... ... etc., for each spectrum in the cells under column right next to the "Include in Quant" column. It gives a calibration curve fit on the points as shown in figure 88.

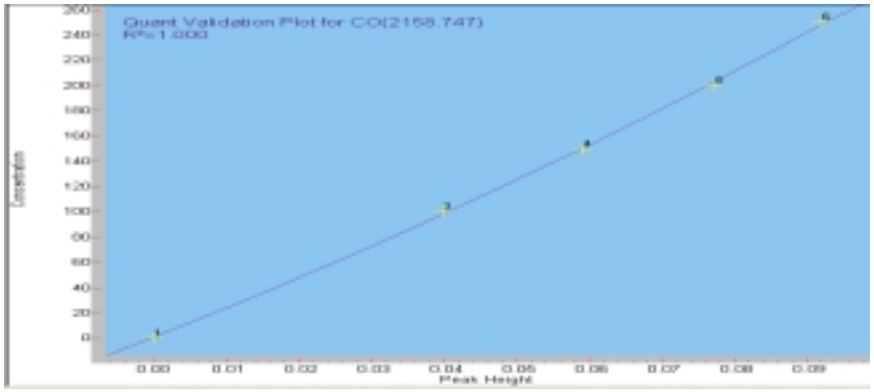

Figure 88. A calibration curve shown on the top-right area in the screen.

(12) In most cases, the peak height and the concentration of the gas species may not be linearly related to each other. To get better matching curve, click the right mouse button in the plot area, then select " Properties" from menu as shown in figure 89.

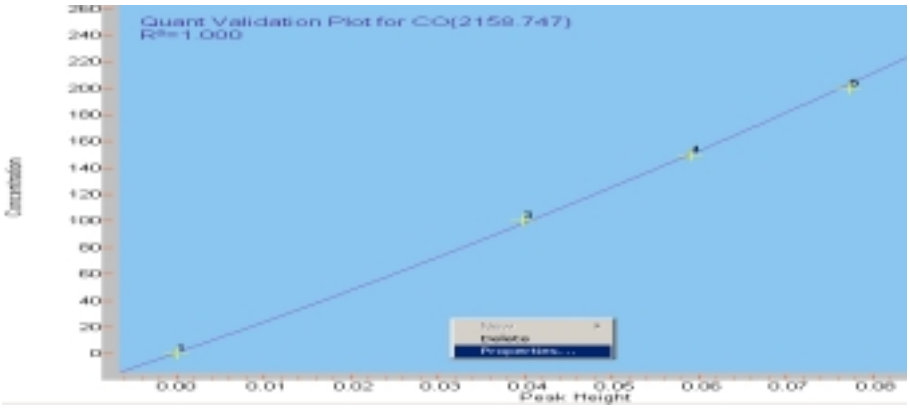

Figure 89. A window after clicking "Properties" on the right button mouse.

(13) Select curve specifications for the better matching in a dialog box "Edit Property" as shown in figure 90.

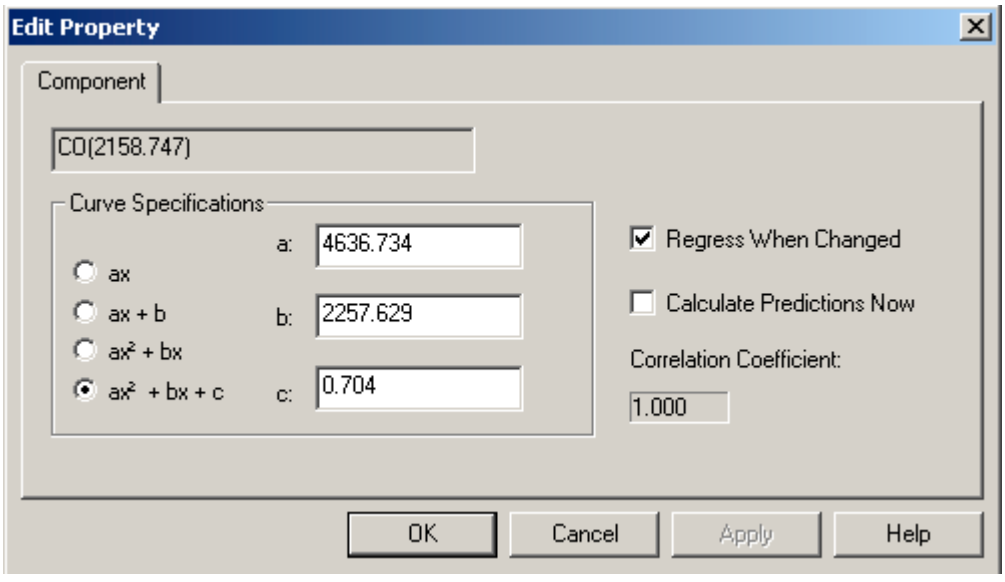

Figure 90. Edit property window for the better match curve.

(14) A calibration document has been created. Save it to a file name into with .bsq extension.

4. Compound specific descriptions

4.1 Carbon monoxide – CO

CO is active only in the range 2250 ~ 2200 cm^{-1}, except that range, there is no evidence CO shape in the whole range. Among lots of peaks, selected 3 peaks for the quantification with these wavenumbers (2166.030, 2169.605, and 2158.747 cm^{-1}) as shown in figure 91. Figure 92 show the relation between absorbance and concentration at 2158.747 cm^{-1} wavenumber.

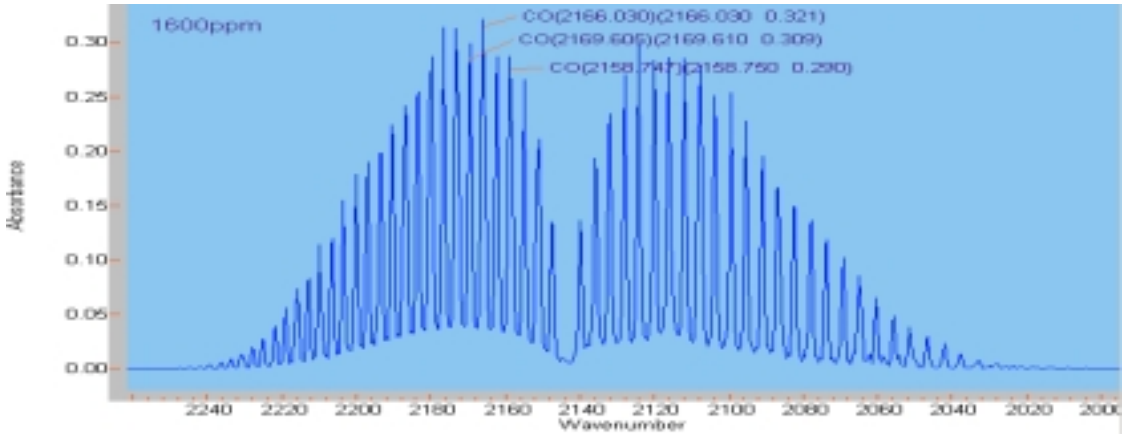

Figure 91. CO absorbance vs wavenumber.

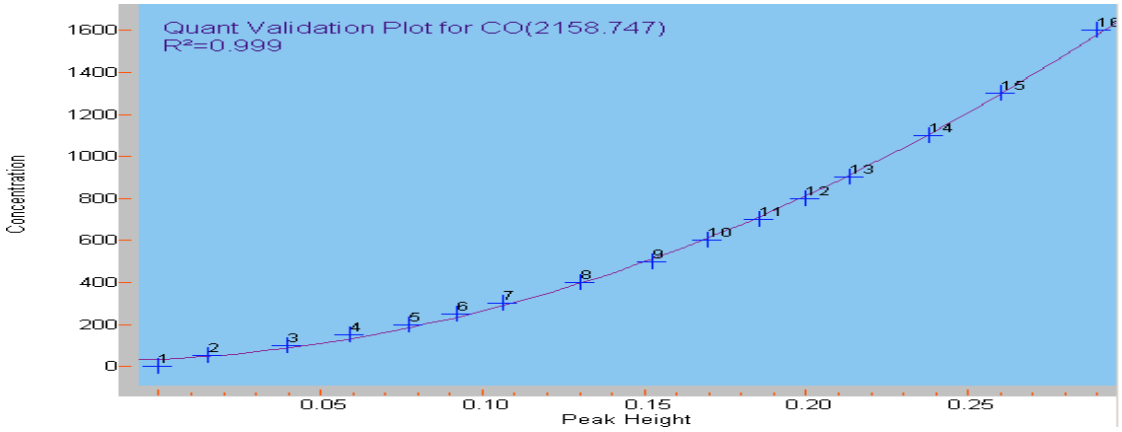

Figure 92. CO concentration vs peak height at wavenumber 2158.747 cm^{-1}.

4.2 Carbon dioxide – CO_2

Carbon dioxide has lots of absorption bands in the infrared. It can be seen 3 regions of CO_2 in the band (3750 ~ 3550, 2400 ~ 2200, and 750 ~ 600 cm^{-1}). The region of 3750~3550 cm^{-1} is interfered by H_2O. Among lots of peaks, selected 3 peaks for the quantification with these wavenumbers (2315.637, 2313.627, and 2311.596 cm^{-1}) as shown in figure 93. Figure 94 show the relation between absorbance and concentration at the wavenumber (2313.627 cm^{-1}). Figure 95 shows calibration spectra of carbon monoxide and carbon dioxide. It is evident that the CO band at 2158.747 cm^{-1} is well separated from the carbon dioxide band at 2313.627 cm^{-1}.

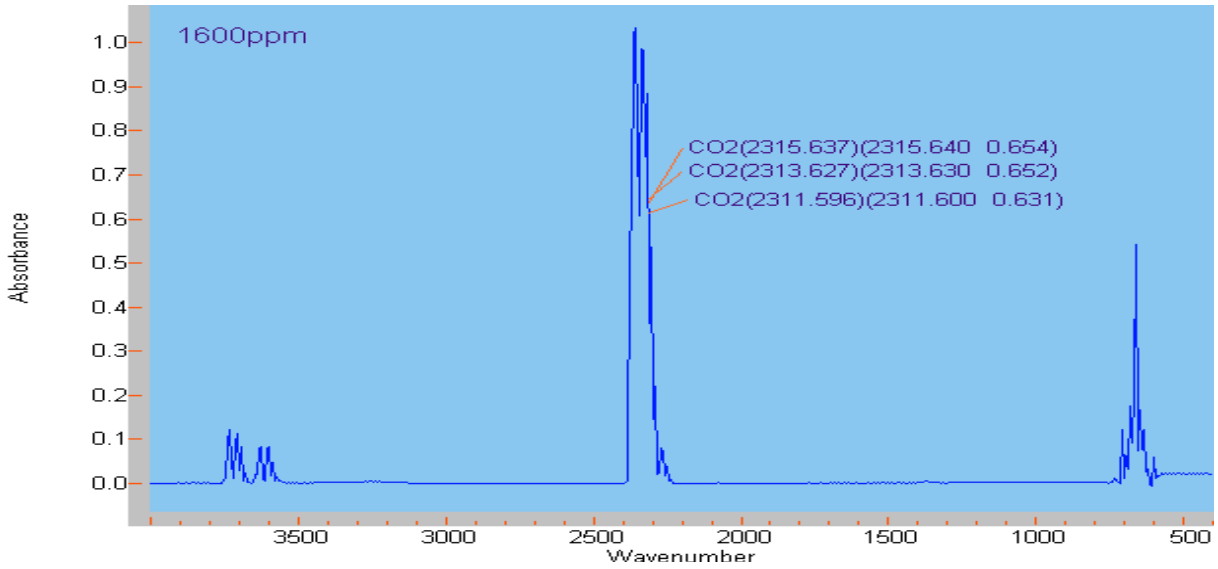

Figure 93. CO_2 absorbance vs wavenumber.

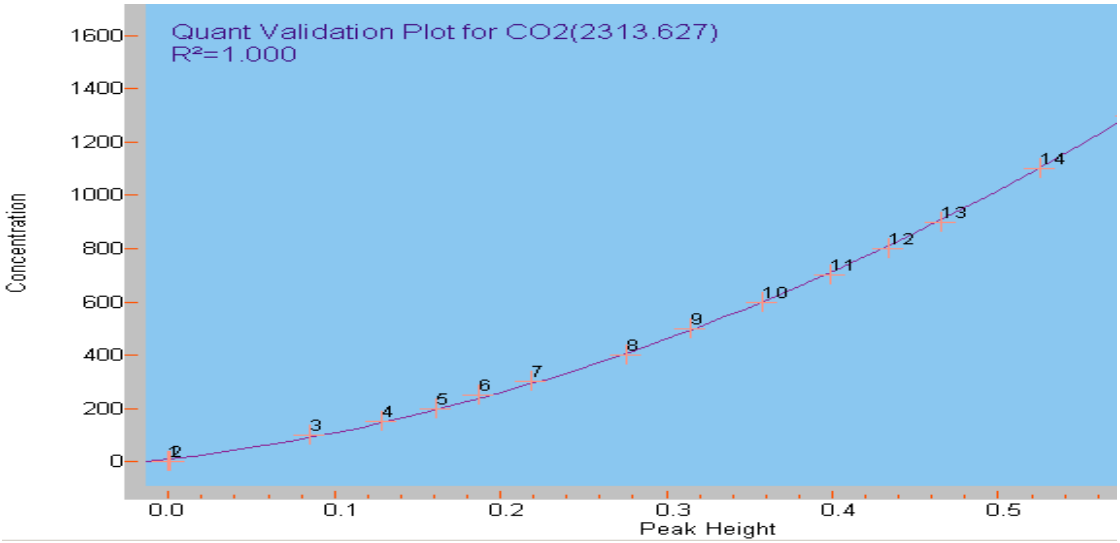

Figure 94. CO_2 concentration vs peak height at wavenumber 2313.627 cm^{-1}.

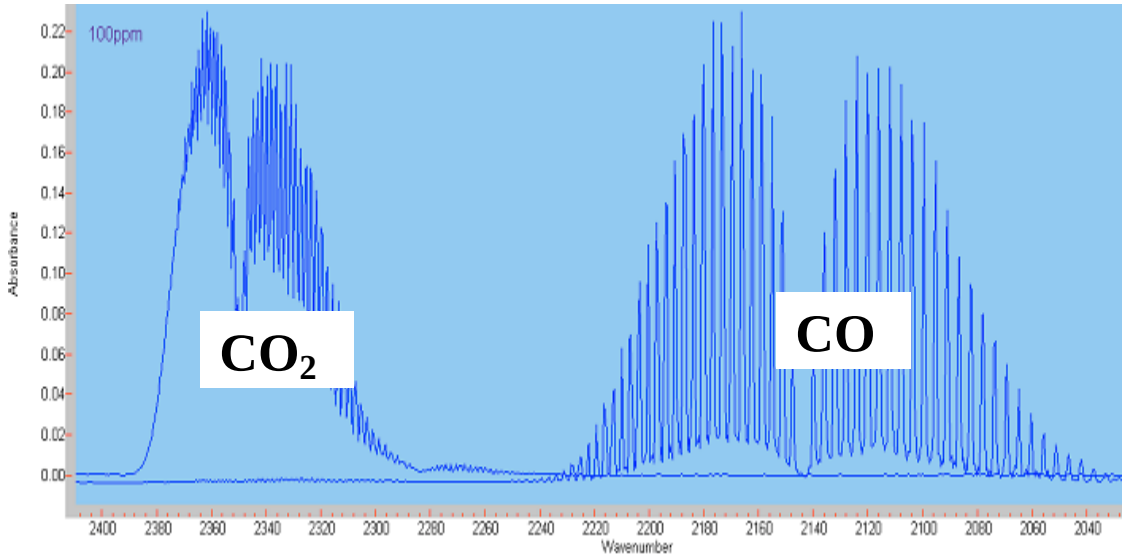

Figure 95. CO_2 and CO absorbance vs wavenumber between 2040 ~ 2400 cm^{-1}.

4.3 Nitric Oxide – NO

Nitric Oxide absorbs infrared radiation only in the range 1950 ~ 1800 cm $^{-1}$. Among lots of peaks, selected 3 peaks for the quantification with this wavenumbers (1903.700, 1906.715, and 1909.714 cm $^{-1}$) as shown in figure 96. Figure 97 show the relation between absorbance and concentration at the wavenumber (1909.714 cm $^{-1}$).

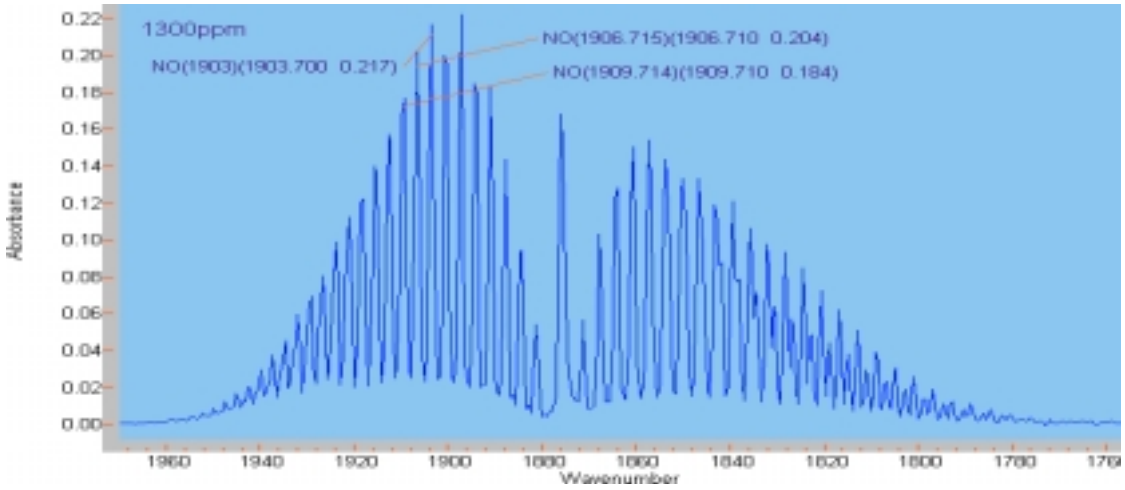

Figure 96. NO absorbance vs wavenumber.

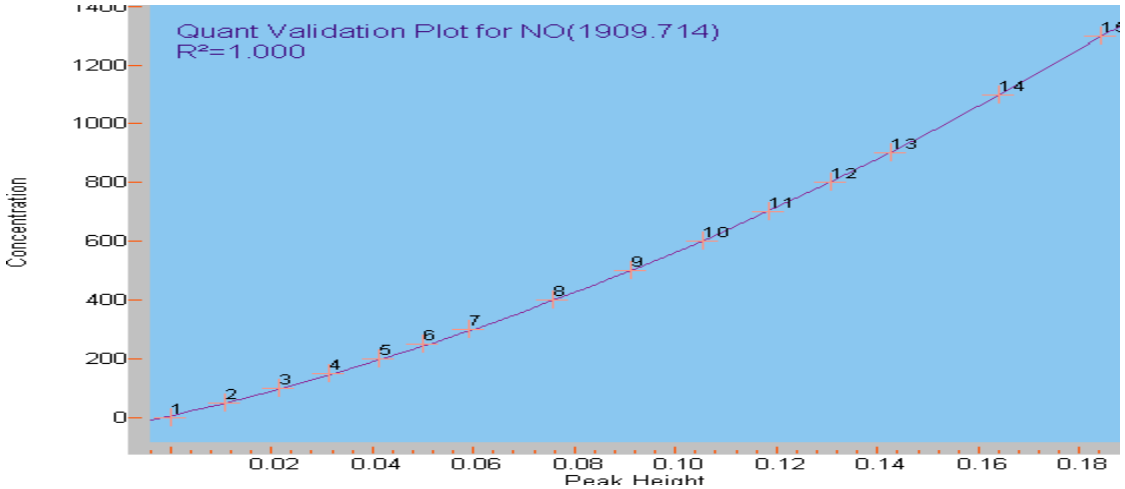

Figure 97. NO concentration vs peak height at wavenumber 1909.714 cm^{-1}.

4.4 Nitrogen Dioxide – NO_2

Nitrogen dioxide has 2 main absorption bands in the infrared (2950 ~ 2850, 1750 ~ 1550 cm^{-1}). Since there is interference from H_2O in the region (1750 ~ 1550 cm^{-1}) that has a relatively high absorption coefficient, selected 3 peaks for the quantification with this wavenumbers (2920.683, 2919.378, and 2918.177 cm^{-1}) as shown in figure 98. Figure 99 show the relation between absorbance and concentration at the wavenumber (2918.177 cm^{-1}).

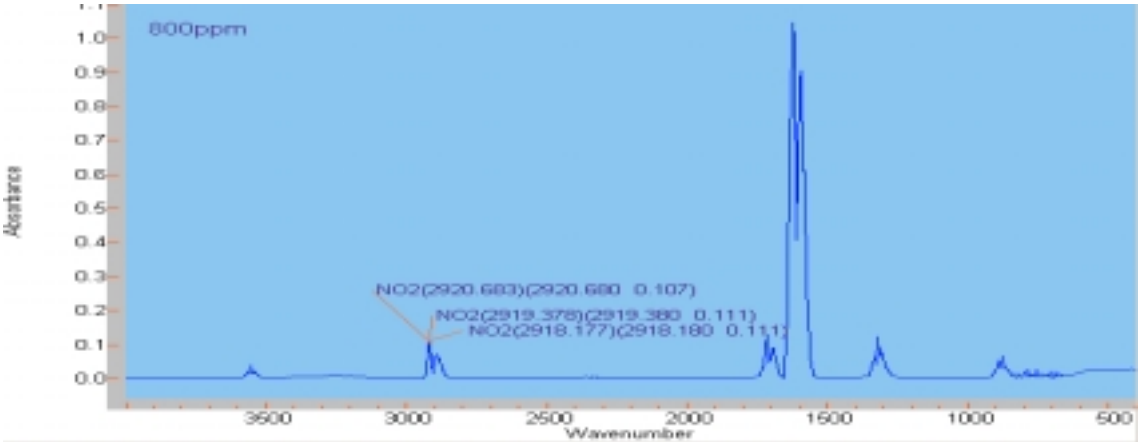

Figure 98. NO_2 absorbance vs wavenumber.

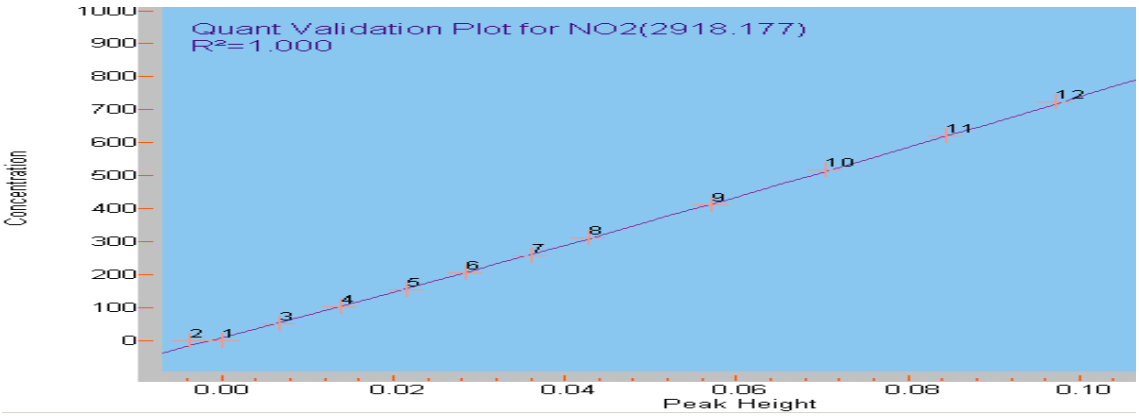

Figure 99. NO_2 concentration vs peak height at wavenumber 2918.177 cm^{-1}.

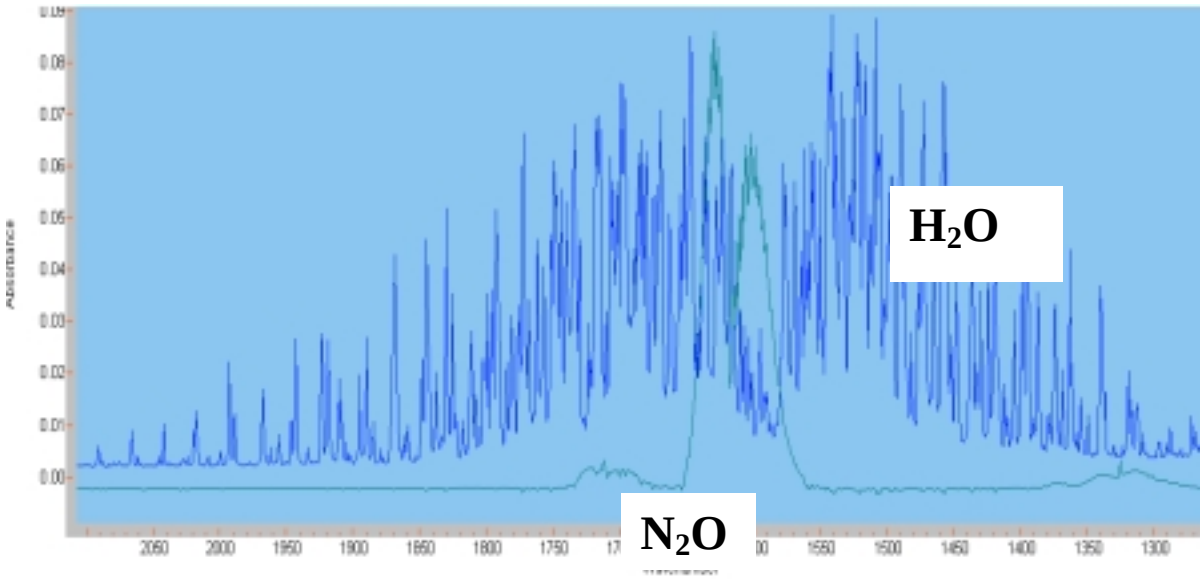

Figure 100. N_2O and H_2O absorbance vs wavenumber between 1300 ~ 2050 cm^{-1}.

Figure 100 shows the interference between H_2O and N_2O in the range 1750 ~ 1550 cm^{-1}. Range between 2950 ~ 2850 cm^{-1} of N_2O band should be detected.

4.5 Nitrous Oxide – N_2O

Nitrous oxide has absorption bands in two ranges in the infrared (1350 ~ 1250 and 2270 ~ 2150 cm^{-1}). In the range around 1300 cm^{-1}, the absorbance is interfered with H_2O. For the accurate determination of N_2O, selected absorbance in the 2200 cm^{-1} region in the spite of strong interference from carbon oxide and carbon dioxide. These two compounds can be determined with good accuracy and therefore their interference can be well compensated. Figure 101 shows a calibration spectrum in the 2200 cm^{-1} range. Below figure 102 shows the N_2O concentration vs peak height at wavenumber 2238.023 cm^{-1}.

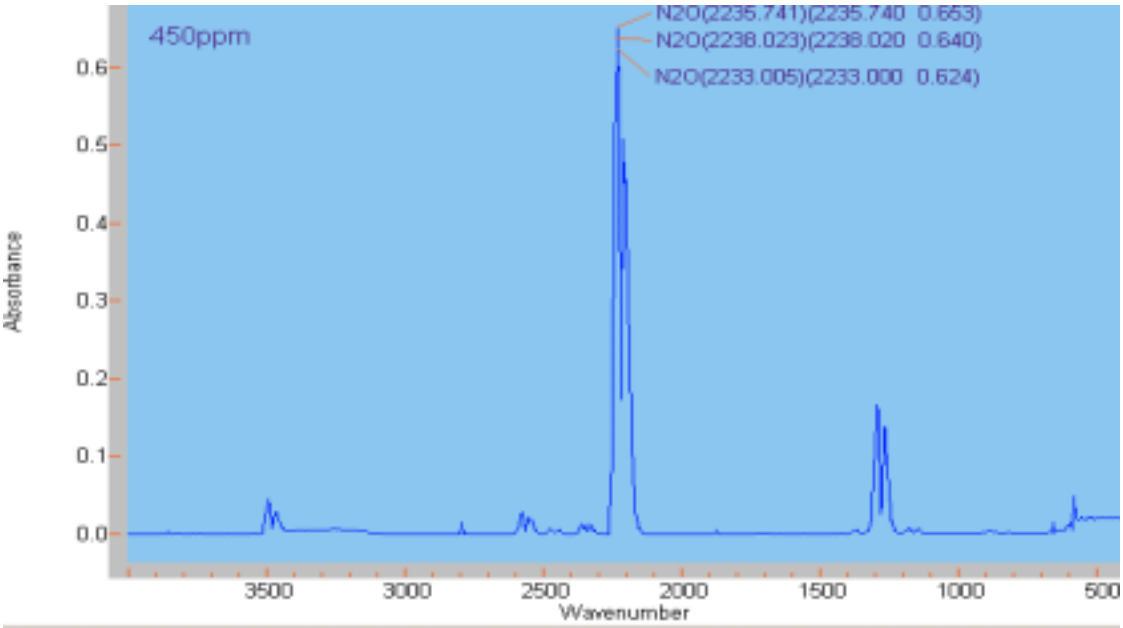

Figure 101. N_2O absorbance vs wavenumber.

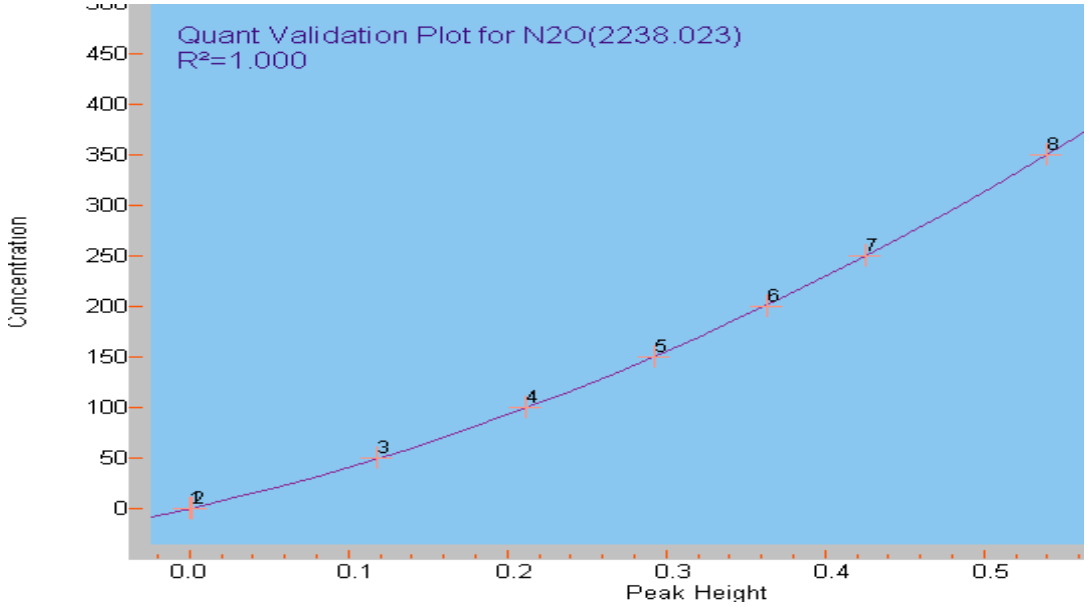

Figure 102. N_2O concentration vs peak height at wavenumber 2238.023 cm^{-1}.

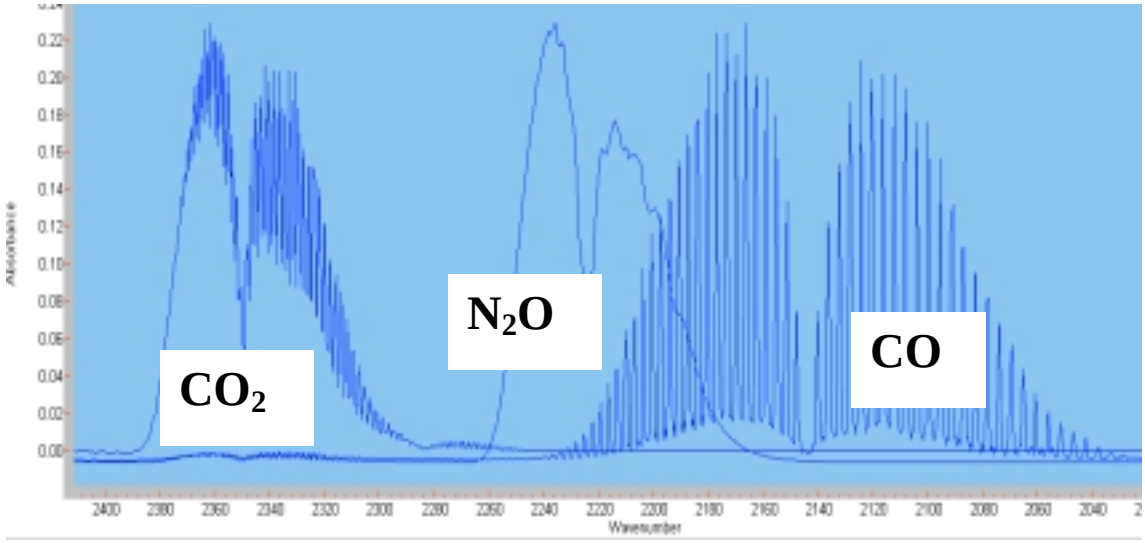

Figure 103. CO_2, N_2O, and CO absorbance vs wavenumber between 2040 ~ 2400 cm^{-1}.

Figure 103 shows the CO_2, N_2O, and CO absorbance vs wavenumber between 2040 ~ 2400cm^{-1}.

4.6 Ammonia – NH_3

Ammonia has a number well separated absorption bands and a relatively high absorption coefficient. Ammonia has absorption bands in three regions in the infrared (3550 ~ 3250, 1800 ~ 1450, and 1200 ~ 750 cm^{-1}) as shown in figure 104. In the ranges around 3550 ~ 3250 and 1800 ~ 1450 cm^{-1}, the absorbance is interfered with H_2O. For the accurate determination of ammonia, selected absorbance in the 1200 ~ 750 cm^{-1} region in the spite of interference from carbon dioxide. Figure 105 shows a calibration spectrum in the 1065 cm^{-1} range. Figure 106 shows the H_2O and NH_3 absorbance vs wavenumber between 800 ~ 3800 cm^{-1}.

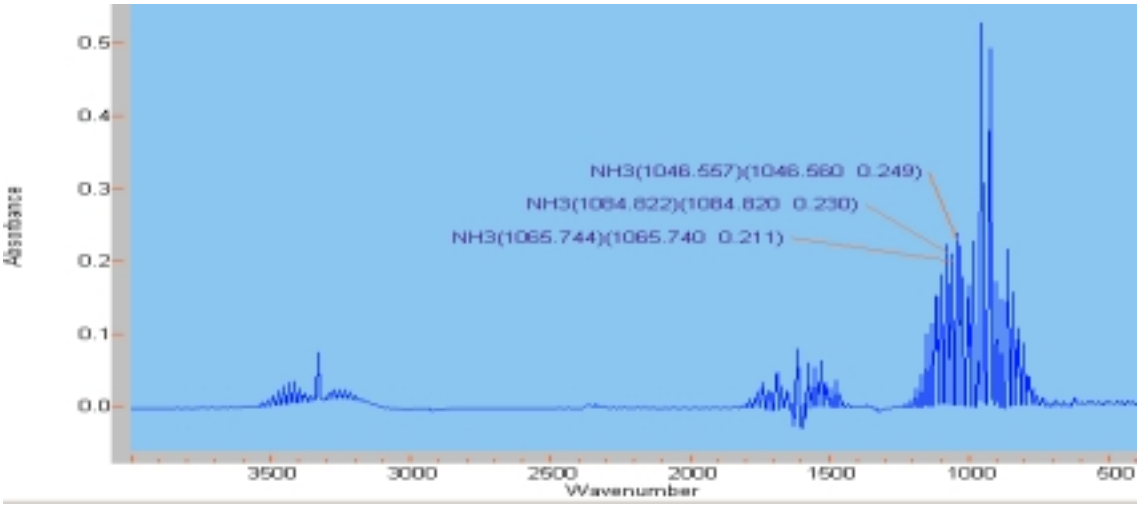

Figure 104. NH_3 absorbance vs wavenumber.

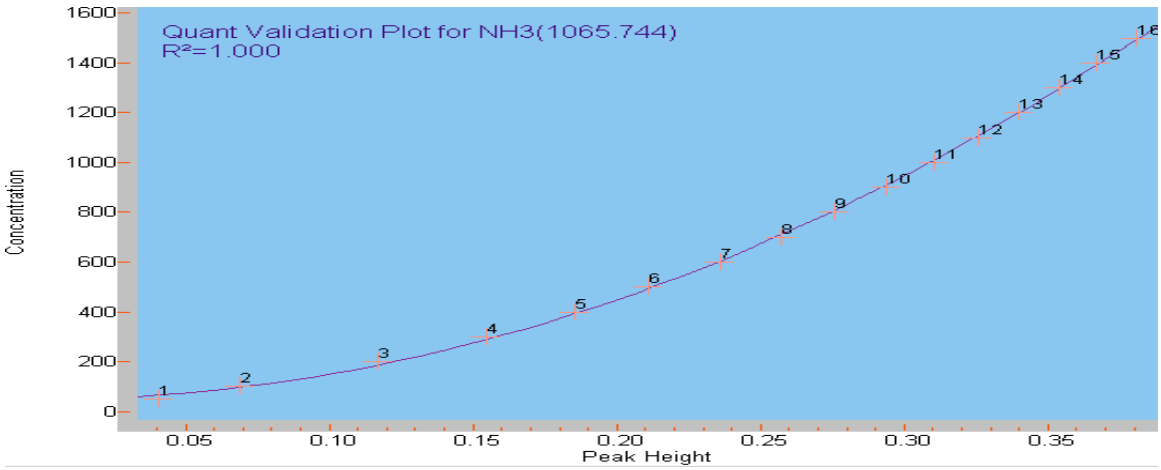

Figure 105. NH_3 concentration vs peak height at wavenumber 1065.744 cm^{-1}.

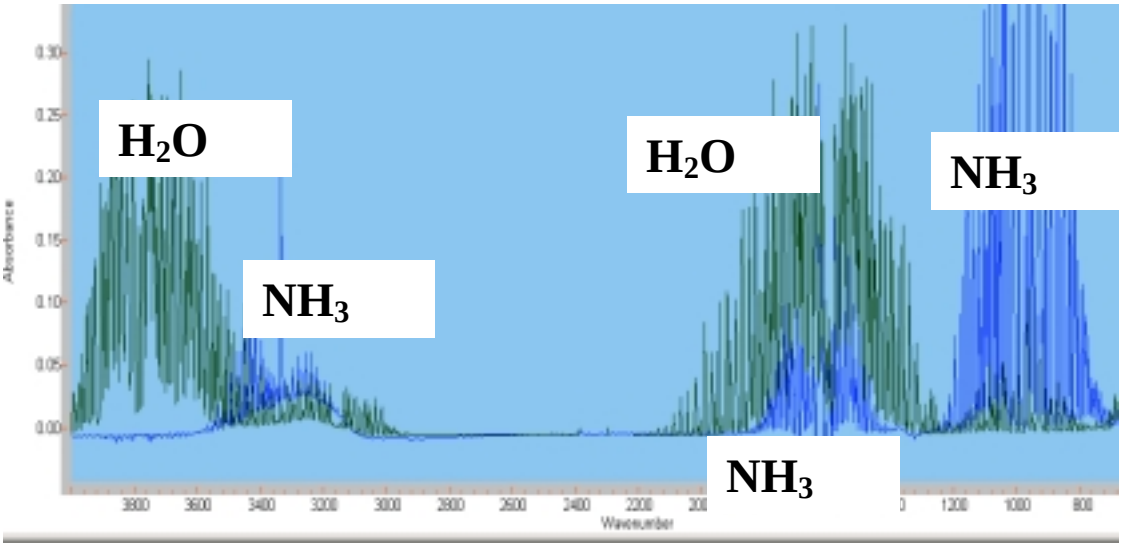

Figure 106. H_2O and NH_3 absorbance vs wavenumber between 800 ~ 3800 cm^{-1}.

4.7 HNCO

Dry urea powder (3.0 g) was placed in the entrance of the reactor. The reactor temperature was increased as only nitrogen gas flowed through the reactor. But calibration was not possible because no source of HNCO for calibrations was available. HNCO absorbs in three regions in the infrared. The main HNCO peak at 2280 cm^{-1} as shown in figure 107, the second strongest peak at 3500 cm^{-1}, the third one at 787 cm^{-1}. In the regions 3500 and 787 cm^{-1}, HNCO absorption band is interfered with H_2O and HN_3. Figure 108 shows the CO_2, HNCO, N_2O, and CO absorbance vs wavenumber between 2040 ~ 2400 cm^{-1}.

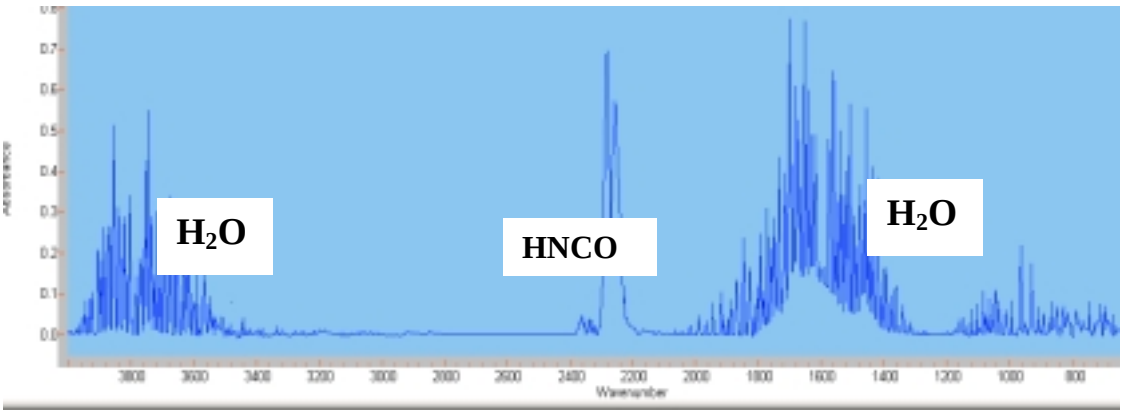

Figure 107. HNCO absorbance vs wavenumber.

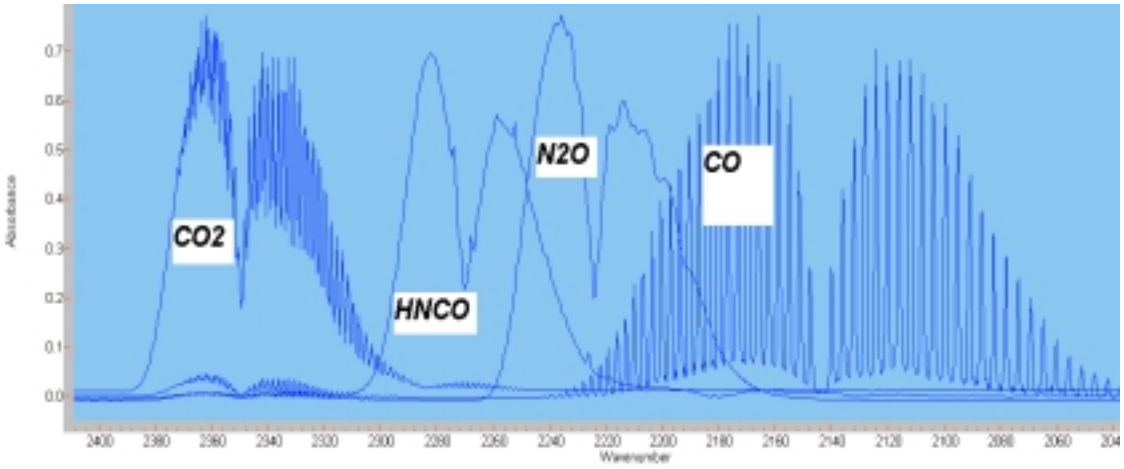

Figure 108. CO_2, HNCO, N_2O, and CO absorbance vs wavenumber between 2040 ~ 2400 cm^{-1}.

VITA

Yong Hun Park was born on July 17th 1972, in Tae-Gu, S. Korea. He enrolled at Kyungpook National University in the spring of 1991 and pursued a Bachelor of Engineering (Mechanical Engineering) in Feb. 1999. He served military service between 1994 and 1996. He had worked at PH Automotive Co.Ltd. as an engineer on a business innovation team since winter in 1998. He enrolled at Texas A&M University in the fall of 2000 to pursue a Master of Science degree in mechanical engineering.

Yong Hun Park can be reached at e-mail: air717@hotmail.com and will maintain his permanent address at his home:

540-3 Bong-Duck-Dong, Nam-Gu, Tae-Gu, S.Korea 705-822